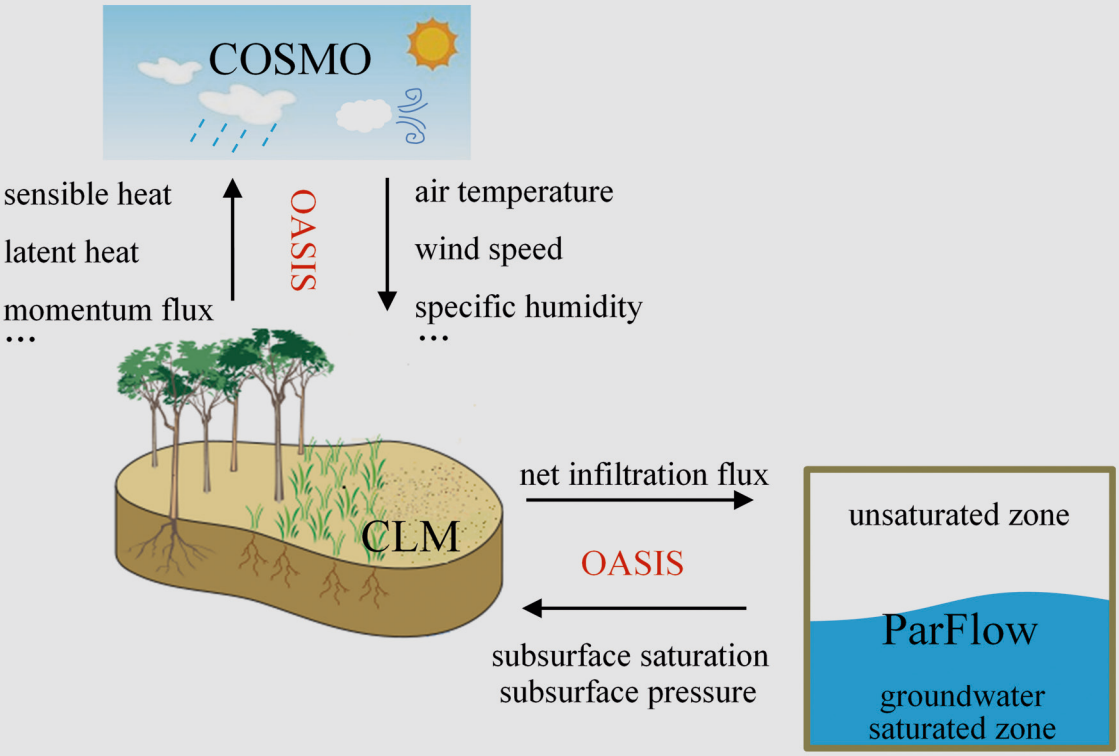

Improved characterization of root zone soil moisture by assimilating groundwater level and surface soil moisture data in an integrated terrestrial system model

Hongjuan Zhang

Energie & Umwelt / Energy & Environment
Band / Volume 427
ISBN 978-3-95806-335-8

Mitglied der Helmholtz-Gemeinschaft

JÜLICH
Forschungszentrum

Schriften des Forschungszentrums Jülich
Reihe Energie & Umwelt / Energy & Environment Band / Volume 427

Forschungszentrum Jülich GmbH
Institut für Bio- und Geowissenschaften
Agrosphäre (IBG-3)

Improved characterization of root zone soil moisture by assimilating groundwater level and surface soil moisture data in an integrated terrestrial system model

Hongjuan Zhang

Schriften des Forschungszentrums Jülich
Reihe Energie & Umwelt / Energy & Environment Band / Volume 427

ISSN 1866-1793 ISBN 978-3-95806-335-8

Bibliografische Information der Deutschen Nationalbibliothek.
Die Deutsche Nationalbibliothek verzeichnet diese Publikation in der
Deutschen Nationalbibliografie; detaillierte Bibliografische Daten
sind im Internet über http://dnb.d-nb.de abrufbar.

Herausgeber und Vertrieb:	Forschungszentrum Jülich GmbH Zentralbibliothek, Verlag 52425 Jülich Tel.: +49 2461 61-5368 Fax: +49 2461 61-6103 zb-publikation@fz-juelich.de www.fz-juelich.de/zb
Umschlaggestaltung:	Grafische Medien, Forschungszentrum Jülich GmbH
Druck:	Grafische Medien, Forschungszentrum Jülich GmbH
Copyright:	Forschungszentrum Jülich 2018

Schriften des Forschungszentrums Jülich
Reihe Energie & Umwelt / Energy & Environment, Band / Volume 427

D 82 (Diss., RWTH Aachen, Univ., 2018)

ISSN 1866-1793
ISBN 978-3-95806-335-8

Vollständig frei verfügbar über das Publikationsportal des Forschungszentrums Jülich (JuSER)
unter www.fz-juelich.de/zb/openaccess.

Contents

List of Figures

List of Tables

List of Acronyms

CLM	Community Land Model
COSMO	Consortium for Small-Scale Modeling
KF	Kalman Filter
EnKF	Ensemble Kalman Filter
EnKF-AUG	State Augmentation Method of EnKF
EnKF-DUAL	Dual Estimation Method of EnKF
LSM	Land Surface Model
MCMC	Markov chain Monte Carlo
NS	Normal Score
NSE	Nash-Sutcliffe Model Efficiency
GWL	Groundwater Level
ParFlow	Parallel Watershed Flow Model
PDAF	Parallel Data Assimilation Framework
PDF	Probability Density Function
PF	Particle Filter
PFT	Plant Function Type
PMCMC	Markov chain Monte Carlo Particle Filter
PWC	Pressure Head to Water Content
RMSE	Root Mean Square Error
RRPF	Residual Resampling Particle Filter
SSM	Surface Soil Moisture
TerrSysMP	Terrestrial System Modeling Platform
VIC	Variable Infiltration Capacity Model
WT	Water Table

Abstract

Soil moisture is an important variable for the cycling of water and energy at the catchment/regional/global scale. Soil moisture content is usually simulated by land surface models, monitored by ground-based sensors, or observed by remote sensing techniques. However, land surface models often have high uncertainties due to simplified parameterizations and uncertainties from input forcing data and hydraulic parameters. For example, in most land surface models, the interaction between groundwater and root zone soil moisture is neglected. The availabilities of in situ monitoring networks are limited because of high costs. Remote sensing can provide soil moisture at the global scale but is limited to the top 5 cm and resolution is coarse. Data assimilation can take advantage of these three different sources of information by assimilating the observations (e.g. from the ground sensors or remote sensing data) into the land surface models to improve soil moisture predictions in both space and time. Furthermore, soil hydraulic parameters in land surface models can also be estimated jointly with soil moisture by data assimilation to further improve soil moisture characterization. In order to make land surface models more robust, integrated land surface-subsurface models have been developed which consider the effect of groundwater on root zone soil moisture in a fully two-way coupled fashion.

In this work, we firstly compared four data assimilation methods in terms of joint estimation of soil moisture and soil hydraulic parameters for two land surface models. The four assimilation methods included Ensemble Kalman Filter (EnKF) with state augmentation (EnKF-AUG) or dual estimation (EnKF-DUAL), the residual resampling Particle Filter (RRPF) and the MCMC-based parameter resampling method (PMCMC). The two land surface models used were the Variable Infiltration Capacity Model (VIC) and the Community Land Model (CLM version 4.5). Real world data (soil properties, soil moisture measurements at 5, 20 and 50 cm depth, climate forcing data) from the Rollesbroich site located in the western Germany were used. We evaluated the usefulness and applicability of the four different data assimilation methods for joint parameter and state estimation of the VIC and the CLM using a 5-month calibration (assimilation) period of the soil moisture measurements. The performance of the "calibrated" VIC and CLM were investigated using water moisture measurements of a 5-month evaluation period. Results from the first study showed that all of the four assimilation methods were able to improve the model predictions of soil moisture after soil hydraulic parameters (for VIC) or sand/ clay/ organic matter fraction (for CLM) were jointly estimated with soil moisture. Overall, EnKF (EnKF-AUG and EnKF-DUAL) performed better than PF (RRPF and PMCMC). The differences between the soil moisture simulations of VIC and CLM were much larger than the discrepancies among the four data assimilation methods. CLM performed better than VIC in the soil moisture simulations at 50 cm depth. The large systematic underestimation of water storage at 50cm depth in VIC is most probably related to the fact that groundwater is not well represented in VIC.

Therefore, one conclusion from this first study was that groundwater was essential for the estimation of the soil moisture content in the deeper soil profile. Therefore in the second study, an integrated model, TerrSysMP, which couples a land surface model and a

groundwater flow model, was used to investigate the potential of assimilating groundwater level data to improve the characterization of root zone soil moisture. We evaluated five data assimilation strategies, based on EnKF, in small scale synthetic experiments. In the groundwater level data assimilation experiments with TerrSysMP, the five data assimilation methodologies demonstrated that EnKF could not handle well strongly skewed state distributions (non-Gaussian distribution). In TerrSysMP, in the unsaturated zone during dry periods very negative pressure heads were calculated. The best methodology to solve this problem was constructing the state vector, to be updated in data assimilation, with pressure head for the saturated zone and soil moisture for the unsaturated zone. This approach gave the best results among the five methodologies and avoided strongly skewed state distribution in EnKF.

It was expected that the relation between groundwater level and root zone soil moisture was affected by different climate conditions, plant functional types (PFTs) and soil textures. So in the third study, we analysed the effect of climate, PFTs and soil textures on the assimilation of groundwater level also with TerrSysMP and small scale synthetic experiments. Results from the third study showed that different climate conditions, PFTs and soil textures generated different groundwater levels and soil moisture distributions. In different data assimilation experiments surface soil moisture and groundwater level were jointly assimilated and results were evaluated in terms of improving root zone soil moisture characterization. Results showed that assimilation performance was more sensitive to climate condition and soil texture, and less sensitive to PFTs. It was also found that assimilation generally worked better if groundwater levels were between -1m and -5m below the soil surface.

In summary, these results showed that data assimilation is a promising way to improve the model predictions and model parameter estimations. The linkage between root zone soil moisture and groundwater is either neglected or simplified in most land surface models. The fully-coupled subsurface-surface model TerrSysMP which is used in this work can properly handle this linkage. Assimilation of groundwater level in TerrSysMP is well suited for improving the characterization of root zone soil moisture.

Zusammenfassung

Bodenfeuchte ist eine wichtige Variable für Wasser- und Energieflüsse auf Einzugsgebietsebene, sowie auf der regionalen und globalen Skala. Der Bodenwassergehalt wird in der Regel mit Hilfe von Landoberflächenmodelle simuliert, von bodenbasierten Sensoren gemessen oder durch Fernerkundungstechniken beobachtet. Allerdings haben Landoberflächenmodelle oftmals hohe Unsicherheiten aufgrund vereinfachter Parametrisierungen sowie Unwägbarkeiten in den Eingabegrößen und hydraulischen Parametern. Zum Beispiel werden bei den meisten Landoberflächenmodellen Wechselwirkungen zwischen Grundwasser und dem Bodenwasser in der Wurzelzone vernachlässigt. Die Verfügbarkeit von in-situ-Monitoring-Netzwerken ist aufgrund der hohen Kosten begrenzt.. Die Fernerkundung kann Bodenfeuchtedaten auf globaler Ebene bereitstellen, ist aber auf die oberen 5 cm des Bodenprofils limitiert und die Auflösung ist grob. Die Datenassimilierung kann diese drei verschiedenen Informationsquellen nutzen, indem die Beobachtungen (z.B. von den Bodensensoren oder Fernerkundungsdaten) in die Landoberflächenmodelle eingebunden werden, um die Bodenfeuchtigkeitsvorhersagen sowohl im Raum als auch über die Zeit zu verbessern. Darüber hinaus können auch bodenhydraulische Parameter in Landoberflächenmodellen gemeinsam mit Bodenfeuchte durch Datenassimilation geschätzt werden, um die Bodenfeuchtebeschreibung weiter zu verbessern. Um Landoberflächenmodelle robuster zu machen, wurden integrierte Landoberflächen-Untergrund-Modelle entwickelt, welche die Interaktionen zwischen Grundwasser und Bodenwasser in der Wurzelzone mit Hilfe einer vollständig wechselseitigen Kopplungberücksichtigen.

In dieser Arbeit verglichen wir zunächst vier Datenassimilationsmethoden in Bezug auf die gemeinsame Schätzung der Bodenfeuchte und der hydraulischen Parameter für zwei Landoberflächenmodelle. Die vier Assimilationsmethoden umfassten den Ensemble Kalman Filter (EnKF) mit „state augmentation“ (EnKF-AUG) oder „dual estimation“ (EnKF-DUAL), den „residual resampling particle filter“- (RRPF) und die „Markov chain Monte Carlo-based parameter resampling“-Methode (PMCMC). Die beiden Landoberflächenmodelle waren das „Variable Infiltration Capacity Model“ (VIC und das „Community Land Model“ (CLM Version 4.5). Es wurden reale Daten (Bodeneigenschaften, Bodenfeuchtemessungen in 5, 20 und 50 cm Tiefe, Klimadaten) vom Standort Rollesbroich in Westdeutschland verwendet. Wir untersuchten die Nützlichkeit und Anwendbarkeit der vier verschiedenen Datenassimilationsmethoden für die gemeinsame Parameter- und Zustandsschätzung mit dem VIC und dem CLM unter Verwendung einer 5-monatigen Kalibrierungsperiode (Assimilation) mit Bodenfeuchtemessungen. Die Güte der "kalibrierten" Modelle, VIC und CLM, wurde anhand von Bodenwassermessungen in einem 5-monatigen Evaluationszeitraum untersucht. Die Ergebnisse der ersten Studie zeigten, dass alle vier Assimilationsmethoden die Modellvorhersagen der Bodenfeuchte verbessern konnten, nachdem die bodenhydraulischen Parameter (für VIC) oder die Anteile an Sand, Ton und organischer Substanz (für CLM) gemeinsam mit der Bodenfeuchte angepasst wurden. Insgesamt lieferte EnKF (EnKF-AUG und EnKF-DUAL) bessere Ergebnisse als PF (RRPF und PMCMC). Die Unterschiede zwischen den Bodenfeuchtesimulationen von VIC und CLM waren viel größer als die Diskrepanzen zwischen den vier Datenassimilationsmethoden. CLM hat in den

Bodenfeuchtigkeitssimulationen in 50 cm Tiefe besser abgeschnitten als VIC. Die große systematische Unterschätzung des Wasserspeichers in 50 cm Tiefe in VIC hängt höchstwahrscheinlich damit zusammen, dass das Grundwasser im VIC nicht gut beschrieben ist.

Eine Schlussfolgerung aus dieser ersten Studie war daher, dass die korrekte Simulation der Grundwasserdynamik für die Schätzung des Bodenfeuchtegehalts im tieferen Bodenprofil unerlässlich war. Daher wurde in der zweiten Studie ein integriertes Modell, TerrSysMP, welches ein Landoberflächen- und ein Grundwasserströmungsmodell koppelt, verwendet, um das Potenzial der Assimilierung von Grundwasserspiegeldaten für eine bessere Beschreibung des Bodenwassers in der Wurzelzone zu untersuchen. Wir haben fünf Datenassimilationsstrategien, basierend auf EnKF, in kleinräumigen synthetischen Experimenten ausgewertet. In den Grundwasserspiegel-Datenassimilationsexperimenten mit TerrSysMP zeigten die fünf Datenassimilationsmethoden, dass EnKF Probleme mit der Verabeitung sehr schiefer Wahrscheinlichkeitsverteilungen (nicht-Gaußsche Verteilungen) der Zustandsgrößen hatte In TerrSysMP wurden in der ungesättigten Zone während Trockenperioden sehr negative Druckhöhen berechnet. Die beste Methode zur Lösung dieses Problems war die Definition des Zustandsvektors, der in der Datenassimilation aktualisiert werden soll, mit Druckhöhe für die gesättigte Zone und Bodenfeuchte für die ungesättigte Zone. Dieser Ansatz ergab die besten Ergebnisse unter den fünf Methoden und vermied eine sehr schiefe Verteilung der Zustandsgrößen in EnKF.

Es wurde erwartet, dass die Beziehungen zwischen Grundwasserspiegel und Bodenwasser in der Wurzelzone durch unterschiedliche Klimabedingungen, funktionale Pflanzentypen (PFTs) und Bodentexturen beeinflusst werden. So analysierten wir in der dritten Studie die Wirkung von Klima, PFTs und Bodentextur auf die Assimilation des Grundwasserspiegels auch in TerrSysMP und mit kleinräumigen synthetischen Experimenten. Die Ergebnisse dieser Studie zeigten, dass unterschiedliche Klimabedingungen, PFTs und Bodentexturen unterschiedliche Grundwasserspiegel und Bodenfeuchtigkeitsverteilungen erzeugten. In verschiedenen Datenassimilationsexperimenten wurden die Bodenfeuchte und der Grundwasserspiegel gemeinsam assimiliert und die Ergebnisse wurden hinsichtlich der verbesserten Schätzung des Bodenwassers in der Wurzelzone bewertet. Die Ergebnisse zeigten, dass die Assimilationsgüte sensibler gegenüber Klimabedingungen und Bodenbeschaffenheit war und weniger gegenüber PFTs. Es wurde auch festgestellt, dass die Assimilation im Allgemeinen bessere Ergebnisse lieferte, wenn die Grundwasserspiegel zwischen -1 m und -5 m unterhalb der Bodenoberfläche lagen.

Zusammenfassend zeigten diese Ergebnisse, dass die Datenassimilation eine vielversprechende Methode ist, welche die Modellvorhersagen und -parameterschätzungen verbessert. Die Verknüpfung zwischen Bodenwasser in der Wurzelzone und Grundwasser wird in den meisten Landoberflächenmodellen entweder vernachlässigt oder vereinfacht. Das vollständig gekoppelte Landoberflächen-Untergrund-Modell TerrSysMP, das in dieser Arbeit verwendet wird, kann diese Verknüpfung richtig behandeln. Die Assimilation des Grundwasserspiegels in TerrSysMP eignet sich hervorragend zur Verbesserung der Beschreibung des Bodenwassers in der Wurzelzone.

Chapter 1 : Introduction

A good knowledge of hydrologic conditions is of critical importance to our daily life such as agricultural irrigation and production, flood and drought prediction, water resources management, weather forecast, water supply and environmental preservation. In land surface hydrologic processes, surface soil moisture and root zone soil moisture content dynamically change in time and space as the result of precipitation and evapotranspiration. Soil moisture content plays an important role in the global energy and water cycles due to its control on the division of net radiation between sensible and latent heat flux at the atmosphere-land-vegetation interface (Koster et al., 2004). Changes in average soil moisture content related to climate change have the potential to significantly impact climate change via feedback processes (Seneviratne et al., 2010). Soil moisture constrains plant transpiration and photosynthesis (Havranek and Benecke, 1978) and affects biogeochemical cycles. For example, high soil moisture content is associated with increased N_2O production (Rubol et al., 2013). Therefore monitoring, estimating and predicting soil moisture content is necessary and essential in many aspects (Houser et al., 2004; Houser et al., 2012).

Soil moisture measurements are available at different scales. Soil moisture can be evaluated by soil samples in the laboratory. Soil samples are collected from field sites which are affected by variability in soil properties, terrain, micro-climate, and vegetation. Indirect methods can establish a relation between soil properties and soil moisture. Information of the soil dielectric constant, variations of the gravity field or soil suction can be converted to soil moisture estimates as the capacity of a soil to retain water is a function of its texture and structure (Park and Xu, 2017). For example, ground-based observational networks provide a good way to precisely measure temporal and spatial variation of soil moisture at the field scale. In a measurement network, soil moisture sensors/probes are installed at different locations and different depths throughout the study site. Based on an empirical (Topp et al., 1980) or semi-theoretical model (Birchak et al., 1974) between soil moisture and dielectric permittivity from sensor/probe response, time series of soil moisture can be monitored by the sensors/probes without disturbing the soil system. However, in situ measurements are very localized and limited in spatial coverage (Robock et al. 2000; Robinson et al., 2008; Dorigo et al., 2011).

The Cosmic-ray Soil Moisture Observation System is a promising method to measure soil moisture at an intermediate spatial scale with a single sensor (Zreda et al., 2012; Han et al., 2014b). The footprint of a cosmic-ray probe measurement is on the scale of ~10 ha and the penetration depth is, depending on soil moisture content, 10-70 cm. Remote sensing techniques make it possible to measure surface soil moisture at large scale (Jackson, 1993). Examples are the ESA Soil Moisture and Ocean Salinity and the NASA Soil Moisture Active Passive missions, launched in 2009 and 2015 respectively. They provide different levels of global soil moisture products with spatial resolutions between 9km and 50km. However, surface soil moisture from remote sensing only represents information from the upper 5 cm. The conversion of the measured brightness temperature into soil moisture is also affected by many factors, like water body fraction, vegetation density, frozen status of soil and

uncertainties in the retrieval parameters. Given these errors, the usefulness of the remotely-sensed soil moisture products is limited.

Land surface models (LSMs) provide a good way to simulate soil moisture content at regional and global scales. They formulate physical understanding of the land surface-vegetation-atmosphere system (Overgaard et al., 2006). LSMs simulate terrestrial biosphere fluxes of matter and energy via numerical solution of the water, energy, carbon and nitrogen balances of the land-surface. The hydrologic processes include soil evaporation, surface runoff, infiltration, canopy interception and transpiration, groundwater drainage and recharge and precipitation. Different LSMs have different parameterizations, simplifications and assumptions for modelling these processes. Generally, the spatial resolution of LSMs is dictated by the applications, changing from hyper-resolution (100 m to 1 km) to very coarse resolution (20km to 100km). LSM predictions are affected by uncertainties in the meteorological forcing variables, model parameters, and model formulations (Reichle et al., 2004).

In most LSMs interaction between root zone soil moisture and groundwater is neglected or not explicitly treated (Liang and Guo, 2003; Chen and Hu, 2004; Kollet and Maxwell, 2008; Miguez-Macho et al., 2008; Zhu et al. 2013). Although groundwater may have a small effect on soil moisture in areas with a deep groundwater table, groundwater can act as a soil water source and have substantial effects in areas where the groundwater table is closer to the land surface. A shallow groundwater table is more likely to cause surface runoff. On the other hand, deep percolation is needed when rainfall or irrigation are in excess to the soil water content deficit, thus producing a downward flux to recharge groundwater through the bottom boundary of the root zone.

As groundwater is a significant water source for soil moisture especially for root zone soil moisture (water rise across the bottom of the soil profile) (Liu et al., 2006; Zhu et al., 2013), there has been increasing interest in incorporating a groundwater component into LSMs to improve the representation of soil moisture at the land surface. Liang et al. (2003) implemented a new parameterization in the VIC (Variable Infiltration Capacity) model to investigate the effects of surface and groundwater interactions on soil moisture, evapotranspiration, runoff and recharge. Yeh and Eltahir (2005) linked a lumped unconfined aquifer model to a LSM and found that most of the simulated hydrological states (e.g., water table depth and soil moisture) and fluxes (e.g., runoff and evaporation) were better simulated. Graham and Butts (2005) developed the MIKE-SHE hydrological model which covers the major processes in the hydrologic cycle and includes process models for evapotranspiration, overland flow, unsaturated flow, groundwater flow, and channel flow and their interactions. Maxwell and Miller (2005) coupled a LSM (Common Land Model) and a variably saturated groundwater flow model (ParFlow) and demonstrated that the soil moisture and water table depth simulated by the coupled model agreed well with observations. More recently the atmosphere-land surface-subsurface Terrestrial System Modeling Platform (TerrSysMP) (Shrestha et al., 2014) was developed to consider land–atmosphere interaction and subsurface hydrodynamics in the terrestrial system.

Land data assimilation provides a good way to merge uncertain observations with predictions of imperfect models to optimally estimate soil moisture dynamics. In situ soil moisture measurements have high accuracy but the sampled spatial volume is limited. Remotely sensed retrievals and LSM estimates show a good spatial coverage but are associated with high uncertainties. Data assimilation combines the complementary information from the measurements and LSMs to produce a superior estimate of soil moisture (Reichle et al., 2002; Reichle et al., 2008). Data assimilation of soil moisture has been tested with soil moisture measurements collected during field campaigns and with synthetic/real satellite retrievals (Houser et al., 2001; Margulis et al., 2002; Reichle et al., 2002; Walker et al., 2002; Crow and Wood 2003; Dunne and Entekhabi 2005; Zhou et al., 2006; Blasone et al., 2008; Huang et al., 2008; Pipunic et al., 2011; Han et al., 2013; De Lannoy and Reichle 2016). Constraining LSMs using data assimilation techniques has been demonstrated to be an effective way to estimate soil moisture dynamics (Ni-Meister 2008; Reichle et al., 2009).

Commonly used data assimilation algorithms in hydrology include Ensemble Kalman Filter (EnKF) (Evensen, 1994), Particle Filter (PF) (Gordon et al., 1993) and their variants, which are Monte Carlo implementations of the Bayesian update problem. The use of the Monte Carlo approach allows to explicitly deal with different sources of modelling error and can also be used in combination with complex non-linear system models. EnKF is more CPU-efficient than PF, but it only shows an optimal performance if the model states and parameters which are updated are Gaussian-distributed. EnKF, PF and their variants are broadly used in hydrology data assimilation and their ability in decreasing the model prediction uncertainty has been demonstrated (Reichle et al., 2002; Zhou et al., 2006; Houser et al., 2012). In these studies the observations used to update model states were soil moisture (Huang et al., 2008; Pipunic et al., 2011; Han et al., 2012; Flores et al., 2012; Yan et al., 2015), discharge (Andreadis et al., 2007; Neal et al., 2009; Pauwels and De Lannoy 2009), runoff (Lorenz et al., 2015) and streamflow (Hirpa, 2013). But most of the works evaluate the ability of EnKF, PF or their variants individually, and the performance of the algorithms is only compared in few studies (Dechant and Moradkhani, 2012; Dumedah and Coulibaly, 2013; Chen et al., 2015).

Moreover, joint estimation of parameters and state variables via EnKF, PF or variants of these algorithms could enhance significantly the predictive capabilities of LSMs. The power and usefulness of such joint state and parameter estimation methods have been investigated by different authors in the hydrologic literature. Most of these publications use synthetic (or twin) experiments with assimilation of artificially generated observations in LSMs, like the Community Land Model (Su et al., 2011; Plaza et al., 2012; Han et al., 2014a; Hoppe et al., 2014), NOAA-Noah LSM (Shi et al., 2014) and Soil and Water Assessment Tool model (Liu et al., 2017).

These synthetic experiments conclude that the joint estimation of parameters and state variables via data assimilation enhances significantly the predictive capabilities of LSMs. Despite this growing body of applications, relatively few studies have focused on real-world joint state-parameter estimation via assimilation in LSMs, like the Community Land Model

(Tian et al., 2008; Lo et al., 2010; Post et al., 2017), the VIC-model (Bi et al., 2014; Peng et al., 2014) and the Flux-PIHM model (Shi et al., 2015b).

Considering the interaction between root zone soil moisture and groundwater in integrated models, assimilation of groundwater level data has a great potential to improve estimation of root zone soil moisture. Moreover, groundwater level is available in many places and at regional and national scales as it can be continuously measured by automatic sensing devices at low cost and high accuracy, like the Collaborative National Groundwater Monitoring Network Program for the United States (Subcommittee on Ground Water, 2011). By assimilating the groundwater level measurements in the integrated models, land surface hydrologic processes can be better simulated as root zone soil moisture will be better reproduced which also affects evapotranspiration. Recently, a few studies were presented where groundwater levels were assimilated in integrated hydrological models (Shi et al., 2014; Rasmussen et al., 2015; Zhang et al., 2016), but this subject is still in its infancy as a research topic.

The objectives of this PhD work are to:

(1) Assimilate soil moisture including state and parameter estimation in two LSMs using the EnKF and the PF. Joint state and parameter estimation is evaluated with real data, which was not done before. EnKF and PF are compared in terms of their ability to jointly estimate states and parameters. Moreover, in our work we use two LSMs to juxtapose the soil moisture simulations and predictions for the comparisons of EnKF and PF.

(2) Develop a methodology to effectively assimilate groundwater levels to improve predictions of root zone soil moisture with the integrated terrestrial systems model TerrSysMP.

(3) Investigate under which conditions assimilation of groundwater levels can improve root zone soil moisture characterization.

Chapter 2 gives a short overview of the integrated model TerrSysMP which was used in our work. Furthermore, this chapter introduces the basic data assimilation schemes of EnKF and PF. In chapter 3 the usefulness and applicability of four different data assimilation methods (variants of EnKF and PF) for joint state and parameter estimation in two LSMs are evaluated. As argued before, people used EnKF or PF but only in few studies the algorithms were compared. Moreover, the methods are compared for a real-world case. The comparison of these data assimilation algorithms for a real-world case including parameter estimation was not documented before. Real world data from the Rollesbroich site in western Germany are used for this comparison. Two LSMs with different parameterizations are also compared and provide contrastive soil moisture simulations for the comparison of data assimilation methods. In chapter 4 the fully-coupled subsurface-land surface model TerrSysMP is used. Root zone soil moisture is closely linked with groundwater, especially when groundwater level is shallow. Therefore assimilation of groundwater levels in the integrated model TerrSysMP has the potential to improve root zone soil moisture characterization. We develop five data assimilation methodologies for assimilating groundwater level data via the EnKF to improve

root zone soil moisture estimation with TerrSysMP. These methodologies are evaluated in synthetic experiments which are performed for different climate conditions, soil types and plant functional types to simulate various root zone soil moisture distributions and groundwater levels. In chapter 5 we use the assimilation methodology which gave the best results in the study presented in chapter 4 to assimilate groundwater levels and surface soil moisture data. As the correlation between groundwater level and root zone soil moisture is expected to depend on the climate conditions, soil textures and vegetation types, it is important to systematically investigate the impact of these factors on the root zone soil moisture characterization with groundwater level data assimilation, which is done in this chapter. 100 synthetic cases which cover 5 climate conditions, 5 plant functional types (PFTs) and 4 soil textures are tested to investigate how climate conditions, PFTs and soil textures affect the assimilation performance in terms of improving root zone soil moisture characterization. Finally, chapter 6 provides a summary of the main results and an outlook for future research.

Chapter 2 : Theory

2.1 Integrated terrestrial systems model TerrSysMP

The integrated terrestrial systems model TerrSysMP (Shrestha et al., 2014) simulates the interaction between the lower atmospheric boundary layer, water and energy cycles at the land surface and subsurface (e.g., overland flow, evapotranspiration and water and energy transport in the unsaturated zone) and subsurface groundwater flow. It features three existing well-established models: an atmospheric model (Consortium for Small-Scale Modeling; COSMO) (Baldauf et al., 2011), a land surface model (the NCAR Community Land Model, version 3.5; CLM) (Oleson et al., 2008), and a three-dimensional variably saturated groundwater flow model (ParFlow) (Ashby and Falgout, 1996; Jones and Woodward, 2001; Kollet and Maxwell, 2006). An external coupler (Ocean Atmosphere Sea Ice Soil, version 3.0; OASIS3) (Valcke, 2013) is used to couple these three models, drive TerrSysMP and control the exchange of fluxes between each component model.

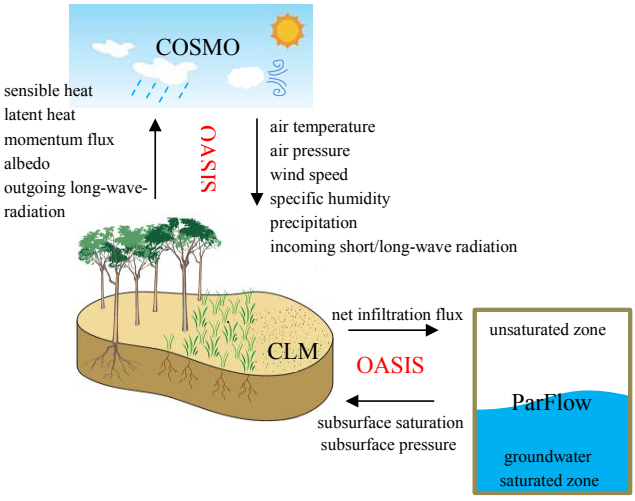

Figure 2.1 Coupling of the TerrSysMP component models COSMO (atmosphere), CLM (land surface) and ParFlow (subsurface) by the coupler OASIS.

Figure 2.1 schematically shows the data exchange among the three component models via the OASIS coupler in TerrSysMP. CLM calculates land surface-atmosphere exchange fluxes, momentum flux, albedo and outgoing long-wave radiation to COSMO. In turn, COSMO provides meteorological forcing data to CLM, including air temperature, air pressure, wind speed, specific humidity, precipitation and incoming short/long-wave radiation. CLM has ten soil layers and provides the net infiltration flux to the upper ten soil layers of ParFlow, which is calculated from precipitation, interception and total evapotranspiration. ParFlow sends back the calculated subsurface saturation and pressure values for the upper ten layers to CLM.

In ParFlow the number of soil layers and soil thicknesses are defined by users and generally it has more than 10 soil layers.

The coupling of the three models improves the physical representation especially at the interfaces of the different terrestrial compartments. For instance, the simplified soil hydrology (1-D only) and surface water routing (uncoupled) schemes in CLM are replaced by ParFlow by a fully integrated 3-D variably saturated surface–subsurface flow model. In COSMO the simplified land surface scheme TERRA is replaced with the more sophisticated land surface scheme of CLM, with an improved representation of vegetation processes. Regarding the parallel performance, TerrSysMP has already shown to be highly scalable on the massively parallel supercomputing environment JUQUEEN (Jülich BlueGene/Q) (Gasper et al., 2014). TerrSysMP is a highly modular model which can be run with fully coupled configuration (COSMO + CLM + ParFlow), partly coupled configuration (COSMO + CLM / CLM + ParFlow) or run for each of the models individually (COSMO / CLM / ParFlow). In our work, the partly coupled configuration with CLM and ParFlow is applied. In the following sections a short overview over the model ParFlow and model CLM is given.

2.1.1 ParFlow

The parallel three-dimensional variably saturated subsurface flow code ParFlow is the result of a long, multi-institutional development history. It was firstly developed by Ashby and Falgout (1996) to simulate groundwater flow with heterogeneous parameter distributions, Jones and Woodward (2001) proposed a Newton-Krylov method to solve Richards' equation, Kollet and Maxwell (2006) incorporated a new two-dimensional overland flow simulator into it and made the parallelism more efficient, and Maxwell (2013) implemented a terrain-following grid transform with variable vertical discretisation to solve groundwater problems with high topographic gradients. It is now a collaborative effort among Colorado School of Mines, University of Bonn, Juelich Research Center, Lawrence Livermore National Laboratory and other universities and institutes. As an open-source, object-oriented and parallel watershed flow model, it includes fully-integrated overland flow and is able to simulate complex topography, geology and heterogeneity. It is available for multi-platforms and runs with a common I/O structure from laptop to supercomputer with excellent parallel efficiency which enables high-resolution large-scale hydrologic simulations (Maxwell et al., 2015).

As one of the main features of ParFlow, the overland flow simulator allows simulation of surface flow based on the shallow water equation (Kollet and Maxwell, 2006). In two spatial dimensions, the continuity equation is given by:

$$\frac{\partial \psi_{\mathrm{s}}}{\partial t} = \nabla(\vec{v}\psi_{\mathrm{s}}) + q_{\mathrm{r}}(x) + q_{\mathrm{e}}(x) \tag{2.1}$$

where ψ_{s} [L] is the surface ponding depth, t [T] the time, $q_{\mathrm{r}}(x)$ [L/T] the general source/sink (e.g. rainfall) rate, $q_{\mathrm{e}}(x)$ [L/T] the exchange rate with the subsurface and $\vec{v}$ [L/T] is vertically averaged surface flow velocity. Equation (2.1) is solved with the Newton-Krylov method and

integrated into the Richards equation as a free surface overland flow boundary condition. More details can be found in the study from Kollet and Maxwell (2006).

Another main feature is the terrain-following grid formulation which transforms the ParFlow grid to conform to topography. Darcy's law includes a topographic slope component:

$$q = -k_{\mathrm{s}}(x)k_{\mathrm{r}}(h)(\nabla(h+z)\cos\theta_x + \sin\theta_y) \tag{2.2}$$

where q [L/T] is the flux, h [L] the pressure head, z [L] the elevation, $k_{\mathrm{s}}(x)$ [L/T] the saturated hydraulic conductivity, k_{r} [-] the relative permeability and θ_x [-] is the local angle of topographic slope S_x [-] in the x direction and $\theta_x = \tan^{-1}S_x$ and θ_y [-] in the y direction as $\theta_y = \tan^{-1}S_y$. More details can be found in the study by Maxwell (2013). The terrain following grid formulation makes groundwater follow the topography which is useful for coupled surface and subsurface flow problems.

ParFlow can calculate a water balance on the basis of solving the Richards' equation, overland flow equation and interaction with CLM, which is given by:

$$\frac{\Delta(V_{\mathrm{subsurface}}+V_{\mathrm{surface}})}{\Delta t} = Q_{\mathrm{overlandflow}} + Q_{\mathrm{evapotranspiration}} + Q_{\mathrm{sourcesink}} \tag{2.3}$$

where $V_{\mathrm{subsurface}}$ [L^3] is the subsurface storage, V_{surface} [L^3] the surface storage, $Q_{\mathrm{overlandflow}}$ [L^3/T] is overland flux, $Q_{\mathrm{evapotranspiration}}$ [L^3/T] the evapotranspiration flux passed from CLM, and $Q_{\mathrm{sourcesink}}$ [L^3/T] any other source/sink fluxes specified in the simulation (e.g. rainfall). $V_{\mathrm{subsurface}}$ and V_{surface} are calculated by:

$$V_{\mathrm{subsurface}} = \sum_{i=1}^{\Omega}[S(h_i)\Delta x\Delta y\Delta z(S_{s,i}h_i + \phi_i)] \tag{2.4}$$

$$V_{\mathrm{surface}} = \begin{cases}\sum_{\Gamma}[h_1\Delta x\Delta y], & h_1 > 0\\ 0, & h_1 \le 0\end{cases} \tag{2.5}$$

where h_1 is the pressure head for the top surface layer. The $V_{\mathrm{subsurface}}$ is calculated over all active grid cells i in the domain Ω [L^3]. V_{surface} is calculated over the upper surface boundary cells in the domain Γ [L^2]. Δx [L], Δy [L] and Δz [L] are the cell resolution in x, y and z directions respectively. $S(h_i)$ [-] is water saturation, $S_{\mathrm{s},i}$ [L^{-1}] the specific storage coefficient, and ϕ_i [-] the porosity of the medium for grid cell i.

2.1.2 Community Land Model (CLM), version 3.5

CLM (version 3.5) is developed by the American National Center for Atmospheric Research to calculate the mass and energy balance at the land surface including soil water infiltration, surface runoff, snow, interception and evapotranspiration (Oleson et al., 2004; Oleson et al., 2008). It was initially developed by Dai et al. (1997), and later further developed by the American National Center for Atmospheric Research including the areas of carbon cycling, vegetation dynamics, and river routing (Oleson and Bonan, 2000). Following this release, Peter Thornton implemented changes to the model structure required to represent carbon and nitrogen cycling in the model which is known as CLM version 2.1 (Vertenstein et al., 2003).

CLM version 3.0 contains further software technical improvements related to the performance and model output. Later CLM version 3.5 features improved biogeophysical parameterizations (Oleson et al., 2008). It also improved the characterization of the land surface by subdividing each CLM3.0 soil cell into 8 sub-cells, improving the accuracy of the estimation of latent and sensible heat fluxes between the land surface and atmosphere.

CLM includes 15 possible plant functional types (PFTs) plus bare soil. Vegetated surfaces are comprised of up to 4 of the 15 PFTs. These PFTs have different physiological and morphological traits along the climatic preferences (Bonan et al., 2002). The composition and abundance of PFTs within a grid cell are time-invariant and prescribed from 1-km satellite data (Bonan et al., 2002). In the 15 PFTs, there are 7 primary PFTs: needleleaf evergreen or deciduous tree, broadleaf evergreen or deciduous tree, shrub, grass, and crop. These 7 primary PFTs are expanded to 15 physiological variants based on climate rules to distinguish arctic, boreal, temperature and tropical PFTs (i.e., different leaf and stem optical properties, different root distributions, and different aerodynamic parameters). CLM has 10 soil layers with internally fixed soil layer depths. Water and energy balances are calculated over the PFTs and the 10 soil layers.

As in TerrSysMP CLM's major contribution is calculating the evapotranspiration from ground and vegetation, here an overview of the parameterization of the evapotranspiration calculation in CLM is given. Precipitation is partitioned into canopy interception, through fall to the soil/snow surface and canopy drip. CLM calculates evaporation and transpiration based on the non-vegetated and vegetated surfaces. For the non-vegetated surface (bare soil), the evaporation E_g [M/L^2/T] from ground is calculated as:

$$E_g = -\frac{\rho_{atm}(q_{atm} - q_g)}{\gamma_{aw}} \tag{2.6}$$

where ρ_{atm} [M/L^3] is air density, q_{atm} [M/M] is the atmospheric specific humidity, q_g [M/M] is the specific humidity of the soil surface and γ_{aw} [T/L] is the aerodynamic resistance to water vapor transfer. q_g is proportional to the saturation specific humidity:

$$q_g = \alpha q_{sat}^{T_g} \tag{2.7}$$

with $q_{sat}^{T_g}$ [M/M] is the saturated specific humidity given the ground surface temperature T_g [Q]. The factor α [-] is a combined value of soil and snow:

$$\alpha = \alpha_{soi,1}(1 - f_{sno}) + f_{sno} \tag{2.8}$$

where f_{sno} [-] is the fraction of snow coverage, $\alpha_{soi,1}$ [-] refers to the surface soil layer and is a function of the surface soil layer water matrix potential ψ_1[L]:

$$\alpha_{soi,1} = \exp\left(\frac{\psi_1 g}{1\times10^3 R_{wv} T_g}\right) \tag{2.9}$$

where R_{wv} [L^2/T^2/Q] is the gas constant for water vapor, g [L/T^2] is the gravitational acceleration, ψ_1 [L] is calculated as:

$$\psi_1 = \psi_{\mathrm{sat},1} s_1^{-B_1} \quad and \quad \psi_1 \geq -1 \times 10^8 \tag{2.10}$$

where $\psi_{\mathrm{sat},1}$ [L] is saturated matric potential for the surface soil layer, B_1 [-] is the Clapp and Hornberger parameter (Clapp and Hornberger, 1978), and s_1[-] is the wetness of the top soil layer with respect to saturation:

$$s_1 = \frac{1}{\Delta z_1 \theta_{\mathrm{sat},1}} \left[\frac{w_{\mathrm{liq},1}}{\rho_{\mathrm{liq}}} + \frac{w_{\mathrm{ice},1}}{\rho_{\mathrm{ice}}} \right] \quad \text{and} \quad 0.01 \leq s_1 \leq 1.0 \tag{2.11}$$

where Δz_1 [L] is the thickness of the top soil layer, $\theta_{\mathrm{sat},1}$ [L^3/L^3] is saturated soil moisture of the top soil layer (i.e., porosity), $w_{\mathrm{liq},1}$ [M/L^2] and $w_{\mathrm{ice},1}$ [M/L^2] are the mass of liquid water and ice of the top soil layer, ρ_{liq} [M/L^3] and ρ_{ice} [M/L^3] are the density of liquid water and ice.

For the vegetated surface, the evapotranspiration flux E [$M/L^2/T$] includes the water vapor flux from vegetation E_{v} and the ground E_{g}:

$$E = E_{\mathrm{v}} + E_{\mathrm{g}} \tag{2.12}$$

$$E_v = -\frac{\rho_{atm}(q_s - q_{sat}^{T_v})}{r_{total}} \tag{2.13}$$

$$E_{\mathrm{g}} = -\frac{\rho_{\mathrm{atm}}(q_{\mathrm{s}} - q_{\mathrm{g}})}{r'_{\mathrm{aw}}} \tag{2.14}$$

where $q_{\mathrm{sat}}^{T_{\mathrm{v}}}$ [M/M] is the saturated specific humidity given the vegetation temperature T_{v} [Q], r'_{aw} [T/L] is the aerodynamic resistance to water vapor transfer between the ground and the canopy air, r_{total} [T/L] is the aerodynamic resistance to water vapor transfer from the canopy to the canopy air. q_{s} [M/M] is the canopy specific humidity:

$$q_{\mathrm{s}} = \frac{c_{\mathrm{a}}^{\mathrm{w}} q_{\mathrm{atm}} + c_{\mathrm{g}}^{\mathrm{w}} q_{\mathrm{g}} + c_{\mathrm{v}}^{\mathrm{w}} q_{\mathrm{sat}}^{T_{\mathrm{v}}}}{c_{\mathrm{a}}^{\mathrm{w}} + c_{\mathrm{g}}^{\mathrm{w}} + c_{\mathrm{v}}^{\mathrm{w}}} \tag{2.15}$$

where $c_{\mathrm{a}}^{\mathrm{w}}$ [L/T], $c_{\mathrm{g}}^{\mathrm{w}}$ [L/T] and $c_{\mathrm{v}}^{\mathrm{w}}$ [L/T] are water vapor conductances from the canopy air to the atmosphere, the leaf to canopy air, and ground to canopy air, respectively.

2.2 Data assimilation

The concept of data assimilation is proposed by Charney et al. (1969) to combine current and past data in an explicit dynamic model which provides time continuity and dynamic coupling amongst the fields. Daley (1991) established data assimilation techniques in weather forecasting. Bennett (1992) successfully used data assimilation in oceanography to improve ocean dynamic prediction. Based on the knowledge derived from the meteorological and oceanographic data assimilation, hydrologists applied data assimilation in hydrology (Houser et al., 1998). Hydrologic data assimilation has been accelerated by the development in hydrologic models and observations, like new satellite sensors which provide suitable large scale observations (Walker et al., 2003a). In essence, hydrologic data assimilation uses both

the hydrological process knowledge from a hydrologic model and information from observations to improve the model predictions with an accuracy level that cannot be obtained when models and observations are used separately.

2.2.1 Posterior inference using Bayes Law

In data assimilation the statistic estimation problem can be approached using Bayes' theorem and conditional probabilities (Lorenc, 1986). Here for illustration, let x denote the model state of interest and $\tilde{y}$ observation data. Assuming that an observation is available at time t, the posterior distribution is presented by $p(\mathbf{x}_t|\tilde{\mathbf{Y}}_{1:t})$, which is the probability of $\tilde{y}$ at time t given all previous and current observation $\tilde{y}$. According to Bayes Law, $p(\mathbf{x}_t|\tilde{\mathbf{Y}}_{1:t})$ can be derived as:

$$p(\mathbf{x}_t|\tilde{\mathbf{Y}}_{1:t}) = p(\mathbf{x}_t|\tilde{\mathbf{y}}_t, \tilde{\mathbf{Y}}_{1:t-1}) = \frac{p(\tilde{\mathbf{y}}_t|\mathbf{x}_t)p(\mathbf{x}_t|\tilde{\mathbf{Y}}_{1:t-1})}{p(\tilde{\mathbf{y}}_t|\tilde{\mathbf{Y}}_{1:t-1})} \tag{2.16}$$

where $p(\mathbf{x}_t|\tilde{\mathbf{Y}}_{1:t-1})$ is the prior distribution of x, $p(\tilde{\mathbf{y}}_t|\mathbf{x}_t)$ is the likelihood of measurements $\tilde{y}$ given x, and $p(\tilde{\mathbf{y}}_t|\tilde{\mathbf{Y}}_{1:t-1})$ is a normalization constant which ensures that the posterior state distribution integrates to unity. $p(\tilde{\mathbf{y}}_t|\tilde{\mathbf{Y}}_{1:t-1})$ can be expanded using the x as intermediate variable:

$$p(\tilde{\mathbf{y}}_t|\tilde{\mathbf{Y}}_{1:t-1}) = \int p(\tilde{\mathbf{y}}_t|\mathbf{x}_t)p(\mathbf{x}_t|\tilde{\mathbf{Y}}_{1:t-1})d\mathbf{x}_t \tag{2.17}$$

By substituting equation (2.17) into (2.16), Bayes Law can compute the posterior distribution sequentially in time:

$$p(\mathbf{x}_t|\tilde{\mathbf{Y}}_{1:t}) = \frac{p(\tilde{\mathbf{y}}_t|\mathbf{x}_t)p(\mathbf{x}_t|\tilde{\mathbf{Y}}_{1:t-1})}{\int p(\tilde{\mathbf{y}}_t|\mathbf{x}_t)p(\mathbf{x}_t|\tilde{\mathbf{Y}}_{1:t-1})d\mathbf{x}_t} \tag{2.18}$$

If the model is assumed to be a first-order Markov process, the prior distribution $p(\mathbf{x}_t|\tilde{\mathbf{Y}}_{1:t-1})$ can be applied in a recursive form through the estimation of the prior distribution via the Chapman-Kolmogorov equation:

$$p(\mathbf{x}_t|\tilde{\mathbf{Y}}_{1:t-1}) = \int p(\mathbf{x}_t|\mathbf{x}_{t-1})p(\mathbf{x}_{t-1}|\tilde{\mathbf{Y}}_{1:t-1})d\mathbf{x}_{t-1} \tag{2.19}$$

2.2.2 Ensemble Kalman Filter (EnKF)

The EnKF was proposed by Evensen (1994) as generalization of the Kalman filter to nonlinear system models with many state variables. This method uses a Monte Carlo approach to generate an ensemble of different model trajectories from which the time evolution of the probability density of the model states, and related error covariances are estimated.

We represent the state-space implementation of the dynamic system model with the following steps (Burgers et al., 1998):

$$\mathbf{x}_t^{i-} = \mathcal{M}(\mathbf{x}_{t-1}^i, \tilde{\mathbf{b}}_{t-1}^i, \mathbf{I}) + \mathbf{w}_t \tag{2.20}$$

where $\mathbf{x}_t^{i-}$ is the $k \times 1$ vector of predicted values of the state variables of the ith ensemble member, $i = \{1,\ldots,N\}$, $\tilde{\mathbf{b}}_{t-1}^i$ signifies the corresponding vector (or matrix) of measured values of the forcing variables, **I** is the matrix of model parameters or variables, $\mathbf{w}_t$ denotes a $k \times 1$ process noise vector that accounts for structural imperfections of the LSM, and t denotes time.

In EnKF, the posterior distribution $p(\mathbf{x}_t|\tilde{\mathbf{Y}}_{1:t})$ in equation (2.18) is estimated as (a Bayesian update on $\mathbf{x}_t$):

$$p(\mathbf{x}_t|\tilde{\mathbf{Y}}_{1:t}) \propto p(\tilde{\mathbf{y}}_t|\mathbf{x}_t)p(\mathbf{x}_t|\tilde{\mathbf{Y}}_{1:t-1}) \tag{2.21}$$

which is found by applying the following equation on each ensemble member *i*:

$$\mathbf{x}_t^i = \mathbf{x}_t^{i-} + \mathbf{K}(\hat{\mathbf{y}}_t^i - \mathbf{H}\mathbf{x}_t^{i-}) \tag{2.22}$$

where $\mathbf{x}_t^i$ denotes the $k \times 1$ vector with updated estimates of the state variables (also called analysis state), $\hat{\mathbf{y}}_t^i$ is the $m \times 1$ vector of measured data at time t, **K** is a $k \times m$ matrix called the Kalman gain, and the $m \times k$ matrix **H** signifies the measurement operator which maps the model output to the measurement space. It is linear for EnKF.

$\hat{\mathbf{y}}_t^i$ is assumed to be Gaussian, and can be written for each individual ensemble member as follows:

$$\hat{\mathbf{y}}_t^i = \tilde{\mathbf{y}}_t + \mathbf{v}_t^i \tag{2.23}$$

where $\mathbf{v}_t^i$ signifies a $m \times 1$ vector of measurement errors drawn randomly from a m-variate normal distribution $\mathcal{N}_m(0, \mathbf{R})$ with zero-mean and $m \times m$ observation error covariance matrix **R**. In our work we assume the measurement errors to have a fixed and common varianceσ^2, and to be uncorrelated in space and time. Thus we can write $\mathbf{R} = \sigma^2\mathbf{I}_m$, where $\mathbf{I}_m$ signifies the $m \times m$ identity matrix with zeros everywhere except on the main diagonal which stores values of σ^2.

The Kalman gain **K** is computed as follows:

$$\mathbf{K} = \mathbf{C}\mathbf{H}^T(\mathbf{H}\mathbf{C}\mathbf{H}^T + \mathbf{R})^{-1} \tag{2.24}$$

where the symbol T denotes transpose, **C** is the $k \times k$ model error covariance matrix. EnKF assume that $\mathbf{x}_t$ has Gaussian probability distribution, from the ensemble of N state vectors, we can calculate **C**, using:

$$\mathbf{C} = \frac{1}{N-1}\sum_{i=1}^{N}(\mathbf{x}_t^{i-} - \bar{\mathbf{x}}_t)(\mathbf{x}_t^{i-} - \bar{\mathbf{x}}_t) \tag{2.25}$$

where $\bar{\mathbf{x}}_t$ denotes the $k \times 1$ vector with ensemble mean values of the states at time *t*.

The updated values of the states $\mathbf{x}_t^i$ from equation (2.22) now enter equation (2.20) and are used to predict the soil moisture values at the next observation time, $t = t + 1$, and so forth.

In some cases it might be appropriate to estimate the model parameters along with the state variables. This requires a slight modification to the state-space formulation of equation (2.24) as the d-vector of parameter values, $\boldsymbol{\alpha}$, must now vary among the N ensemble members to facilitate parameter estimation from the measured data. Three different approaches have been published in the literature for joint estimation of model states and parameters in the EnKF. This includes, state augmentation, dual and outer estimation. The first two approaches assume the LSM parameters to be time-variant, and infer their values sequentially along with the model states. The third approach assumes the parameters to be time-invariant, and estimates their posterior distribution in a loop outside the EnKF by maximizing the marginal likelihood of the N state trajectories (Vrugt et al., 2005, 2013). In our study we will consider herein only the first two approaches, that is, state augmentation and dual estimation, as these two methods are most CPU-efficient.

In state augmentation, the $k \times 1$ vector of state variables, $\mathbf{x}_t$, the model error covariance matrix $\mathbf{C}$, the measurement operator $\mathbf{H}$, and the Kalman gain $\mathbf{K}$ consist of two separate blocks (Franssen and Kinzelbach, 2008):

$$\mathbf{x}^{*i} = \begin{bmatrix} \mathbf{x}^i \\ \boldsymbol{\alpha}^i \end{bmatrix} \tag{2.26}$$

$$\mathbf{C}^* = \begin{bmatrix} \mathbf{C_{xx}} & \mathbf{C}_{\boldsymbol{\alpha x}}^T \\ \mathbf{C}_{\boldsymbol{\alpha x}} & \mathbf{C}_{\boldsymbol{\alpha\alpha}} \end{bmatrix} \tag{2.27}$$

$$\mathbf{H}^* = [\mathbf{H_x}, 0] \tag{2.28}$$

where the subscripts $\mathbf{x}$ and $\boldsymbol{\alpha}$ refer to the model states and parameters respectively. The state vector, $\mathbf{x}^*$, now consists of $k + d$ elements, the model error covariance matrix $\mathbf{C}^*$ is made up of four smaller matrices, $\mathbf{C_{xx}}$, $\mathbf{C}_{\boldsymbol{\alpha x}}^T$, $\mathbf{C}_{\boldsymbol{\alpha x}}$, and $\mathbf{C}_{\boldsymbol{\alpha\alpha}}$, and the measurement operator $\mathbf{H}^*$ includes $\mathbf{H_x}$ and additional values of zero. The Kalman gain matrix $\mathbf{K}$ is now given by:

$$\begin{aligned} \mathbf{K} = \mathbf{C}^*\mathbf{H}^{*T}(\mathbf{H}^*\mathbf{C}^*\mathbf{H}^{*T} + \mathbf{R})^{-1} &= \begin{bmatrix} \mathbf{C_{xx}} & \mathbf{C}_{\boldsymbol{\alpha x}}^T \\ \mathbf{C}_{\boldsymbol{\alpha x}} & \mathbf{C}_{\boldsymbol{\alpha\alpha}} \end{bmatrix} \begin{bmatrix} \mathbf{H_x}^T \\ 0 \end{bmatrix} \left([\mathbf{H_x}, 0] \begin{bmatrix} \mathbf{C_{xx}} & \mathbf{C}_{\boldsymbol{\alpha x}}^T \\ \mathbf{C}_{\boldsymbol{\alpha x}} & \mathbf{C}_{\boldsymbol{\alpha\alpha}} \end{bmatrix} \begin{bmatrix} \mathbf{H_x}^T \\ 0 \end{bmatrix} + \mathbf{R} \right)^{-1} \\ &= \begin{bmatrix} \mathbf{C_{xx}}\mathbf{H_x}^T(\mathbf{H_x}\mathbf{C_{xx}}\mathbf{H_x}^T + \mathbf{R})^{-1} \\ \mathbf{C}_{\boldsymbol{\alpha x}}\mathbf{H_x}^T(\mathbf{H_x}\mathbf{C_{xx}}\mathbf{H_x}^T + \mathbf{R})^{-1} \end{bmatrix} \\ &= \begin{bmatrix} \mathbf{K_x} \\ \mathbf{K}_{\boldsymbol{\alpha}} \end{bmatrix} \end{aligned} \tag{2.29}$$

This results in the following equation for the updated states and parameter values:

$$\begin{bmatrix} \mathbf{x}_t^i \\ \boldsymbol{\alpha}_t^i \end{bmatrix} = \begin{bmatrix} \mathbf{x}_t^{i-} \\ \boldsymbol{\alpha}_t^{i-} \end{bmatrix} + \begin{bmatrix} \mathbf{K_x}(\hat{\mathbf{y}}_t^i - \mathbf{H_x}\mathbf{x}_t^{i-}) \\ \mathbf{K}_{\boldsymbol{\alpha}}(\hat{\mathbf{y}}_t^i - \mathbf{H_x}\mathbf{x}_t^{i-}) \end{bmatrix}. \tag{2.30}$$

In the dual estimation approach, the state variables and model parameters are stored in two separate vectors and updated using their own individual steps (Moradkhani et al., 2005a). The parameter values of each ensemble member are first updated according to:

$$\boldsymbol{\alpha}_t^i = \boldsymbol{\alpha}_t^{i-} + \mathbf{K}_{\boldsymbol{\alpha}}(\hat{\mathbf{y}}_t^i - \mathbf{H}_{\mathbf{x}}\mathbf{x}_t^{i-}) \tag{2.31}$$

Then, the updated parameter values are used with equation (2.20) to predict, for the second time, the state variables at time t, after which their values are updated via equation (2.24). This approach necessitates running the LSM twice for the time period between two successive measurements, thereby doubling the required CPU-time of each ensemble member for this dual estimation method compared to the state augmentation approach.

2.2.3 Particle Filter (PF)

The PF was first suggested in the research area of object recognition, robotics and target tracking (Gordon et al., 1993) and was introduced to hydrology by Moradkhani et al. (2005a). The PF differs from the EnKF in that it describes the evolving probability density function (PDF) of the LSM state variables by a set of N random samples, also called particles. Each particle carries a non-zero weight which determines its underlying probability, and these weights are updated as soon as a new datum (observation) becomes available. Before we proceed with a brief theoretical description of the PF we must first explicate our notation. We denote with symbol $\mathbf{X}_{1:t}$ the collection of simulated values of the LSM state variables between the first observation at $t = 1$ and the present datum, t, hence $\mathbf{X}_{1:t} = [\mathbf{x}_1, \dots, \mathbf{x}_t]$ is a $k \times t$ matrix with the LSM states at each measurement time stored as a column vector. The corresponding observations are stored in the $m \times t$ matrix, $\widetilde{\mathbf{Y}}_{1:t} = [\tilde{\mathbf{y}}_1, \dots, \tilde{\mathbf{y}}_t]$. Finally, we use braces, $\{\cdot\}$, to denote our Monte Carlo ensemble of N particle trajectories, $\{\mathbf{X}_{1:t}^{1:N}\}$, and thus $\{\mathbf{x}_t^{1:N}\}$ is a $k \times N$ matrix with sampled values of the LSM state variables at time t. The subsequent description of the PF follows closely the description of Vrugt et al. (2013). Interested readers are referred to this publication for further details.

If we assume the parameters to be known, then we can write the evolving posterior distribution, $p_{\boldsymbol{\alpha}}(\mathbf{X}_{1:t}|\widetilde{\mathbf{Y}}_{1:t})$, for the state-space formulation of equation (2.20) as follows:

$$p_{\boldsymbol{\alpha}}\left(\mathbf{X}_{1:t}\middle|\widetilde{\mathbf{Y}}_{1:t}\right) = \overbrace{p_{\boldsymbol{\alpha}}\left(\mathbf{X}_{1:t-1}\middle|\widetilde{\mathbf{Y}}_{1:t-1}\right)}^{\text{prior}} \frac{\overbrace{\mathcal{M}_{\boldsymbol{\alpha}}(\mathbf{x}_t|\mathbf{x}_{t-1})}^{\text{model}} \overbrace{L_{\boldsymbol{\alpha}}(\tilde{\mathbf{y}}_t|\mathbf{x}_t)}^{\text{likelihood function}}}{\underbrace{p_{\boldsymbol{\alpha}}(\tilde{\mathbf{y}}_t|\widetilde{\mathbf{Y}}_{1:t-1})}_{\text{normalization constant}}}, \tag{2.32}$$

where $p_{\boldsymbol{\alpha}}\left(\mathbf{X}_{1:t-1}\middle|\widetilde{\mathbf{Y}}_{1:t-1}\right)$ denotes the prior state distribution, $\mathcal{M}_{\boldsymbol{\alpha}}(\mathbf{x}_t|\mathbf{x}_{t-1})$ signifies the transition probability density of the state variables (= equation (2.20)), $L_{\boldsymbol{\alpha}}(\tilde{\mathbf{y}}_t|\mathbf{x}_t)$ is the likelihood function, and $p_{\boldsymbol{\alpha}}(\tilde{\mathbf{y}}_t|\widetilde{\mathbf{Y}}_{1:t-1})$ represents the normalization constant. Equation (2.32) follows directly from Bayes' law (see Appendix A of Vrugt et al. (2013)), and does not use at once the data up to time t to estimate $p_{\boldsymbol{\alpha}}\left(\mathbf{X}_{1:t}\middle|\widetilde{\mathbf{Y}}_{1:t}\right)$ but rather estimates the evolving system state recursively over time using some mathematical model and new incoming measurements. If we integrate out the state trajectory $\mathbf{X}_{1:t-1}$ from equation (2.32) then we can derive an

expression for the marginal PDF of the state variables $p_{\boldsymbol{\alpha}}(\mathbf{x}_t|\tilde{\mathbf{Y}}_{1:t})$ at time t (= equation (2.16) in the state-space):

$$p_{\boldsymbol{\alpha}}(\mathbf{x}_t|\tilde{\mathbf{Y}}_{1:t}) = \frac{L_{\boldsymbol{\alpha}}(\tilde{\mathbf{y}}_t|\mathbf{x}_t)p_{\boldsymbol{\alpha}}(\mathbf{x}_t|\tilde{\mathbf{Y}}_{1:t-1})}{p_{\boldsymbol{\alpha}}(\tilde{\mathbf{y}}_t|\tilde{\mathbf{Y}}_{1:t-1})}, \tag{2.33}$$

which is also referred to as the **update step** of the optimal filter (conditional independence of measurements). The state **prediction step** is equivalent to the Chapman-Kolmogorov equation (= equation (2.19) in the state-space):

$$p_{\boldsymbol{\alpha}}(\mathbf{x}_t|\tilde{\mathbf{Y}}_{1:t-1}) = \int_{\boldsymbol{\Omega}} \mathcal{M}_{\boldsymbol{\alpha}}(\mathbf{x}_t|\mathbf{x}_{t-1})\, p_{\boldsymbol{\alpha}}(\mathbf{x}_{t-1}|\tilde{\mathbf{Y}}_{1:t-1})\mathrm{d}\mathbf{x}_{t-1}, \tag{2.34}$$

where $\boldsymbol{\Omega}$ signifies the feasible state space.

We conveniently assume herein, a Gaussian likelihood function:

$$L_{\boldsymbol{\alpha}}(\tilde{\mathbf{y}}_t|\mathbf{x}_t) = \frac{1}{(2\pi)^{m/2}|\mathbf{R}|^{1/2}} \exp\left(-\frac{1}{2}(\tilde{\mathbf{y}}_t - \mathbf{H}_{\mathbf{x}}\mathbf{x}_t)^T\mathbf{R}^{-1}(\tilde{\mathbf{y}}_t - \mathbf{H}_{\mathbf{x}}\mathbf{x}_t)\right), \tag{2.35}$$

where $\mathbf{R}$ is the $m \times m$ measurement error covariance matrix, $|\cdot|$ signifies the determinant operator, and m denotes the length of the observation vector, $\tilde{\mathbf{y}}_t$, at time t.

The PF makes use of the following identity of equation (2.32) to approximate the evolving state PDF:

$$p_{\boldsymbol{\alpha}}(\mathbf{X}_{1:t}|\tilde{\mathbf{Y}}_{1:t}) \propto p_{\boldsymbol{\alpha}}(\mathbf{X}_{1:t-1}|\tilde{\mathbf{Y}}_{1:t-1})\mathcal{M}_{\boldsymbol{\alpha}}(\mathbf{x}_t|\mathbf{x}_{t-1})L_{\boldsymbol{\alpha}}(\tilde{\mathbf{y}}_t|\mathbf{x}_t). \tag{2.36}$$

This recursion implies that we can reuse the particles (samples) at $t-1$ that define the prior distribution, $p_{\boldsymbol{\alpha}}(\mathbf{X}_{1:t-1}|\tilde{\mathbf{Y}}_{1:t-1})$, to approximate the posterior state PDF, $p_{\boldsymbol{\alpha}}(\mathbf{X}_{1:t}|\tilde{\mathbf{Y}}_{1:t})$, at the next observation time. Yet, such recycling poses a problem, that is, we cannot sample directly from $p_{\boldsymbol{\alpha}}(\mathbf{X}_{1:t}|\tilde{\mathbf{Y}}_{1:t})$ as we do not know its multivariate distribution. We therefore resort to an easy-to-sample-from importance density, $q_{\boldsymbol{\alpha}}(\cdot\,|\mathbf{x}_{t-1}, \tilde{\mathbf{y}}_t)$, and draw $\{\mathbf{x}_t^{1:N}\}$ taking into consideration the current observation, $\tilde{\mathbf{y}}_t$, and previous state samples, $\{\mathbf{x}_{t-1}^{1:N}\}$. We then calculate the unnormalized importance weight of the ith particle, W_t^i, as follows

$$W_t^i \propto \bar{W}_{t-1}^i w_t(\{\mathbf{X}_{1:t}^i\}), \tag{2.37}$$

where $w_t(\mathbf{X}_{1:t}^i)$ signifies the incremental importance weight:

$$w_t(\{\mathbf{X}_{1:t}^i\}) = \frac{\mathcal{M}_{\boldsymbol{\alpha}}(\{\mathbf{x}_t^i\}|\{\mathbf{x}_{t-1}^i\})L_{\boldsymbol{\alpha}}(\tilde{\mathbf{y}}_t|\{\mathbf{x}_t^i\})}{q_{\boldsymbol{\alpha}}(\{\mathbf{x}_t^i\}|\{\mathbf{x}_{t-1}^i\}, \tilde{\mathbf{y}}_t)}, \tag{2.38}$$

and $\bar{W}_t^i = W_t^i / \sum_{i=1}^N W_t^i$ denote the normalized importance weights, which vary between 0 and 1.

Before we can implement the PF in practice, we need to specify the importance density, $q_{\boldsymbol{\alpha}}(\cdot\,|\{\mathbf{x}_{t-1}^{1:N}\}, \tilde{\mathbf{y}}_t)$, for $t = \{2, \ldots, n\}$. We follow Gordon et al. (1993) and set $q_{\boldsymbol{\alpha}}(\mathbf{x}_t|\mathbf{x}_{t-1}, \tilde{\mathbf{y}}_t) = \mathcal{M}_{\boldsymbol{\alpha}}(\mathbf{x}_t|\mathbf{x}_{t-1})$ which results in the following equation for the incremental particle weights:

$$w_t\left(\{\mathbf{X}_{1:t}^i\}\right) = \frac{\mathcal{M}_{\boldsymbol{\alpha}}(\{\mathbf{x}_t^i\}|\{\mathbf{x}_{t-1}^i\})L_{\boldsymbol{\alpha}}(\tilde{\mathbf{y}}_t|\{\mathbf{x}_t^i\})}{\mathcal{M}_{\boldsymbol{\alpha}}(\{\mathbf{x}_t^i\}|\{\mathbf{x}_{t-1}^i\})} = L_{\boldsymbol{\alpha}}\left(\tilde{\mathbf{y}}_t\middle|\{\mathbf{x}_t^i\}\right). \tag{2.39}$$

This chapter is adopted from Zhang et al. (2017).

2.2.4 TerrSysMP-PDAF

TerrSysMP-PDAF is developed by Kurtz et al. (2016) which couples TerrSysMP and a Parallel Data Assimilation Framework (PDAF) (Nerger and Hiller, 2013). PDAF is a parallelized data assimilation system and provides interface with numerical models to do efficient data assimilation. It parallelizes both the forward ensemble simulations and the analysis step to provide a fully parallelized framework. TerrSysMP-PDAF can do data assimilation for the land surface-subsurface part of TerrSysMP (CLM and ParFlow). To improve the computational efficiency, an online coupling approach is used in coupling TerrSysMP and PDAF, where data exchange is via main memory so that frequent re-initialisations and I/O operations are avoided, which affords the application of the system to very large problem sizes. More technical implementations can be referred to (Kurtz et al., 2016). The current version 1.0 of TerrSysMP-PDAF has only EnKF as data assimilation algorithm activated. In the coupled (ParFlow + CLM) and uncoupled (ParFlow stand alone) TerrSysMP configuration, measurements of pressure or soil moisture can be assimilated in ParFlow. TerrSysMP-PDAF also allows for joint state-parameter update to estimate spatially distributed saturated hydraulic conductivity or the Manning's roughness parameter.

Kurtz et al. (2016) investigated the scaling properties of TerrSysMP-PDAF with a simple synthetic data assimilation exercise. They assimilated soil moisture in a virtual catchment for CLM + ParFlow of TerrSysMP. Their experiments showed that the TerrSysMP-PDAF system runs efficiently and scales well even for a large number of processors, which proved that this system is promising for large scale applications of high resolution models which are extremely computationally demanding. Baatz et al. (2017) applied a catchment tomography approach in synthetic experiments to assimilate frequent stream water level measurements and update spatially distributed Manning's roughness coefficients with TerrSysMP-PDAF. The subsurface part ParFlow was used to simulate 2D overland flow which was forced by high resolution radar precipitation data. Their results showed that TerrSysMP-PDAF worked successfully with the joint state-parameter estimation. Given the effectiveness and reliability of TerrSysMP-PDAF we also used it in this work to conduct assimilation experiments.

Chapter 3 : State and parameter estimation of two land surface models using the Ensemble Kalman Filter and the Particle Filter

*adapted from: Zhang, H., Hendricks Franssen, H.-J., Han, X., Vrugt, J. A., and Vereecken, H.: State and parameter estimation of two land surface models using the ensemble Kalman filter and the particle filter, Hydrology and Earth System Sciences, 21, 4927-4958, https://doi.org/10.5194/hess-21-4927-2017, 2017.

3.1 Introduction and scope

Land surface models (LSMs) are used widely to simulate and predict the exchanges of momentum, energy, and mass between the terrestrial biosphere and overlying atmosphere at local, regional, and global scales. These models also play a key role in assessing impacts of environmental changes (climate, land-use, and land-cover) on energy, water, and biogeochemical fluxes (e.g. CO2, CH4, N2O) at the soil-atmosphere interface, and simplify analysis of cause-effect relationships among the myriad of processes that govern land-atmosphere interactions and feedbacks, and emulate spatiotemporal variations in climate through greenhouse gas exchanges, carbon-nitrogen feedbacks, soil moisture-precipitation, and soil moisture-temperature coupling. LSMs use relatively simple mathematical equations to conceptualize and aggregate the complex, spatially distributed, and interrelated (bio)physical, chemical, and ecological processes that govern the exchange of mass, energy, and momentum between the land-surface and the atmosphere. This approach simplifies considerably the topology of the land-surface system, and reduces to much lower dimensions its state and parameter space. The consequence of this process aggregation and simplification is, however that the LSM parameters often do not represent directly measurable entities, and instead must be estimated via calibration by fitting the model against measured data records of soil moisture, soil temperature, and/or CO2, water vapour, and/or energy fluxes across a range of biomes and timescales. These measurements are of crucial importance to quantify properly LSM parameter and predictive uncertainty, and to identify poorly represented or missing processes (Williams et al., 2009; Bonan, 2008).

Many of the parameters of a LSM are model dependent and therefore difficult to transfer between different land-surface schemes. Nevertheless, all LSMs use soil hydraulic, vegetation, and thermal parameters to describe heat transport, water flow, and root water uptake (canopy transpiration) in the variably saturated soil domain, and share a reflection coefficient (aka surface albedo) to calculate the reflected shortwave radiation. Two main approaches exist to determine the hydraulic and thermal properties of the considered soil domain. Some LSMs such as the Community Land Model (CLM) use basic soil data (soil texture and organic matter fraction) to estimate hydraulic and thermal parameters via pedotransfer functions (Oleson et al., 2013; Han et al., 2014a; Vereecken et al., 2016). Other land-surface schemes such as the Variable Infiltration Capacity Model (VIC) (Liang et al., 1994; Gao et al., 2010) expect users to specify values for the hydraulic and thermal parameters. Pedotransfer functions are particularly useful in large-scale application of CLM as they simplify tremendously soil hydraulic characterization. Nevertheless, soil hydraulic

parameter values derived from pedotransfer functions are subject to considerable uncertainty, and might therefore not accurately describe soil water movement and storage, particularly at larger spatial scales. What is more, (measurement) errors of the atmospheric forcing (e.g. wind speed, temperature, radiation, vapour pressure deficit, and precipitation) and errors in the auxiliary model input (e.g. topographic properties, vegetation characteristics) further enhance LSM prediction uncertainty.

In the past decades, many different search and optimization methods have been developed for automatic calibration of dynamic system models. Of these, Bayesian methods have found widespread application and use in Earth systems modelling due to their innate ability to treat, at least in principle, model input (forcing), output (forecast), parameter and structural errors. The Bayesian approach relaxes the assumption of a single optimum parameter value in favour of a posterior parameter and forecast distribution which summarizes the coordinated impact of different uncertainties on the modelling results. Yet, general-purpose methods such as DREAM (Vrugt et al., 2008, 2009; Vrugt, 2016) require a relatively large number of LSM evaluations to estimate parameter and forecast uncertainty. This can pose significant computational challenges for CPU-intensive and parameter-rich LSMs, and complicates treatment of input data uncertainty via latent variables (e.g. Vrugt et al., 2008).

Data assimilation offers an attractive alternative as general framework to account for LSM parameter, input, output, and other sources of uncertainty to take advantage of all available ground-based, airborne or spaceborne observations to improve the compliance between numerical models and corresponding data. This approach enables joint estimation of model state variables and parameters and simplifies treatment of forcing data errors (Liu and Gupta, 2007). Many different studies published in the hydrologic literature have demonstrated the benefits of parameter estimation in the context of data assimilation for soil moisture characterization (e.g., Montzka et al., 2011; Lee, et al., 2014), rainfall-runoff (e.g., Moradkhani et al., 2005a; Vrugt et al., 2005) and land surface modelling (e.g., Pauwels et al., 2009).

Data assimilation methods merge uncertain observations with predictions (output) of imperfect models to optimally estimate the state of a dynamical system. The prototype of this method, the Kalman filter (KF) was developed in the 1960s by Rudy Kalman for optimal control of linear dynamical systems (Kalman, 1960). The KF is a maximum likelihood estimator of the dynamic state of the system if the model error and measurement error distributions are (multivariate) normal. For nonlinear dynamical models this Gaussian assumption is not generally valid, and the KF will not give a maximum likelihood state estimate. The ensemble Kalman Filter, or EnKF, is a stochastic generalization of the KF to nonlinear system models, in which the evolution of the model error covariance matrix is derived from a finite set of state realizations (Evensen, 1994). The use of this Monte Carlo ensemble not only makes possible state estimation for complex system models but also enables the explicit treatment of different sources of modelling error. Two decades on from its inception, the EnKF has received operational status in real-time weather, tsunami, and flood prediction systems (amongst others) due its proven ability to enhance a model's forecast skill and characterize accurately prediction uncertainty.

State estimation via the EnKF advances significantly the capabilities of hydrologic and land-surface models to predict spatiotemporal dynamics of water movement and storage in soils, lakes, and reservoirs, and fluxes of mass, energy, and momentum between the soil and the atmosphere. The predictive skill of these models is, however determined in large part by their parameterization. This has led hydrologists and hydrometeorologists to develop data assimilation approaches that permit the simultaneous inference of model state variables and parameter values. The power and usefulness of such joint state and parameter estimation methods have been investigated by many different authors in the water resources literature. Most of these publications use synthetic (or twin) experiments with assimilation of artificially generated data. Examples include studies with simulated measurements of the groundwater table depth or hydraulic head (Franssen and Kinzelbach, 2008; Bailey and Bau, 2012; Kurtz et al., 2014; Shi et al., 2014; Song et al., 2014; Tang et al., 2015), discharge/streamflow (Bailey and Bau, 2012; Moradkhani et al., 2012; Vrugt et al., 2013; Rasmussen et al., 2015), groundwater temperature (Kurtz et al., 2014), soil moisture (Wu and Margulis, 2011; Plaza et al., 2012; Erdal et al., 2014; Shi et al., 2014; Song et al., 2014; Pasetto et al., 2015), brightness temperature from passive remote sensing (Montzka et al., 2013; Han et al., 2014a), and contaminant concentration (Gharamti et al., 2013). These studies use a variety of different methods for joint parameter and state estimation, among which the EnKF (Franssen and Kinzelbach, 2008; Wu et al., 2011; Gharamti et al., 2013; Erdal et al., 2014; Kurtz et al., 2014; Shi et al., 2014; Pasetto et al., 2015), the iterative EnKF (Song et al., 2014), the extended KF (Pauwels et al., 2009), the local ensemble transform KF (Han et al., 2014a), the ensemble transform KF (Rasmussen et al., 2015), and the normal score EnKF (Tang et al., 2015).

The overarching conclusion from the body of synthetic experiments is that the joint estimation of parameters and state variables via data assimilation enhances significantly the predictive capabilities of hydrologic and land-surface models. This finding is corroborated by results for real-world assimilation studies documented in a rapidly growing list of publications and involving model structural inadequacies, measurement errors of the atmospheric forcing variables and calibration (assimilation) data, inadequate characterization of the lower boundary condition (aquifer), and uncertainty of other, auxiliary, model inputs. This includes assimilation of measurements of the electrical conductivity (Wu and Margulis, 2013), hydraulic head in wells (Kurtz et al., 2014; Shi et al., 2015b), groundwater temperature (Kurtz et al., 2014), streamflow and discharge (Moradkhani et al., 2012; Shi et al., 2015b), active remote sensing (Pauwels et al., 2009), passive brightness temperature (Qin et al., 2009), soil moisture from lysimeters (Lue et al., 2011; Wu and Margulis, 2013; Erdal et al., 2014; Shi et al., 2015a), land surface temperature (Bateni and Entekhabi, 2012) and sensible and latent heat fluxes (Shi et al., 2015b) using methods such as the PF (Qin et al., 2009), PMCMC (Moradkhani et al., 2012), EnKF (Bateni and Entekhabi, 2012; Wu and Margulis, 2013; Erdal et al., 2014; Kurtz et al., 2014; Shi et al., 2015b) and the extended KF (Pauwels et al., 2009; Lue et al., 2011). Despite this growing body of applications, relatively few studies (e.g. Lue et al., 2011; Shi et al., 2015b) have focused on an accurate characterization of soil moisture dynamics simulated by LSMs. This is particularly surprising, as root zone moisture storage modulates spatiotemporal variations in climate and weather,

and governs the production and health status of crops, and the organization of natural ecosystems and biodiversity (Vereecken et al., 2008).

In this study, we evaluate the usefulness and applicability of four different data assimilation methods for joint parameter and state estimation of VIC and CLM using a 5-month calibration (assimilation) period of soil moisture measurements at 5, 20 and 50 cm depth in the Rollesbroich experimental test site in the Eifel mountain range in western Germany. This grassland site is part of the TERENO network of observatories and extensively monitored since 2011 to catalogue long-term ecological, social and economic impact of global change at regional level. We used the EnKF with state augmentation (Chen and Zhang, 2006) or dual estimation (Moradkhani et al., 2005a), respectively, and the residual resampling PF (Douc et al., 2005) with a simple, statistically deficient (Moradkhani et al., 2005b), or more sophisticated, MCMC-based (Vrugt et al., 2013) parameter resampling method. The "calibrated" LSM models were tested using SPADE water content measurements from a 5-month evaluation period. To the best of our knowledge, this is only the second study after Chen et al. (2015) that compares sequential data assimilation methods for joint parameter and state estimation of a LSM. Related work by Dechant and Moradkhani (2012) and Dumedah and Coulibaly (2013) consider application to the rainfall-runoff transformation of a watershed.

The three main objectives of our study may be summarized as follows, (1) to evaluate the usefulness and applicability of joint parameter and state estimation for soil moisture characterization with LSMs, (2) to compare the performance of four commonly used parameter and state estimation methods in their ability to predict soil moisture dynamics at different depths in the Rollesbroich experimental test site, and (3) to compare, contrast and juxtapose the soil moisture simulations and predictions of CLM and VIC.

The remainder of this study is organized as follows. Section 3.2 discusses briefly VIC and CLM which are used as our LSMs to characterize soil moisture dynamics of the Rollesbroich experimental site in Germany. In this section, we contrast the numerical approaches, boundary conditions, and spatial discretization (soil layers), that are used by VIC and CLM to describe water flow and storage in the modelled soil domain, and are particularly concerned with selection of their calibration parameters. Section 3.3 then reviews the basic concepts and theory of the four different data assimilation algorithms used herein. This is followed in section 3.4 with a detailed discussion of the Rollesbroich experimental site, and the numerical implementation and setup of each data assimilation method. Section 3.5 introduces the results of the different parameter and state estimation methods and two LSMs, and section 3.6 discusses the main findings of our numerical experiments and assimilation studies. Finally, this study concludes in section 3.7 with a summary of our main findings.

3.2 Land surface models and calibration parameters

LSMs simulate terrestrial biosphere fluxes of matter and energy via numerical solution of the water, energy, and carbon balance of the land-surface. This includes hydrologic processes such as soil evaporation, infiltration, surface runoff, canopy interception and transpiration, aquifer discharge, groundwater recharge, and precipitation (Schaake et al., 1996) and energy

fluxes such as latent and sensible heat from soil, snow, surface water and vegetated surfaces (Bertoldi, 2004). Their respective equations contain parameters whose values depend on global or regional distributions of vegetation and soil properties (Milly and Shmakin, 2002).

The Rollesbroich site investigated herein covers an area of about 270,000 m2 with grassland vegetation that is dominated by perennial ryegrass (Loliumperenne) and smooth meadow grass (Poapratensis). The limited size of our site and its rather uniform vegetation and topography, justify treatment of our land surface domain as a single grid cell in LSM with apparent parameters that characterize the mass and energy exchange between the soil and atmosphere. This assumption of homogeneity is computationally convenient and also simplifies somewhat our subsequent mathematical notation. We conveniently write the LSM as a (nonlinear) regression function, $\mathcal{M}(\cdot)$, which returns a $m \times n$ matrix $\mathbf{Y}$ with the simulated (predicted) values of m different variables (e.g. soil moisture content, latent and sensible heat fluxes) at discrete times, $t \in \{1, \dots, n\}$, as follows

$$\mathbf{Y} \leftarrow \mathcal{M}(\boldsymbol{\alpha}, \tilde{\mathbf{x}}_0, \widetilde{\mathbf{B}}, \widetilde{\mathbf{U}}), \tag{3.1}$$

where $\boldsymbol{\alpha} = \{\alpha_1, \dots, \alpha_d\}$ is the d-vector of model parameters, $\tilde{\mathbf{x}}_0$ signifies the $k \times 1$-vector with measured (inferred) values of the state variables of the land surface model for the domain at the start of simulation, $\widetilde{\mathbf{B}}$ denotes the $l \times n$ control matrix with temporal measurements of l forcing variables (e.g. air temperature, precipitation, vapour pressure deficit, wind speed, short and long-wave radiation), $\widetilde{\mathbf{U}}$ represents a matrix with auxiliary constants, variables, or properties (e.g. plant functional type, land cover, soil texture, and other variables/constants) deemed necessary to simulate the water and energy balance of the land-surface domain of interest, and $\mathbf{Y} = [\mathbf{y}_{1:n}^1, \dots, \mathbf{y}_{1:n}^m]^T$, where T denotes transpose. Without loss of generality, we restrict the model parameters to a closed space, $\mathbf{A}$, equivalent to some d-dimensional hypercube, $\boldsymbol{\alpha} \in \mathbf{A} \in \mathbb{R}^d$, called the feasible parameter space.

The assumption of homogeneity simplifies considerably the model definition in equation (3.1). Yet, this lumped topology might not characterize adequately real-world soil-land-surface systems that exhibit considerable spatial variations in soils, vegetation, and land properties. Such systems might necessitate distributed application of equation (3.1) via spatial discretization of the considered land-surface domain into different grid cells. This discretization should honour spatial variations in vegetation and soil properties, and could account for small-scale (within-grid-cell) variability. Nevertheless, in our present application of LSM we the treat the Rollesbroich site as a single grid cell with grassland vegetation and homogeneous, but layered, soil (details to follow).

We now discuss briefly two different land surface schemes, VIC and CLM which are used to describe temporal variations in soil water storage at different depths in the Rollesbroich experimental site in Germany.

3.2.1 The Variable Infiltration Capacity Model (VIC)

The VIC model is a macro-scale semi-distributed hydrological model which solves for the water and energy balance of each grid cell using explicit consideration of within-grid-cell

vegetation variations. Accordingly, each grid cell is divided into land cover tiles (Liang et al., 1994; Liang et al., 1996; Cherkauer and Lettenmaier, 1999), and assumes constant values of the soil properties (e.g., soil texture, hydraulic conductivity, thermal conductivity). The total evapotranspiration, sensible heat flux, effective land surface temperature and runoff are then obtained for each grid cell by summing over all the land cover tiles (vegetation types and bare soil) weighted by their respective fractional coverage (Gao et al., 2010). The VIC model can either be executed in a water balance mode or a water-and-energy balance mode. In this study, we assume the latter and use a 70 cm deep soil composed of a 10 cm surface layer followed by a middle and bottom layer of 20 and 40 cm, respectively. The relatively thin surface layer is used to capture rapid fluctuations in soil moisture due to rainfall and bare soil evaporation, and the deepest and thickest layer summarizes seasonal water content dynamics and base flow. We use herein, VIC, and force the model with atmospheric boundary conditions (e.g. precipitation, wind speed, air temperature, longwave and shortwave radiation, and relative humidity) for the Rollesbroich experimental site in Germany. In the absence of detailed information about the hydraulic properties of the considered soil domain, we treat each layer's saturated hydraulic conductivity, $\log_{10}k_s$ [$\log_{10}$(m/s)] and exponent of Brooks-Corey's drainage equation, β [-], as calibration parameters. What is more, we also include the infiltration shape parameter, b [-], and the maximum baseflow velocity, D_{m} [mm/day] as calibration parameters. Thus, this involves estimation of $d = 8$ parameters in VIC for the Rollesbroich site. Appendix 3.A summarizes the soil module of VIC, including a brief description of the main processes and model parameters.

3.2.2 The Community Land Model (CLM)

CLM is the land model for the Community Earth System Model (Oleson et al., 2013), and is made up of multiple different building blocks, or modules, which resolve processes related to land biogeophysics, the hydrological cycle, biogeochemistry, and dynamic vegetation composition, structure, and phenology. The model recognizes explicitly surface heterogeneity by dividing each individual grid cell into multiple subgrid levels. For example, a grid cell can be made up of different land cover types, each with their own respective patches of plant functional types (PFTs) and associated stem area index and canopy height. The first subgrid level is defined by land units (vegetated, lake, urban, glacier, and crop), each composed of a number of different columns (second subgrid level) for which separate energy and water calculations are made. Vegetated land units, as well as lakes and glaciers, use one column. Urban land uses five separate columns, and for crop land there is a distinction between irrigated and unirrigated columns with one single crop occupying each column. The third subgrid level is composed of PFTs and includes bare soil. The vegetated column has 16 possible PFTs besides bare soil. For the crop column, several crop types are available. Processes such as canopy evaporation and transpiration are calculated for each individual PFT, whereas soil and snow processes are calculated at the column level using areal-weighted values of the properties of the PFTs of individual patches. Note, that a similar aggregation approach is used by VIC.

In our application of CLM to the Rollesbroich experimental site in Germany, we calculate soil temperature for 15 different soil layers, and simulate hydrological states and fluxes for the top 10 soil layers only. Appendix 3.B presents a brief description of the soil module of CLM, and discusses the main parameters used. The CLM is forced with atmospheric conditions (e.g. precipitation, vapour pressure deficit, wind speed, incoming short wave and long wave radiation) using values for the model parameters and initial states, and land surface data and other physical constants and/or variables as auxiliary input. The soil hydraulic (e.g. saturated hydraulic conductivity) and thermal parameters of CLM are derived from built-in pedotransfer functions (see equation (3.B1) - equation (3.B4) of Appendix 3.B) using as inputs the auxiliary matrix $\tilde{\mathbf{U}}$ with sand, clay and organic matter fractions of each individual soil layer. We treat these auxiliary soil variables as unknown parameters in the present application of CLM. Thus, this involves $d = 30$ parameters in CLM for the Rollesbroich site.

3.2.3 Main differences of VIC and CLM

Before we proceed, we first summarize the main differences of VIC and CLM in their calculations of the water and energy balance of the land-surface. In the first place, VIC treats the vadose zone as a multi-layer bucket with variable infiltration capacity, whereas CLM uses a more physics-based description of soil water movement, storage, and associated hydrological fluxes (e.g. root water uptake) by numerical solution of a modified form of Richards' equation (Zeng and Decker, 2009). A bucket model is computationally convenient, but sacrifices important detail regarding the vertical distribution of soil water storage. The latter is a prerequisite to characterize accurately processes such as infiltration, redistribution, root-water uptake, drainage, and groundwater recharge. We refer the interested reader to Romano et al. (2011) for a detailed comparison of bucket-type and Richards' based vadose zone flow models.

Second, VIC treats the saturated and variably-saturated soil domain as two separate, lumped, control volumes which are decoupled from the underlying groundwater reservoir. In other words, a fixed lower boundary condition is imposed. CLM, on the contrary, simulates interactions between the modelled soil domain and an unconfined aquifer. The resulting water table variations of the aquifer affect soil water movement in the unsaturated zone via a variable recharge flux. In our application of CLM, this recharge flux emanates at the bottom of the tenth soil layer. The calculation of this recharge flux may be best explained via the use of a virtual soil layer, say layer 11, whose depth extends from the bottom of layer 10 to the groundwater table. If we assume hydrostatic conditions in layer 11, then we can calculate the recharge flux from layer 10 using equation (3.B9) in Appendix 3.B. This recharge flux then changes the depth of the water table according to equation (3.B11). This equation also takes into consideration drainage from the water table due to topographic gradients. If the groundwater table is within the upper 10 soil layers, a drainage flux emanates from the upper most saturated layer according equation (3.B10).

Third, VIC expects the user to specify values for the soil hydraulic (e.g. saturated hydraulic conductivity), thermal, and baseflow parameters of the first, second, and third layer of each grid-cell, respectively, whereas CLM derives their counterparts (e.g. hydraulic conductivity at

saturation, matric head at saturation, Clapp-Hornberger exponent B, and soil thermal conductivity) for each of the fifteen soil layers using built-in pedotransfer functions.

Finally, VIC allows the user to determine freely the number and thickness of the soil layers in the bucket model (default is three layers), whereas CLM assumes a fixed thickness of each soil layer.

3.2.4 Selection of calibration parameters

LSMs contain a large number of parameters whose values can be adjusted by fitting model output to observed data. Yet, only a few of those parameters will affect noticeably model performance. Various authors have investigated the parameter sensitivity of VIC via Monte Carlo simulation, Generalized Likelihood Uncertainty Estimation (GLUE), or model calibration methods (Demaria et al., 2007; Xie et al., 2007; Troy et al., 2008). These studies demonstrated a strong dependency of parameter sensitivity on climatic conditions. Table 3.1 lists the VIC and CLM parameters that have been selected for calibration via data assimilation, and reports their units, feasible ranges, perturbation, and spatial configuration. To honour prior information (e.g. soil textural data) we do not draw the model parameters from their feasible ranges, but rather sample their initial values around some best-guess VIC and CLM parameterization using the normal and uniform distributions listed under the header "Perturbation". This makes up the prior parameter distribution and is further explained in section 3.4.2.

Appendix 3.A (VIC) and 3.B (CLM) summarize the main variables, processes, and equations which are used by both models to describe the storage and vertical and/or horizontal movement of water in the variably-saturated soil domain of the Rollesbroich site. These two appendices help to better understand the role of the different calibration parameters of table 3.1, and will be most beneficial to readers which are rather unfamiliar with both models. Note that CLM estimates the hydraulic and thermal parameters of each soil layer from built-in pedotransfer functions (Oleson et al., 2013; Han et al., 2014a) using as input the sand, clay, and organic matter fraction of each soil layer.

Table 3.1 Description of the soil parameters of VIC and CLM that are subject to inference with the different data assimilation methods using the 5-month soil moisture calibration data period of the Rollesbroich site. We list the symbol, unit, feasible range, perturbation, and domain of application of each parameter of VIC and CLM. The column with header "perturbation" lists the statistical distributions that are used to create the initial parameter ensemble for each data assimilation algorithm. The notation $\mathcal{N}(\mathbf{a}, \mathbf{b})$ signifies the univariate normal distribution with mean **a** and standard deviation **b**, whereas $\mathcal{U}(\mathbf{a}, \mathbf{b})$ denotes the univariate uniform distribution between **a** and **b**. These perturbation distributions are centred on the best-guess parameter values of VIC and CLM (see section 3.4.2) and define together the prior parameter distribution. This prior distribution honours textural measurements of each soil layer and its dispersion is in agreement with previously published studies.

Model	Parameter	Description	Units	Ranges	Perturbation	Configuration
VIC	$\log_{10}k_s$	Saturated hydrologic conductivity	$\log_{10}$(m/s)♦	[-7, -3]	$\mathcal{N}(0,1)$	Layer
	β	Exponent of Brooks-Corey drainage equation	-	[8, 30]	$\mathcal{U}(-5,5)$	Layer
	b	Infiltration shape parameter	-	[10^{-3}, 0.8]	$\mathcal{U}(-0.1,0.1)$	Profile
	D_m	Maximum baseflow velocity	mm/d	(0, 30]	$\mathcal{U}(-10,10)$	Profile
CLM	f_{cl}	Clay fraction	-	[0.01, 1]	$\mathcal{U}(-0.1,0.1)$	Layer
	f_{sd}	Sand fraction	-	[0.01, 1]	$\mathcal{U}(-0.1,0.1)$	Layer
	f_{om}	Organic matter fraction	-	[0, 1]	$\mathcal{U}(-0.12,0.12)$	Layer

†Note that the sand, clay, and organic matter fraction of each layer serve as input to pedotransfer functions in CLM which compute the hydraulic properties of each layer. See equation (3.B2) – (3.B5) of Appendix 3.B.

♦In the figures of this study we conveniently use labels with units of m/s for $\log_{10}k_s$.

3.3 Data assimilation methods

Data assimilation methods merge uncertain observations with predictions (output) of imperfect models to optimally estimate the state and/or parameters of a dynamical system. This includes the use of four-dimensional variational data assimilation (4D-Var), EnKF, PF, and related assimilation schemes. These methods have been applied successfully to a large number of different fields for model-data fusion in the atmospheric, oceanic, biogeochemical and hydrological sciences.

3.3.1 EnKF and PF

In chapter 2 the theory of EnKF and PF (state estimation/joint estimation of states and parameters) is described. Here the state augmentation method and dual estimation method of EnKF are referred to as EnKF-AUG and EnKF-DUAL, respectively. The EnKF suffers from filter inbreeding, that is, the ensemble spread degrades after several data assimilation steps. In extreme cases, the covariance matrix $\mathbf{C}$, of the state ensemble is so small that the measurements receive a negligible weight via equation (2.24) and do not affect much the

state trajectories of the individual ensemble members. This reflects a situation similar to model calibration in which state variable errors are ignored and all uncertainty in the input-output representation of the model is attributed to the parameters. Filter inbreeding is aggravated by the use of a relatively low number of ensemble members (small N) which results in spurious correlations among state variables and/or parameters, and underestimation of the spread of the ensemble. Other reasons for an insufficient ensemble spread are model structural errors, and the use of an underdispersed prior parameter distribution or too small variance of the measurement errors of the forcing variables. Ensemble inflation methods are an effective way to ameliorate filter inbreeding (Anderson, 2007; Whitaker and Hamill, 2012). We apply the inflation algorithm of Whitaker and Hamill (2012) to the d parameter values of each ensemble member as follows:

$$\alpha_{j,t}^{i} = \bar{\alpha}_{j,t} + \frac{V_j}{W_j}\left(\alpha_{j,t}^{i} - \bar{\alpha}_{j,t}\right), \tag{3.2}$$

where $\bar{\alpha}_{j,t}$ signifies the analysis mean (after update) of the jth parameter at time t, the scalars V_j and W_j denote the prior (before update) and analysis standard deviation of the j th parameter (derived from ensemble), and $j = \{1, \dots, d\}$. This method promotes a parameter spread that is in agreement with the width of the prior parameter distribution, and is particularly important to avoid a strong underestimation of ensemble variance and associated filter inbreeding in applications with relatively small ensemble sizes. As the spread is kept artificially constant, it cannot be assessed properly how data assimilation affects reduction of prediction uncertainty. In addition, it is important that the initial ensemble spread is adequate. This is a drawback of the applied inflation.

We now briefly discuss two different data assimilation methods of PF which are used herein with VIC and CLM to characterize spatiotemporal soil moisture dynamics at our experimental site. PF gives satisfactory results if the transition density or model operator, $\mathcal{M}_{\boldsymbol{\alpha}}(\mathbf{x}_t|\mathbf{x}_{t-1})$, adequately describes the observed system dynamics, and/or the observations, $\widetilde{\mathbf{Y}}_{1:t}$, are not too informative. Otherwise, the repeated application of equation (2.37) causes particle impoverishment in which the sampled particle trajectories drift away from the actual posterior state distribution, and receive a negligible importance weight. This ensemble degeneracy (e.g. Carpenter et al., 1999) deteriorates PF performance and results in a poor computational efficiency of the filter as much of the CPU-time is devoted to carrying forward particle trajectories whose contribution to $p_{\boldsymbol{\alpha}}\left(\mathbf{X}_{1:t}\middle|\widetilde{\mathbf{Y}}_{1:t}\right)$ for $t > 1$ is virtually zero.

To combat particle degeneracy we monitor the effective sample size (ESS) after assimilation of each new observation:

$$\text{ESS} = 1/\sum_{i=1}^{N}\left(\overline{W}_t^i\right)^2. \tag{3.3}$$

If the ESS is smaller than some default threshold, say $N/2$, then the particle ensemble is said to be degenerating. Several methods have been developed in the statistical literature to rejuvenate the particle ensemble. Gordon et al. (1993) introduced Sequential Importance Resampling (SIR), where N particles are drawn from the ensemble using selection

probabilities equal to their normalized importance weights. This step replaces samples with low importance weights with exact copies of the most promising particles, and produces a resampled set of N particles with equal weights of $1/N$. In our application of the PF we implement Residual Resampling (RR) developed by Liu and Chen (1998). This method has an important advantage over SIR in that it produces a resampled set of particles with more diverse weights (Weerts and Serafy, 2006). First, we compute a selection probability, $p_{\{\mathrm{x}_t^i\}}$, of each individual particle as follows:

$$p_{\{\mathbf{x}_t^i\}} = \frac{N\bar{W}_t^i - \lfloor N\bar{W}_t^i \rfloor}{N-M}, \tag{3.4}$$

where the $\lfloor\cdot\rfloor$ operator rounds down to the nearest integer, and $M = \sum_{j=1}^{N} \lfloor N\bar{W}_t^j \rfloor$. Then, the M particles with largest normalized importance weights are retained, and the remaining $N - M$ spots are filled by drawing from the M retained particles using their selection probabilities from equation (3.4). The resulting filter is referred to as RRPF.

In the present application of the RRPF, we not only estimate the LSM states but also jointly infer the values of the model parameters. We use state augmentation and add the model parameters to the vector of LSM state variables. Yet, this approach requires definition of an importance density for the parameters to avoid parameter impoverishment after several successive assimilation steps. This has been demonstrated numerically by Plaza et al. (2012) using a series of data assimilation experiments. In principle, we could corrupt the posterior parameter distribution using the ensemble inflation method of Whitaker and Hamill (2012) detailed in equation (3.2). This approach was used by Qin et al. (2009) to avoid degeneracy of the parameter values. Instead, we use the approach described by Plaza et al. (2012) and perturb the parameter values of the resampled particles using draws from a zero-mean d-variate Gaussian distribution with diagonal covariance matrix. This $d \times d$ matrix has zero entries everywhere (uncorrelated dimensions) except on the main diagonal which stores values of $s^2\mathrm{Var}\left[\{\alpha_{0,j}^{1:N}\}\right]$, where s is a scaling factor, $\mathrm{Var}\left[\{\alpha_{0,j}^{1:N}\}\right]$ signifies the prior variance of the jth parameter (at $\mathrm{t} = 0$), and $\mathrm{j} = \{1, \ldots, \mathrm{d}\}$. This is an adaptation of the method introduced by Moradkhani et al. (2005b) and uses the prior variance of the parameters rather than their variance at the previous measurement time, $t - 1$. Yet, in the absence of a formal guidelines on the choice of s, this perturbation approach suffers from a lack of adequate statistical underpinning (Vrugt et a., 2013; Yan et al., 2015). In our present application, we set $s = 0.1$, and evaluate the RRPF performance for VIC model using other values for this scaling factor as well.

The RR procedure produces a sample with more evenly distributed weights, but many of the particles are exact copies of one another. To enhance sample diversity, we therefore evaluate another resampling step using Markov chain Monte Carlo (MCMC) simulation. We follow herein the MCMC resampling method of Vrugt et al. (2013) and create candidate particles after RR using a discrete proposal distribution with state and parameter jumps equal to a multiple of the difference of two or more pairs of resampled particles. Each candidate particle is then re-evaluated between $t - 1$ and t by the LSM model, and the Metropolis acceptance

probability is used to determine whether to replace the "old" particle or not. This combined PF and MCMC methodology is also referred to as PMCMC. Interested readers are referred to Vrugt et al. (2013) for a detailed description of this method.

3.1.2 Important differences of EnKF and PF

Before we proceed with application of the EnKF-AUG, EnKF-DUAL, RRPF and PMCMC data assimilation methods, we reminisce about the key differences of the EnKF and PF. These differences are often overlooked and misunderstood but of crucial importance to help understand the two filters, and analyse and interpret our findings (see Vrugt et al., 2013). Most critically, the EnKF uses the measured values of the state variables (via measurement operator, if appropriate) to correct (update) the forecasted states of each ensemble member. The state PDF at each time is approximated by a weighted average of the distributions of the measured and forecast states. The PF on the other hand does not use a state analysis step, but rather assigns a likelihood to each particle. This likelihood is a dimensionless scalar which measures in a probabilistic sense the distance between the measured and forecasted state variables. The state PDF at each time is then constructed via the likelihoods (normalized importance weights) of the particles. Resampling is required to rejuvenate the ensemble, but this step is rather inefficient compared to the state analysis step of the EnKF as the measured states are only used indirectly in the PF via calculation of the likelihood. What is more, a single resampling step in RRPF or PMCMC does not guarantee a good approximation of the actual state PDF, as the particles' forecasted states may be systematically biased. Consequently, the PF may need a very large ensemble and/or many resampling steps to characterize properly the state PDF. On the contrary, the state analysis step of the EnKF resurrects rapidly a biased ensemble by migrating the members' forecasted states in closer vicinity of their measured values. This crucial difference between the EnKF and PF is the result of their dichotomous design, as is also evident from our mathematical notation. The EnKF estimates separately at each time the state PDF via equation (2.22), whereas the PF is designed to estimate the posterior distribution of the entire state trajectory via the recursion of equation (2.36). This latter task is much more difficult in practice, and requires use of the laws of probability to ensure that each particles' state trajectory constitutes a plausible realization from the transition density, $\mathcal{M}\left(\{\mathbf{x}_t^i\}\middle|\{\mathbf{x}_{t-1}^i\}\right)$, juxtaposed by the distribution of the model errors. This latter requirement of plausibility renders impossible the use of an analysis step in the PF (such as EnKF), as the resulting state updates may violate the statistics of the transition density and model error distribution and jeopardize the realism of each particle's state trajectory. Therefore, the PF requires a proper resampling method that takes into explicit account the statistical properties of the state transition density and model error distribution to replace bad particles and ensure an exact characterization of the evolving state PDF.

3.4 Case study

3.4.1 The Rollesbroich experimental site

We apply the four data assimilation approach to characterize soil moisture dynamics of the 27 ha Rollesbroich experimental test site (50°37'27"N, 6°18'17"E) in Germany. This site is located in the Eifel hills and ranges in elevation between 474 and 518 m with mean slope of 1.63°. The watershed constitutes a sub-basin of the TERENO Rur experimental catchment (Bogena et al., 2010; Qu et al., 2014) and consists of grassland with a soil texture that is predominantly silty loam. The mean annual air temperature and precipitation are 7.7 °C and 1033 mm, respectively. An eddy covariance tower (50°37'19"N, 6°18'15"E, elevation 514.7 m) and a soil moisture and soil temperature sensor network (with measurements at 5, 20 and 50 cm depth) have been installed (amongst others) at the Rollesbroich site. Water content data are measured at 41 different locations (see figure 3.1) using SPADE soil moisture probes (sceme.de GmbH i.G., Horn-Bad Meinberg, Germany) (Hübner et al., 2009) installed at 5 cm, 20 cm and 50 cm depth along a vertical profile. The SPADE probe is a ring oscillator and the frequency of the oscillator is a function of the dielectric permittivity of the surrounding medium, which depends strongly on local soil water content because of the high relative permittivity of water (≈ 80) as compared to mineral soil solids (≈ 2-9), and air (≈ 1). The SPADE probe was calibrated following the procedure outlined in (Qu et al., 2014). The soil moisture measurements are subject to several sources of error. This includes an inadequate contact of the sensors with the surrounding soil, and structural imperfections of the equations which relate the sensor response to the dielectric permittivity, and this permittivity to soil moisture.

The atmospheric LSM forcing data in this study were measured at the eddy covariance tower and include hourly measurements of air temperature, air pressure, relative humidity, wind speed, and incoming shortwave and longwave radiation. Precipitation was measured by a tipping bucket located in close proximity of the eddy covariance station. Soil texture was determined using 273 soil samples, taken from three different depths, ranging between 5 and 11 cm, 11 and 35 cm, and 35 to 65 cm. The sample locations coincided exactly with the location of the SoilNet sensors. The soil textural composition, organic carbon content, and bulk density were determined for each sample using standard laboratory experiments. These values were averaged to obtain mean values for the listed depths. Soil hydraulic parameters were then estimated for each of these three measurement depths from pedotransfer functions using as input data the basic soil measurements.

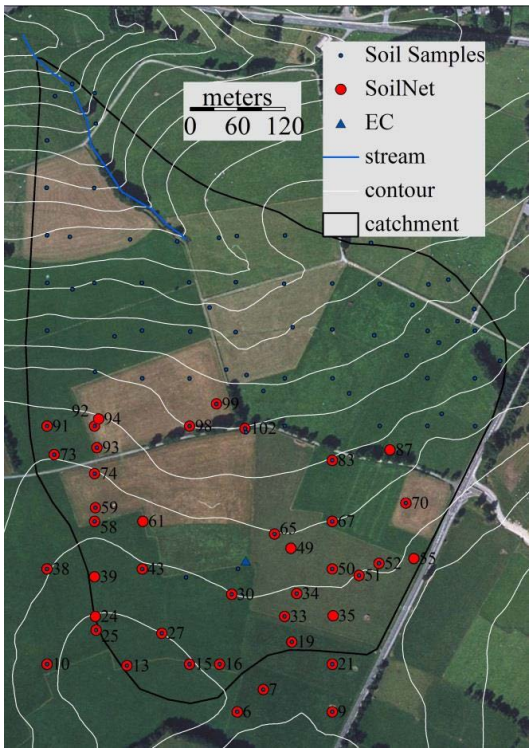

Figure 3.1 Aerial photograph of the 270,000 m2 Rollesbroich experimental test site near the city of Rollesbroich in the Eifel mountain range, western Germany (photo is taken from Qu et al., (2014)). The solid black line signifies the outer perimeter of our site and is determined in part by topographic gradients except for the Rollesbroich Straße which acts as border in the East-Southeast part of our domain. The small blue dots characterize locations within the watershed where soil samples were taken. The larger red dots are locations of the sensor network where soil moisture and temperature were recorded at depths of 5, 20, and 50 cm. The blue triangle symbolizes the eddy covariance tower.

In this work, we conveniently assume the soil-land-surface domain of the Rollesbroich site to be homogeneous and characterized by areal average values of soil moisture content at 5, 20 and 50 cm depth. In other words, we consider only vertical variations in soil water storage. Common LSM data assimilation experiments published in the literature usually involve application to much larger spatial scales, especially when remote sensing data are used. Hence, it is important to evaluate the LSM performance for a site where heterogeneities are neglected. Qu et al. (2014) investigated the geostatistical properties of the soils of the Rollesbroich test site. This work demonstrated a rather small spatial variability of the soil texture. This does not suggest, however that we can ignore spatial variations in the measured soil moisture values. Indeed, the standard deviations of soil moisture vary between 0.04 and 0.07 cm3/cm3 depending on the actual soil layer. This spatial heterogeneity of the soil moisture data documents variability in the soil hydraulic properties, and complicates the application and upscaling of LSMs.

3.4.2 Numerical experiments

A total of $N = 100$ ensemble members (particles) were used in all our data assimilation experiments. The period from January 1, 2011 to February 29, 2012 was used to spin-up VIC and CLM using measured hourly forcing data. The subsequent period between March 1, 2012 and July 31, 2012 served as our "calibration period" during which the daily soil moisture observations at the three measurement depths were used to update the LSM state variables and possibly also its parameter values. The following 5-months from August 1, 2012 to December 31, 2012 were used as an independent evaluation period. During this last period, we did not update the states and set the parameters to their "optimized" values derived from the calibration period. Soil moisture assimilation was initiated in March 2012 as the SPADE water content sensors were deemed unreliable (at least in February) in the preceding winter season due to soil freezing. We terminated our numerical experiments at the end of December 2012, as a large number of sensors seemed to be malfunctioning in subsequent readings which could impact too much the mean soil moisture values.

Soil moisture contents measured at 5 cm, 20 cm and 50 cm depth were assimilated jointly. The three (default) soil layers in VIC (0-10 cm, 10-30 cm, and 30-70 cm) were synchronized to match the three measurement depths. Soil parameters were defined separately for all individual layers, measured or not. In CLM, we used ten (default) soil layers with increasing thickness downwards (see table 3.2). The 5, 20 and 50 cm measurement depths correspond to the third, fifth and the sixth layer in CLM. Spatial relationships (covariance matrices) between the soil parameters of the measured layers and their values of the unmeasured layers were used in the EnKF to update the parameterization of layers 1, 2, 4, 7, 8, 9 and 10. A slightly different approach was followed in RRPF and PMCMC, in which the soil parameters of the unmeasured moisture layers in CLM were updated to their weighted-average values of the resampled particles using the vector of normalized importance weights.

The measurement errors of the soil moisture observations are assumed to be zero-mean Gaussian with standard deviation, $\sigma = 0.02$ m^3/m^3. This results in $\mathbf{R} = 4 \cdot 10^{-4}\mathbf{I_m}$ in equation (2.24) and equation (2.35), respectively. We admit that 0.02 m^3/m^3 is clearly larger than the uncertainty of the mean soil moisture content averaged over the 41 values. A larger observation error alleviates potential problems with filter inbreeding. Also, we account crudely for errors in LSM model formulation via parameter uncertainty and the use of a stochastic description of the precipitation record of the Rollesbroich site (discussed next). In other words, the $k \times 1$ process noise vector, $\mathbf{w}_t$, in equation (2.20) consists of zeros. However, we agree that it can be expected that we have other model structural errors, for example in relation to the representation of photosynthesis.

The hyetograph of each ensemble member is derived by multiplying the measured hourly precipitation rates of the tipping bucket with multipliers drawn from a unit-mean normal distribution with standard deviation of 0.10. This is equivalent to a heteroscedastic error of 10% of the observed precipitation (Hodgkinson et al., 2004). Forcing variables which govern evapotranspiration (incoming shortwave and longwave radiation, air temperature, relative humidity, and wind speed) were not corrupted.

Table 3.2 Nodal depth, $\boldsymbol{z}$, thickness, $\Delta\boldsymbol{z}$, and depth at layer interface, $\boldsymbol{zh}$, of the ten soil layers used by CLM.

Layer $\boldsymbol{i}$	$\boldsymbol{z}$ [m]	$\Delta\boldsymbol{z}$ [m]	$\boldsymbol{zh}$ [m]
1 (top)	0.0071	0.0175	0.0175
2	0.0279	0.0276	0.0451
3	0.0623	0.0455	0.0906
4	0.1189	0.0750	0.1655
5	0.2122	0.1236	0.2891
6	0.3661	0.2038	0.4929
7	0.6198	0.3360	0.8289
8	1.0380	0.5539	1.3828
9	1.7276	0.9133	2.2961
10	2.8646	1.5058	3.8019

The initial values of the VIC and CLM parameters are sampled at random using a simple two-step procedure. This approach honours soil textural data and is consistent with related results published in the literature. First, we draw N times from each marginal distribution listed in Table 1 under the column "perturbation". These distributions originate from Han et al. (2014) for CLM, and Demaria et al. (2007) and Troy et al. (2008) in case of VIC. This results in a $N \times d$ matrix of perturbations for VIC and CLM, respectively. We then create the initial $N \times d$ parameter ensemble of VIC and CLM by adding each perturbation matrix to a deterministic vector of "best-guess" parameter values for each model. This initial parameter ensemble is the same for all the assimilation methods. For CLM, this best-guess vector is simply equivalent to the areal-averaged sand, clay, and organic matter fraction of each of the ten soil layers, respectively. In case of VIC, we guess that $\beta = 15$ (all layers), $b = 0.2$, and $D_{\mathrm{m}} = 13$ (mm/d), and derive the value of $\log_{10}k_s$ ($\log_{10}$(m/s)) of all three soil layers from the measured mean areal sand fraction at each of those depths. The best-guess parameter values of VIC and CLM and their respective marginal distributions are jointly also referred to hereafter as prior parameter distribution. We want to compare EnKF and PF starting from the same prior distribution in order to make a more meaningful comparison. EnKF assumes a Gaussian distribution, but the PF not. We believe that assuming an initial uniform distribution is a neutral assumption good for comparing EnKF and PF.

One may debate our best-guess parameter values of VIC and CLM and their respective marginal distributions. Nevertheless, the prior parameter distribution used herein introduces more than sufficient dispersion in the best-guess parameter values to rapidly overcome a

possibly deficient initial model parameterization. Note, that the prior uncertainty of the two texture parameters (sand and clay fraction) in CLM is much larger than their spread derived from the texture measurements of each soil layer. This inflation of the prior distribution is done purposely to account indirectly for the epistemic uncertainty of the pedotransfer functions that are used to predict the soil hydraulic parameters. Indeed, the prior parameter uncertainty of the sand and clay fraction should be large enough to guarantee a sufficient soil moisture spread of the ensemble, which is of crucial importance for an adequate performance of the different data assimilation methods.

Figure 3.2 shows the measured records of daily precipitation and daily air temperature for the 10 month measurement period used herein. The measurement period is rather wet with several intensive precipitation events during the summer. For example, notice the event on the 27th of July in 2012 in which 31 mm of precipitation fell in just one hour. Our experience suggests that such extreme rainfall events corrupt the parameter estimates, in large part due to an inadequate description and/or characterization of surface runoff. What is more, the correlation between the hydraulic parameters of the different layers of our soil domain and the moisture state deteriorates rapidly close to saturation. Therefore, on days with rainfall in excess of 20 mm we resort to state estimation only, and proceed with this the next two consecutive days to give VIC and CLM sufficient opportunity to remove, via deficient surface transport or state updating, the excess water. On the third day after each 20 mm+ precipitation event, we resume joint LSM state and parameter estimation.

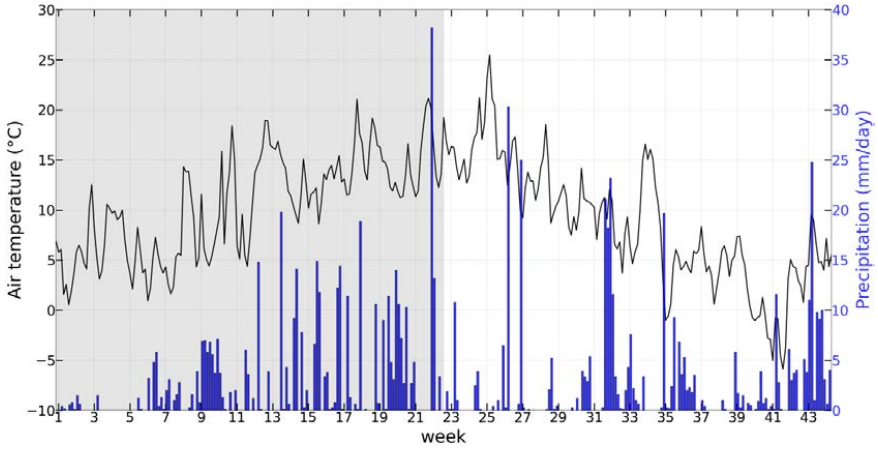

Figure 3.2 Historical records of daily mean air temperature (solid black line; left y-axis) and precipitation (blue bars; right y-axis) in the period from March 1, 2012 to December 31, 2012 for the Rollesbroich experimental test site in the Eifel mountain range in western Germany. The grey region demarcates the 5-month assimilation period (March 1, 2012 to July 31, 2012) which is used for VIC and CLM calibration using joint parameter and state estimation. The subsequent 5-month period between August 1, 2012 and December 31, 2012 serves as our evaluation period to verify the performance of the calibrated VIC and CLM models without state estimation.

To evaluate joint state-parameter estimation algorithms for the two LSMs and the four different data assimilation algorithms, we carried out the following three numerical experiments for VIC and CLM (see also table 3.3):

(1) Open loop simulation. We evaluate the LSMs from March 1, 2012 to December 31, 2012 with time-invariant parameters via Monte Carlo simulation using a large number of draws from the prior parameter distribution summarized in table 3.1 and section 3.4.2.

(2) State updating with EnKF. The soil moisture state variables were updated during the five-month calibration period using the SPADE moisture content measurements. In theory, soil moisture assimilation should improve our estimates of the initial states of the evaluation period. We posit that this enhanced state-value characterization should improve the accuracy of the LSM simulated (predicted) soil moisture values during the first few days/weeks of the evaluation period, after which the model performance deteriorates rapidly over time in the absence of recursive state adjustments.

(3) Joint state-parameter estimation using RRPF, PMCMC, and EnKF with state augmentation and dual estimation. The soil moisture state variables and model parameters are estimated during the five-month calibration period using the SPADE soil moisture measurements. The parameter values and state variables at the end of the calibration data period are used for the evaluation period.

Table 3.3 Summary of the different numerical experiments used in this study for CLM and VIC and their respective abbreviations used in the subsequent tables and figures.

scenario description	**Abbreviation**
Open loop simulation	OpenLoop
EnKF with state estimation	noParamUpdate
EnKF with state augmentation	EnKF-AUG
EnKF with dual estimation	EnKF-DUAL
RRPF with ad-hoc parameter perturbations	RRPF
PMCMC	PMCMC

3.4.3 Summary statistics

We used the Nash-Sutcliffe model efficiency (NSE) and the Root Mean Square Error (RMSE) to evaluate the quality-of-fit of the VIC and CLM predicted (simulated) soil moisture values during the calibration (assimilation) and evaluation period. These two metrics are computed separately for the 5, 20, and 50 cm measurement depths as follows:

$$\mathrm{NSE}_i = 1 - \frac{\sum_{t=1}^{n}\left(\tilde{\mathbf{y}}_{i,t} - \bar{\mathbf{y}}_{i,t}\right)^2}{\sum_{t=1}^{n}\left(\tilde{\mathbf{y}}_{i,t} - \frac{1}{n}\sum_{t=1}^{n}\tilde{\mathbf{y}}_{i,t}\right)^2}; \qquad \mathrm{RMSE}_i = \sqrt{\frac{1}{n}\sum_{t=1}^{n}\left(\tilde{\mathbf{y}}_{i,t} - \bar{\mathbf{y}}_{i,t}\right)^2}, \tag{3.5}$$

where $\tilde{\mathbf{y}}_{i,t}$ and $\bar{\mathbf{y}}_{i,t}$ denote the measured and ensemble mean predicted soil moisture contents at time t, the subscript i constitutes an index for measurement depth, $i = \{1, \dots, 3\}$, and $t = \{1, \dots, n\}$. The 3×1 vector of ensemble mean predicted moisture contents, $\bar{\mathbf{y}}_t$, is simply equivalent to the mean of the VIC or CLM forecasted state variables at these respective measurement depths. Larger values of the NSE and smaller values of the RMSE are preferred as they indicate a better LSM performance. In the absence of reliable information about the soil hydraulic properties of the different layers, the soil moisture observations were the only data available to evaluate the results of VIC and CLM and each data assimilation method.

3.5 Results

In this section we present the results of our numerical experiments. We first discuss our findings for VIC followed by the results of CLM. Section 3.6 proceeds with a discussion of the main findings.

3.5.1 VIC

Figure 3.3 displays the observed (blue dots) and VIC predicted soil moisture values (solid lines) at (a) 5, (b) 20, and (c) 50 cm depths using PMCMC (black), RRPF (red), EnKF-AUG (green), and EnKF-DUAL (cyan). As the Rollesbroich test site experiences a yearly average precipitation of more than about 1000 mm it is not surprise that the upper soil layer at 5 cm is rather wet with volumetric soil moisture contents that vary dynamically between 0.3 and 0.5 cm^3/cm^3 in response to atmospheric forcing. This is especially true during the summer months (week 12 – 22) and explained by a rapid succession of rainfall and drying events. The larger porosity values of the surface layer explain the relatively high soil moisture contents of the 5 cm measurement depth. The storage time series of the deeper soil layers at 20 and 50 cm depth exhibit a rather negligible temporal variation with soil moisture values that range between 0.3-0.4 cm^3/cm^3 and show a damped and lagged response to rainfall. Note that the soil water storage of the deepest layer increases steadily during the year. This implies a drainage flux from the top soil to the aquifer (and drainage channels).

The different data assimilation methods demonstrate a rather similar performance with VIC predicted moisture contents that track reasonably well the three different layers. Note, however that RRPF does not reproduce well the measured data at 50cm depth in the period from March (week 1) to June (week 17). This might be caused by filter inbreeding of the states, and will be discussed later (see also figure 3.9(b)). Nevertheless, RRPF recovers the observed soil moisture data in week 18. Although difficult to see, the EnKF produces the best results at 50 cm depth (state augmentation and dual estimation).

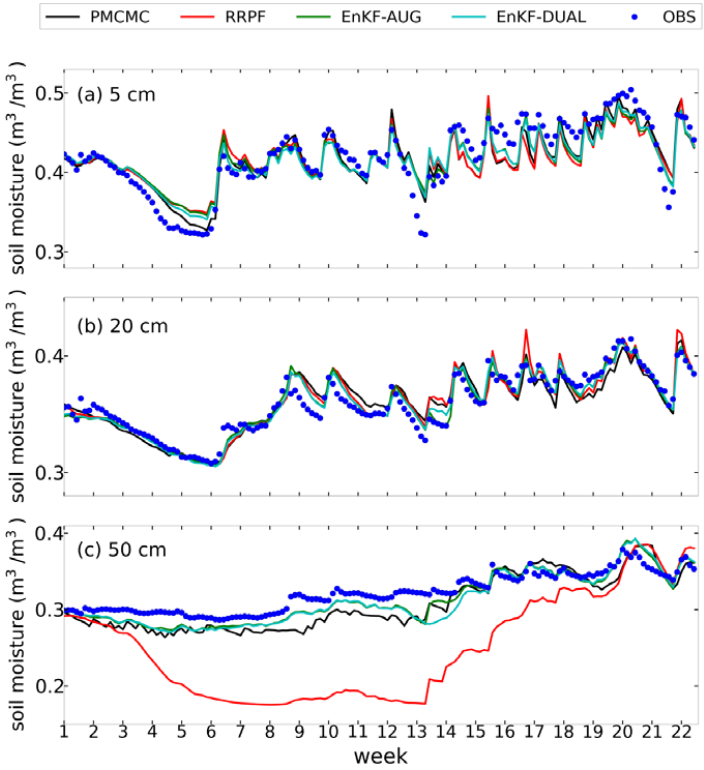

Figure 3.3 Assimilation period: Observed (blue dots) and VIC predicted time series (solid lines) of soil moisture content at depths of (a) 5, (b) 20, and (c) 50 cm in the Rollesbroich site. Colour coding is used to differentiate between the results of PMCMC [black], RRPF [red], EnKF-AUG [green], and EnKF-DUAL [cyan]. The first days of week 1 and 22 are 01-03-2012 and 26-07-2012, respectively.

Table 3.4 summarizes the NSE and RMSE values of PMCMC, RRPF, EnKF-DUAL and EnKF-AUG for the calibration (assimilation) period. We also list the performance of VIC without data assimilation (OpenLoop) using the mean soil moisture time series of many different realizations of the prior parameter distribution, and include RMSE and NSE values of the EnKF for state estimation only (noParamUpdate) using VIC parameterizations drawn randomly from its prior parameter distribution. The open loop deviates most from the measured values with RMSE values of 0.036, 0.037 and 0.129 cm^3/cm^3 for the 5, 20, and 50 cm measurement depths. The different data assimilation methods improve significantly the quality of fit of VIC compared to the open loop run. EnKF-AUG and EnKF-DUAL exhibit an almost identical performance with similar NSE and RMSE values. The particle filters, RRPF and PMCMC demonstrate comparable results for the 5 and 20 cm depth, but exhibit somewhat inferior performance compared to EnKF-AUG and EnKF-DUAL for the 50 cm layer. The Table confirms our previous finding that the PF exhibits difficulties to track the soil moisture data of the deepest measurement layer. Indeed, the RMSE value of 0.088 of the PF for this layer is much larger than its counterparts of 0.021, 0.014 and 0.016 derived from PMCMC, EnKF-AUG and EnKF-DUAL, respectively. Perhaps surprisingly, but the best

performance of VIC is obtained for state estimation only (noParamUpdate) using model parameterizations drawn randomly from the prior parameter distribution. We posit that the nonlinear relationship between states and parameters may introduce inconsistencies in PMCMC, RRPF, EnKF-AUG and EnKF-DUAL which jointly estimate VIC states and parameters. Overall, the EnKF gives somewhat better results than the PF, particularly for the deepest measurement layer, and PMCMC exhibits a better performance than RRPF.

Table 3.4 Calibration period: Values of the NSE and RMSE summary statistics of the quality of fit of VIC for the Rollesbroich soil moisture observations at 5, 20, and 50 cm depth using the PMCMC, RRPF, EnKF-AUG and EnKF-DUAL data assimilation methods. For completeness, we also list the performance of the EnKF for state estimation only (noParamUpdate) using VIC parameter values drawn randomly from the prior parameter distribution, and the performance of an open loop run of VIC (OpenLoop) using the mean simulation of many different VIC parameterizations drawn randomly from the prior parameter distribution (see table 3.1 and section 3.4.2).

Criteria	**Soil depth**	**PMCMC**	**RRPF**	**EnKF-AUG**	**EnKF-DUAL**	**noParamUpdate**	**OpenLoop**
NSE (-)	5 cm	0.82	0.73	0.80	0.82	0.89	0.33
	20 cm	0.80	0.84	0.92	0.91	0.86	-1.16
	50 cm	0.27	-11.77	0.69	0.58	0.91	-26.65
RMSE (m^3/m^3)	5 cm	0.019	0.023	0.020	0.019	0.015	0.036
	20 cm	0.011	0.010	0.007	0.007	0.009	0.037
	50 cm	0.021	0.088	0.014	0.016	0.008	0.129

Figure 3.4 presents traceplots of the VIC parameters during the 5-month calibration period using the PMCMC (black), PF (red), EnKF-AUG (green), and EnKF-DUAL (cyan) data assimilation methods. We display the ensemble mean saturated hydraulic conductivity ($\log_{10}k_s$ in m/s) at (a) 5 cm, (b) 20 cm, and (c) 50 cm depth, (d) b, β at (e) 5 cm, (f) 20 cm, and (g) 50 cm depth, and (h) the maximum baseflow velocity, D_{m} in mm/day. In general, the different data assimilation methods result in somewhat similar trajectories of the ensemble mean parameter values during the calibration period. In particular, the parameter traceplots of EnKF-AUG and EnKF-DUAL appear almost identical, with the exception of parameter b and β at 50 cm depth. Note that the parameters of the surface layer exhibit most dynamics in response to atmospheric forcing. PMCMC exhibits significant temporal dynamics. This is not surprising, and a consequence of the MCMC resampling step that is used to rejuvenate the parameter samples (e.g. Vrugt et al., 2013). In the first place, the DREAM-type proposal distribution that is used to create candidate particles allows for relatively large moves in the parameter space. Second, only a small LSM trajectory between two successive soil moisture observations is used to determine the acceptance probability of each candidate particle. With such a short (re)-simulation period, insensitive parameters are allowed to transition to very

different values, as they do not affect the model output between the two observations, and thus likelihood of a candidate particle. Altogether, this also contributes to a stronger dependency of PMCMC on the initial parameter ensemble. This collection of parameter vectors is drawn randomly from the prior parameter distribution and differs per trial depending on the random seed. The use of a larger historical simulation period (going back further in time) would better constrain the VIC parameters, but also increase significantly the computational burden of resampling. Nonetheless, the ensemble mean VIC parameter values of the different data assimilation methods are remarkably similar at the end of the calibration period, after assimilating the soil moisture observations of week 22. The exception to this is parameter b whose trajectories differ most with values at the end of the calibration period that range between values of 0.11 for RRPF and 0.25 for EnKF-DUAL. Finally, parameter D_{m} converges systematically to values of 1 - 2 mm/day but at a different rate for the data assimilation methods. The EnKF-AUG, EnKF-DUAL and PMCMC methods need just a few soil moisture observations to determine the value of D_{m}, whereas RRPF converges at a much slower pace. This might explain the rather inferior performance of RRPF for the 50 cm measurement depth during a substantial part of the assimilation period.

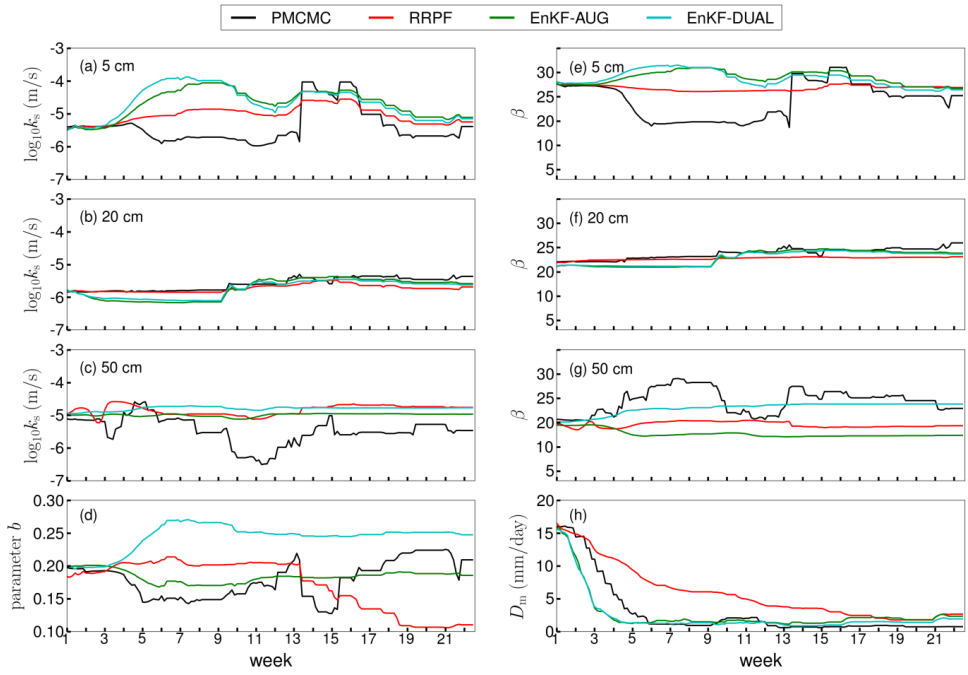

Figure 3.4 Traceplots (solid lines) of the VIC parameters, Saturated hydraulic conductivity ($\log_{10}\boldsymbol{k_s}$ in m/s) at (a) 5 cm, (b) 20 cm, and (c) 50 cm depth, (d) $\boldsymbol{b}$, $\boldsymbol{\beta}$ at (e) 5 cm, (f) 20 cm, and (g) 50 cm depth, and (h) the maximum baseflow velocity, $\boldsymbol{D_{\mathrm{m}}}$, in mm/day during the 5-month assimilation period. Colour coding is used to differentiate between the results of PMCMC [black], RRPF [red], EnKF-AUG [green], and EnKF-DUAL [cyan]. The first days of week 1 and 22 are 01-03-2012 and 26-07-2012, respectively.

To provide a better understanding of the ensemble spread of the VIC parameters, please consider Figure 3.5 which presents traceplots of the sampled $\log_{10}k_s$ (left column) and β (right column) values at the 20 cm measurement depth for the $N = 100$ members. Results are presented in order of (a-b) PMCMC (gray), (c-d) RRPF (red), (e-f) EnKF-AUG (green) and (g-h) EnKF-DUAL (cyan) and the ensemble mean is indicated with the solid black line. The ensemble members cover a relatively large part of the prior distribution of both parameters, with the exception of RRPF which seems to underestimate the actual uncertainty of $\log_{10}k_s$ and β. This is an artefact of equation (3.2) which discourages large parameter adjustments with small s. Nevertheless, note that the ensemble mean of the parameters is rather unaffected by assimilation of the soil moisture data, except for the small increase of $\log_{10}k_s$ and β late April due to increased precipitation in the following months (see also figure 3.2).

Figure 3.6 displays VIC simulated soil moisture time series for the independent 5-month evaluation period at (a) 5, (b) 20, and (c) 50 cm depths using initial states and parameter values derived from PMCMC (black), PF (red), EnKF-AUG (green), and EnKF-DUAL (cyan). The observed soil moisture values are separately indicated with the solid blue dots.

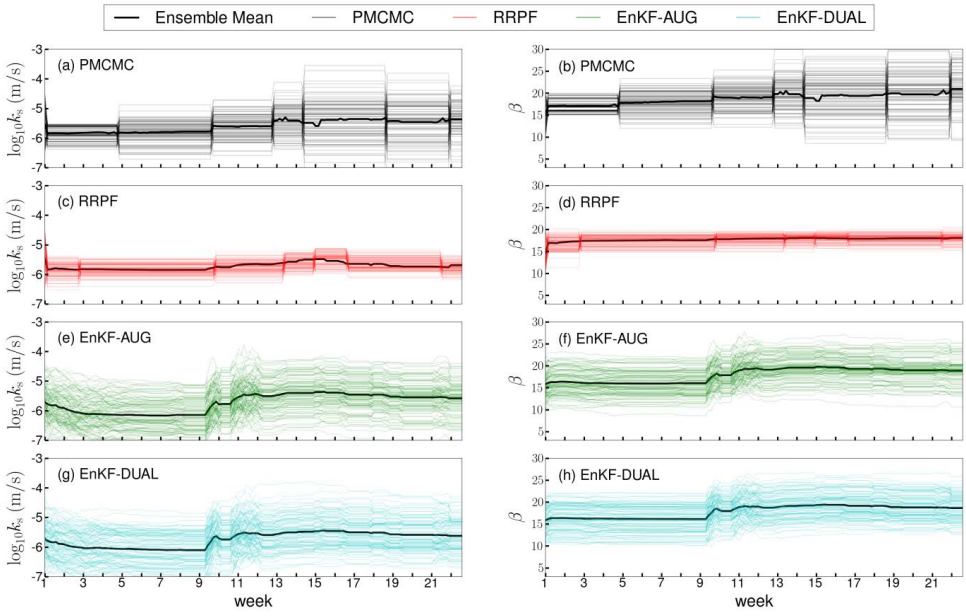

Figure 3.5 Sampled trajectories of the $\boldsymbol{N = 100}$ ensemble members of the saturated hydraulic conductivity ($\log_{10}\boldsymbol{k_s}$ in m/s) at 20 cm depth (left column) and parameter $\boldsymbol{\beta}$ (right column) of VIC during the 5-month assimilation period of week 1 to 22 using (a-b) PMCMC [grey] (c-d) RRPF [red], (e-f) EnKF-AUG [green], and (g-h) EnKF-DUAL [cyan]. The trajectory of the ensemble mean is separately indicated in each panel using the solid black line.

The water content simulations of VIC are hardly distinguishable, except for the deepest soil layer at 50 cm depth. Apparently, it does not matter which data assimilation method is used to estimate the VIC parameter values and initial states of the evaluation period. VIC tracks very well the soil moisture data at 20 cm depth, but does not do a particularly good job in

describing water content dynamics at 5 and 50 cm depth. In particular, the model systematically underestimates the observed storage of the bottom soil layer between weeks 25-36. This might be a consequence of the use of a fixed lower boundary condition (no connection with underlying aquifer) and/or the relatively simple baseflow parameterization. Although not further shown herein, a separate VIC run using state estimation only (noParamUpdate) produces similar results after a few days to an open loop simulation.

We summarize in table 3.5 the NSE and RMSE values of PMCMC, RRPF, EnKF-DUAL and EnKF-AUG during the 5-month evaluation period. We also list the performance of VIC without data assimilation (OpenLoop) using the mean soil moisture time series of many different realizations of the prior parameter distribution, and include RMSE and NSE values of the EnKF for state estimation only (noParamUpdate) using VIC parameterizations drawn randomly from its prior parameter distribution. In general, the RMSE values of the evaluation period are much higher than their counterparts of the assimilation period, and noParamUpdate produces RMSE values similar to that of an open loop simulation. VIC parameter estimation is productive, as it substantially reduces the RMSE values of 20 and 50 cm measurement depths compared to a model run with state estimation only (noParamUpdate) and parameters drawn randomly from their prior distribution. More specifically, the PMCMC, RRPF, EnKF-AUG and EnKF-DUAL show a RMSE improvement of about 54% and 42% for the second and third measurement depth compared to OpenLoop and noParamUpdate. The NSE values of VIC for the 50 cm depth are negative for all six methods, conclusively demonstrating an inferior performance of the model for this soil layer.

Table 3.5 Table 3.5 Evaluation period: Values of the NSE and RMSE summary statistics of the quality of fit of VIC for the Rollesbroich soil moisture observations at 5, 20, and 50 cm depth using the calibrated parameter values and initial states derived from the PMCMC, RRPF, EnKF-AUG and EnKF-DUAL data assimilation methods. For completeness, we also list the performance of the EnKF using state estimation only (noParamUpdate) using VIC parameter values drawn randomly from the prior parameter distribution, and the performance of an open loop run of VIC (OpenLoop) using the mean simulation of many different VIC parameterizations drawn randomly from the prior parameter distribution.

Criteria	**Soil depth**	**PMCMC**	**RRPF**	**EnKF-AUG**	**EnKF-DUAL**	**noParamUpdate**	**OpenLoop**
NSE (-)	5 cm	0.39	0.39	0.39	0.39	0.35	0.36
	20 cm	0.38	0.47	0.40	0.39	-1.75	-1.87
	50 cm	-10.33	-8.41	-10.54	-11.33	-26.83	-32.96
RMSE (m^3/m^3)	5 cm	0.052	0.052	0.052	0.052	0.054	0.053
	20 cm	0.026	0.024	0.026	0.026	0.055	0.056
	50 cm	0.076	0.069	0.077	0.079	0.119	0.132

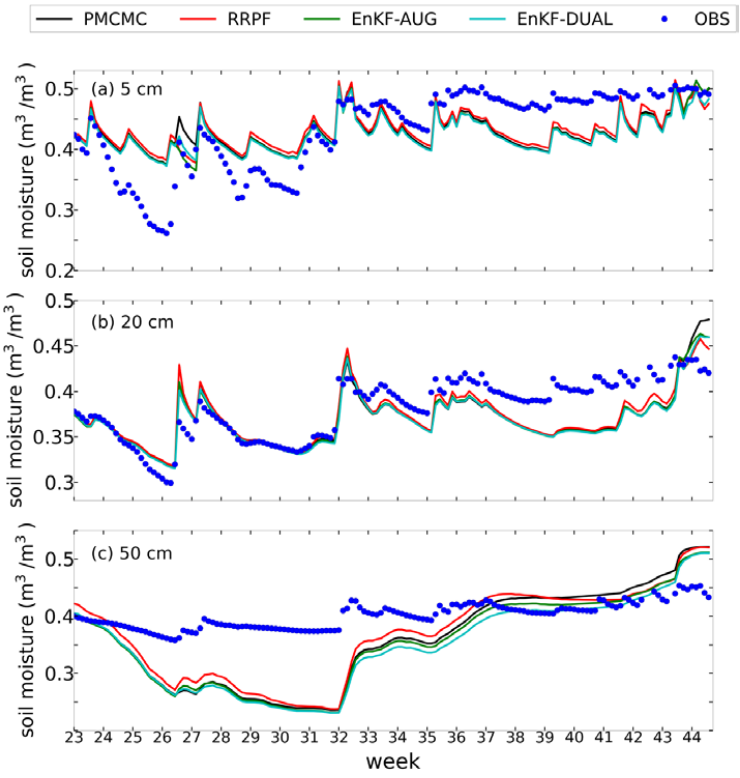

Figure 3.6 Evaluation period: Observed (blue dots) and VIC simulated time series (solid lines) of soil moisture content at depths of (a) 5 cm, (b) 20 cm, and (c) 50 cm in the Rollesbroich site. Colour coding is used to differentiate between the results of PMCMC [black], RRPF [red], EnKF-AUG [green], and EnKF-DUAL [cyan]. The first days of week 23 and 44 are 01-08-2012 and 26-12-2012, respectively.

We now investigate in more detail the effect of MCMC resampling with the PF as figure 3.4 has demonstrated that PMCMC produces rather dynamic trajectories of the sampled parameter values. Nevertheless, the parameters converge to stable values at the end of the assimilation period. This suggests that the choice of the length of the calibration period is crucially important in determining the performance of PMCMC during the evaluation period. To investigate this in more detail we use June 11, June 30, July 20, and July 31, 2012 as end dates of the PMCMC calibration period and verify VIC performance for the same 5-month evaluation period. The different end dates are conveniently referred to as PMCMC_0611, PMCMC_0630, PMCMC_0720 and PMCMC_0731 in figure 3.7. The simulated soil moisture trajectories of PMCMC_0630, PMCMC_0720 and PMCMC_0731 are in excellent agreement, but deviate from PMCMC_0611. Thus, a 4-month calibration period would have led to the same results of PMCMC.

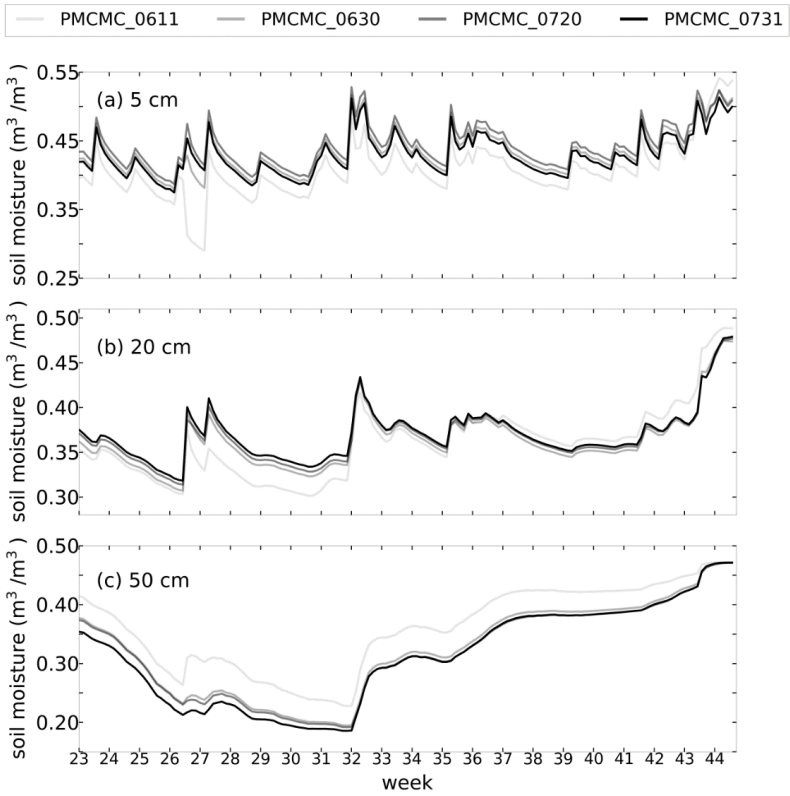

Figure 3.7 Evaluation period: VIC simulated volumetric moisture contents at (a) 5 cm, (b) 20 cm, and (c) 50 cm depth in the soil of the Rollesbroich experimental test site using parameter values derived from PMCMC via assimilation periods ending on 06-11 [platinum], 06-30 [silver], 07-20 [grey] and 07-31 [black], respectively. For PMCMC_0611, PMCMC_0630 and PMCMC_0720, the soil moisture state on 01-08-12, the first day of the 5-month evaluation period, was derived from VIC simulation using the analysis state and parameter values of the last day of the assimilation period.

The effect of initial uncertainties on the performance of EnKF with the ensemble inflation method is also tested with the VIC model. Table 3.6 compares the RMSE values of EnKF-AUG and EnKF-DUAL for the calibration and evaluation period using heteroscedastic precipitation data errors equivalent to 10% (default) and 20% of their measured hourly rates plotted in figure 3.2. We list separate RMSE values for each soil moisture measurement depth. In short, the results are equivalent for both EnKF implementations.

Next, we evaluate the effect of the choice of the scaling factor s in RRPF on VIC output. This scalar plays a crucial role in the resampling of the parameters in the PF. If s is taken too large, the resampling step will introduce parameter drift and corrupt the approximation of $p(\mathbf{X}_{1:t}|\widetilde{\mathbf{Y}}_{1:t})$ and $p(\mathbf{x}_t|\widetilde{\mathbf{Y}}_{1:t})$. On the contrary, if s is too small, then the resampled parameters exhibit insufficient dispersion, and underestimate the actual parameter uncertainty. In the absence of theoretical convergence proofs and clear guidelines on the selection of s, the RRPF cannot estimate exactly the posterior state and parameter PDF (Vrugt et al., 2013; Yan et al., 2015). Previous applications of RRPF have suggested a value of $s = 0.01$ (DeChant

and Moradkhani, 2012; Plaza et al., 2012), but thus far we have used $s = 0.1$ to avoid sample impoverishment. Table 3.7 lists RMSE values of VIC for the 5, 20, and 50 cm measurement depth for the calibration and evaluation period using RRPF with $s = 0.01$, $s = 0.1$, and $s = 0.5$, respectively. These three runs are coined RRPF-0.01, RRPF-0.1 and RRPF-0.5, respectively. These results demonstrate that a value of $s = 0.5$ significantly enhances the performance of RRPF during the calibration period. The RMSE values are reduced from 0.025, 0.012, and 0.113 to 0.015, 0.007, and 0.037 for the 5, 20 and 50 cm measurement depths. RRPF-0.5 also shows substantial improvements over RRPF-0.01 during the evaluation period. This improvement is most apparent for the 20 and 50 cm soil depths with RMSE values that have decreased from 0.025 and 0.119 to 0.020 and 0.071, respectively. These results are on par with our default setting of $s = 0.1$ in RRPF. These findings provide evidence for our claim that the scaling factor s plays a crucial role in RRPF. What is more, it provides support for our conclusion in figure 3.5 that RRPF underestimates the actual uncertainty of $\log_{10}k_s$ and β. Larger values of s will increase the parameter spread, which in turn will enhance the uncertainty among the particles' forecasted states. This makes it easier for RRPF to track the observed soil moisture data during the calibration period.

Table 3.6 RMSE values of VIC for the Rollesbroich soil moisture measurements at 5, 20, and 50 cm depth using the EnKF with state AUGmentation or DUAL estimation during the calibration period. We also summarize the subsequent performance of the VIC model using the calibrated parameter values and initial states derived from AUG and DUAL. The subscripts 10% and 20% signify the standard deviations of the measurements errors that are used to corrupt the hourly precipitation data.

Period	**Soil depth**	**EnKF-AUG_10%**	**EnKF-AUG_20%**	**EnKF-DUAL_10%**	**EnKF-DUAL_20%**
Calibration (Assimilation)	5 cm	0.020	0.019	0.019	0.019
	20 cm	0.007	0.007	0.007	0.007
	50 cm	0.014	0.014	0.016	0.014
Evaluation	5 cm	0.052	0.052	0.052	0.052
	20 cm	0.026	0.025	0.026	0.025
	50 cm	0.077	0.077	0.079	0.079

Figure 3.8 displays traceplots of the sampled $N = 100$ trajectories of the saturated hydraulic conductivity ($\log_{10}k_s$ in m/s) at 50 cm depth (left column) and parameter β (right column) of VIC during the 5-month assimilation period using (a-b) RRPF-0.01, (c-d) RRPF-0.1, and (e-f) RRPF-0.5. As expected, larger values of s increase the spread of the sampled values of the VIC parameters as evidenced by an increasingly larger particle coverage of the prior parameter distribution. This larger spread of the particles' parameter values also enhances the ability of RRPF to track properly the joint parameter and state PDF. Yet, larger values of s

have two important drawbacks. Not only can it obstruct parameter convergence (as evidenced in figure 3.8(e)), but also many of the resampled parameter values might be deemed nonbehavioral, enhancing considerably the chances of particle degeneration. To demonstrate this more explicitly, Figure 3.9 shows traceplots of the VIC predicted soil moisture contents of the $N = 100$ particles at 50 cm depth using (a) RRPF-0.01, (b) RRPF-0.1, and (c) RRPF-0.5. The RRPF is excessively optimistic for $s = 0.01$ with a negligible uncertainty in the predicted soil moisture values between weeks 2-14. Note that in weeks 2-4 the ensemble has collapsed to a deterministic simulation (appears as single line). A similar result is observed for RRPF-0.1 but with enhanced uncertainty in soil moisture values for the second part of the calibration period. In PF-0.1 particle degeneration from March to June explains its bad performance from March to June in figure 3.3. The use of $s = 0.5$ enhances considerably the spread of the VIC soil moisture predictions. Yet, the ensemble spread has become quite large from week 15 onwards. For these reasons, we are satisfied with our value of $s = 0.1$ in RRPF, although this decision is subjective and would require much testing via trial-and-error. This has stimulated Vrugt et al. (2013) to introduce a parameter resampling method which is properly rooted in statistical theory and uses laws of probability to rejuvenate the ensemble.

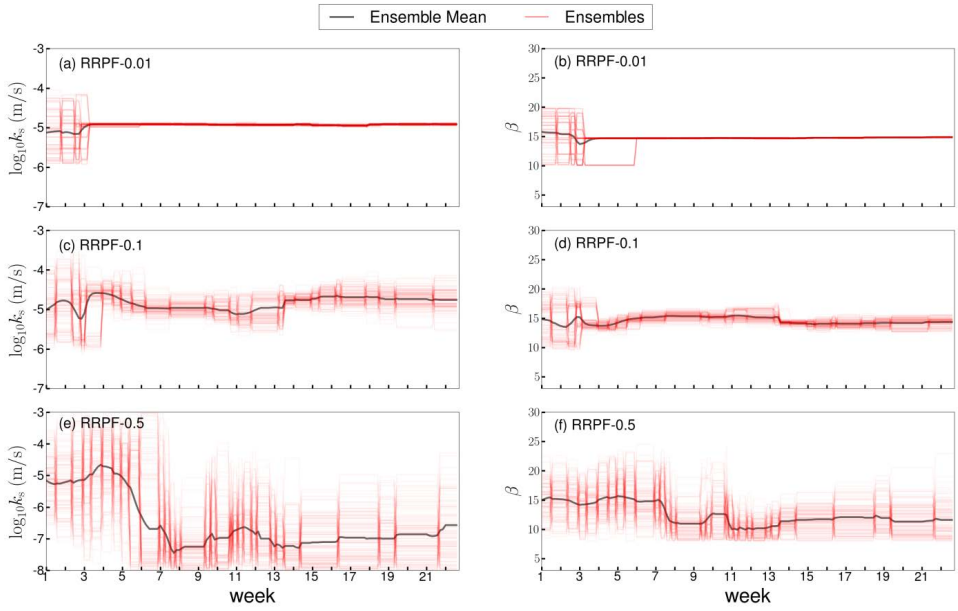

Figure 3.8 Sampled trajectories of the $\boldsymbol{N = 100}$ ensemble members (solid red lines) of the saturated hydraulic conductivity ($\log_{10}\boldsymbol{k_s}$ in m/s) at 50 cm depth (left column) and parameter $\boldsymbol{\beta}$ (right column) of VIC during the 5-month assimilation period of week 1 to 22 using (a-b) RRPF-0.01, (c-d) RRPF-0.1, and (e-f) RRPF-0.5. The ensemble mean is separately indicated in each panel with the solid grey line.

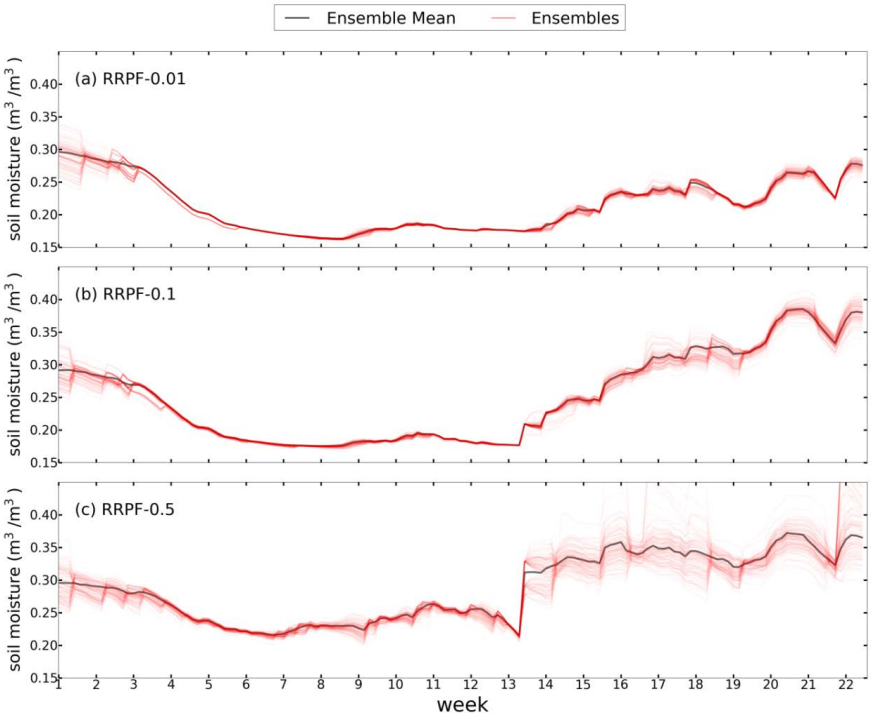

Figure 3.9 Soil moisture trajectories of the $\boldsymbol{N = 100}$ ensemble members at 50 cm depth for the 5-month assimilation period (week 1 to 22) of the Rollesbroich site using VIC and (a) RRPF-0.01, (b) RRPF-0.1, and (c) RRPF-0.5. The solid black line signifies the ensemble mean soil moisture prediction.

Table 3.7 RMSE values of VIC for the Rollesbroich soil moisture observations at 5, 20, and 50 cm depth using data assimilation with RRPF during the calibration period. We also summarize the subsequent performance of the VIC model using the calibrated parameter values and initial states derived from RRPF. The subscripts 0.01, 0.1, and 0.5 signify the value of the scaling factor s of the multivariate normal distribution that is used to perturb the parameter values (importance density).

Table 3.7 RMSE values of VIC for the Rollesbroich soil moisture observations at 5, 20, and 50 cm depth using data assimilation with RRPF during the calibration period. We also summarize the subsequent performance of the VIC model using the calibrated parameter values and initial states derived from RRPF. The subscripts 0.01, 0.1, and 0.5 signify the value of the scaling factor **s** of the multivariate normal distribution that is used to perturb the parameter values (importance density).

Period	Soil depth	RRPF-0.01	RRPF-0.1	RRPF-0.5
Calibration (Assimilation)	5 cm	0.025	0.023	0.015
	20 cm	0.012	0.010	0.007
	50 cm	0.113	0.088	0.037

	5 cm	0.053	0.052	0.056
Evaluation	20 cm	0.025	0.024	0.020
	50 cm	0.119	0.069	0.071

3.5.2 CLM

Figure 3.10 shows the observed (blue dots) and ensemble mean predicted soil moisture values by CLM (solid lines) at (a) 5, (b) 20, and (c) 50 cm depths during the assimilation period using PMCMC (black), PF (red), EnKF-AUG (green), and EnKF-DUAL (cyan). The most important results are as follows. First, the ensemble mean soil moisture time series of CLM exhibit a larger spread than VIC depicted previously in figure 3.3. Second, the EnKF-AUG and EnKF-DUAL exhibit a superior performance with ensemble mean CLM simulations that track closely the observed soil moisture observations at each depth. Third, the moisture time series (and data) demonstrate most dynamics at the 5 cm depth in response to the variable atmospheric boundary conditions. Fourth, the worst performance is observed for RRPF, as evidenced by systematic deviations of this filter´s soil moisture predictions with the observed data between weeks 3-6 and 18-21 for the 5 cm depth, weeks 1-14 and weeks 18-21 for the 20 cm depth, and weeks 1-15 and 19-22 for the 50 cm measurement depth. Fourth, the initial soil moisture values of CLM at 50 cm depth appear positively biased with a distance of approximately 0.05 cm^3/cm^3 to the areal-mean value of the soil water contents measured by the SPADE sensors on 01-03-2012 (first day of week 1). A smaller bias of 0.03 cm^3/cm^3 is observed at the 20 cm depth. The ENKF-AUG and EnKF-DUAL methods need a few days to recover from this erroneous initialization.

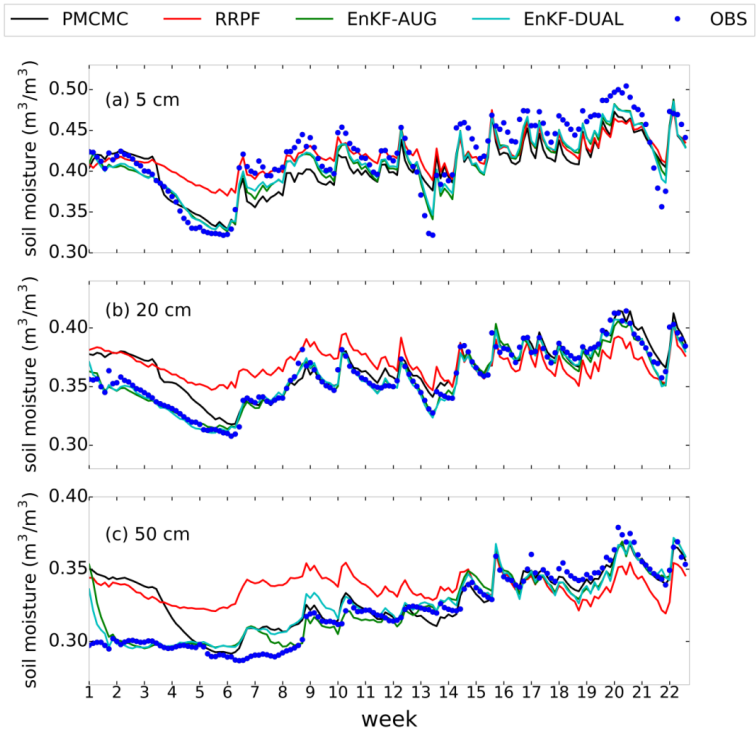

Figure 3.10 CLM predicted time series of soil moisture content at (a) 5 cm, (b) 20 cm, and (c) 50 cm depth during the 5-month calibration period using PMCMC [black], RRPF [red], EnKF-AUG [green], and EnKF-DUAL [cyan]. The first day of week 1 is 01-03-2012 and week 22 starts with 26-07-2012.

Table 3.8 lists the NSE and RMSE values of PMCMC, RRPF, EnKF-DUAL and EnKF-AUG for the CLM calibration (assimilation) period. We also list the performance of CLM without data assimilation (OpenLoop) using the mean soil moisture time series of many different realizations of the prior parameter distribution, and list in column with header "noParamUpdate" the RMSE and NSE values of the EnKF using state estimation only with CLM parameterizations drawn randomly from the prior parameter distribution. These results demonstrate that soil moisture assimilation enhances considerably the ability of CLM to predict the observed data. Compared to open loop CLM simulation, the RMSE is reduced from 0.051, 0.031 and 0.069 to values of about 0.020, 0.012, and 0.016 (average) for the different data assimilation methods, respectively. Yet, the RMSE and NSE values of a CLM run with state estimation only (noParamUpdate) appear as good as those derived from joint parameter and state estimation using PMCMC, RRPF, EnkF-AUG and EnKF-DUAL. Overall, the best performance is observed for EnKF-AUG and EnKF-DUAL followed by PMCMC and RRPF.

Table 3.8 Calibration period: Values of the NSE and RMSE summary statistics of the quality of fit of CLM for the Rollesbroich soil moisture measurements at 5, 20, and 50 cm depth with the PMCMC, RRPF, EnKF-AUG and EnKF-DUAL data assimilation methods. For completeness, we also list the performance of the EnKF for state estimation only (noParamUpdate) using CLM parameter values drawn randomly from the prior parameter distribution, and the performance of an open loop run of CLM (OpenLoop) using the mean simulation of many different CLM parameterizations drawn randomly from the prior parameter distribution.

Criteria	**Soil depth**	**PMCMC**	**RRPF**	**EnKF-AUG**	**EnKF-DUAL**	**noParamUpdate**	**OpenLoop**
NSE (-)	5 cm	0.63	0.63	0.82	0.85	0.72	-0.31
	20 cm	0.73	0.23	0.94	0.95	0.98	-0.57
	50 cm	0.50	-0.26	0.85	0.86	0.47	-6.90
RMSE (m^3/m^3)	5 cm	0.027	0.027	0.019	0.017	0.024	0.051
	20 cm	0.013	0.022	0.006	0.006	0.004	0.031
	50 cm	0.017	0.028	0.009	0.009	0.018	0.069

We proceed in figure 3.11 with traceplots of the $N = 100$ sampled trajectories of the saturated hydraulic conductivity ($\log_{10} k_s$ in m/s) at 50 cm depth (left column) and soil hydraulic parameter B at 50 cm depth (right column) during the 5-month assimilation period using (a-b) PMCMC (c-d) RRPF, (e-f) EnKF-AUG, and (g-h) EnKF-DUAL. The evolution of the ensemble mean $\log_{10} k_s$ and B values is separately indicated with the solid black line. The largest spread of the ensemble members is observed for EnKF-AUG and EnKF-DUAL and explained by the inflation method of equation (3.2) which inherits and sustains the prior parameter uncertainty. The RRPF sampled trajectories of $\log_{10} k_s$ and B exhibit a rather small uncertainty with PDF´s of these two parameters that appear well defined at all measurement times. This might explain the inferior performance of RRPF as detailed previously in table 3.8. Overall, the two CLM parameters do not exhibit large temporal changes and converge to stable values in the last few weeks of the calibration period.

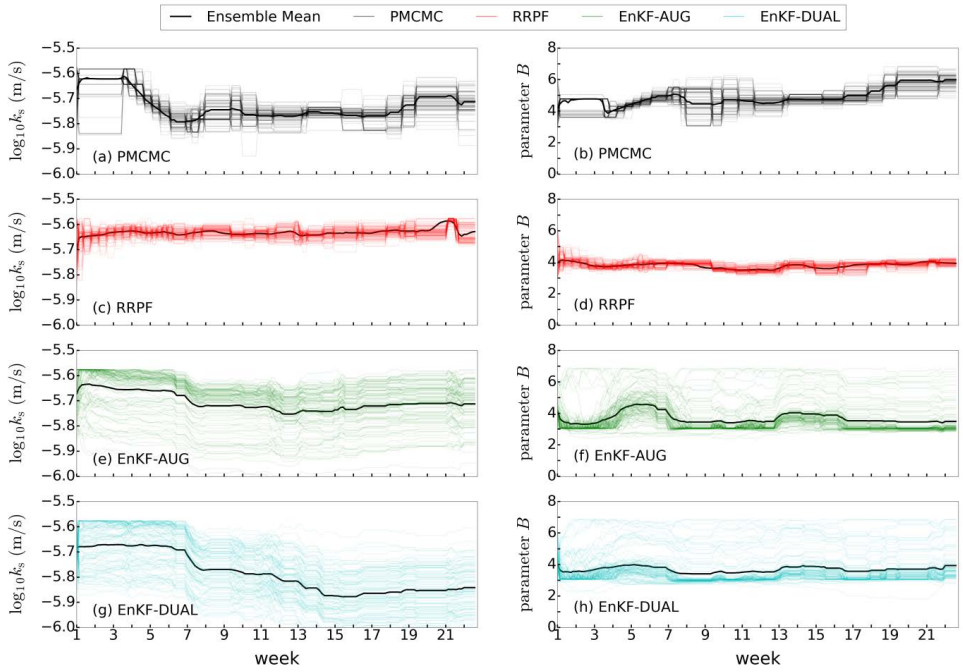

Figure 3.11 Sampled trajectories of the $\boldsymbol{N = 100}$ ensemble members of the saturated hydraulic conductivity ($\log_{10}\boldsymbol{k_s}$ in m/s) at 50 cm depth (left column) and soil hydraulic parameter $\boldsymbol{B}$ at 50 cm depth (right column) of CLM during the 5-month assimilation period of week 1 to 22 using (a-b) PMCMC [grey] (c-d) RRPF [red], (e-f) EnKF-AUG [green], and (g-h) EnKF-DUAL [cyan]. The solid black line signifies the evolution of the ensemble mean values of $\log_{10}\boldsymbol{k_s}$ and B. Please note that $\log_{10}$ks (in $\log_{10}$(m/s)) and parameter $\boldsymbol{B}$ are derived from the sand, clay, and organic matter fractions of each soil layer, which are estimated during the assimilation period.

Figure 3.12 displays the observed (blue dots) and ensemble mean predicted soil moisture values by CLM (solid lines) at (a) 5, (b) 20, and (c) 50 cm depths during the evaluation period using PMCMC (black), PF (red), EnKF-AUG (green), and EnKF-DUAL (cyan). The soil moisture time series of the different data assimilation methods appear rather similar with largest differences observed at the 50 cm depth. In general, the PMCMC, RRPF, EnKF-AUG and EnKF-DUAL methods do not do a particularly good job in tracking the soil moisture observations of the top soil layer. Indeed, the CLM soil moisture predictions derived from the different data assimilations are systematically biased, either underestimating (weeks 35-41 and 43-44) or overestimating (weeks 24-31 and 42) the observed soil moisture data during large parts of the evaluation data set. CLM much better tracks the soil moisture data of the 20 and 50 cm depth.

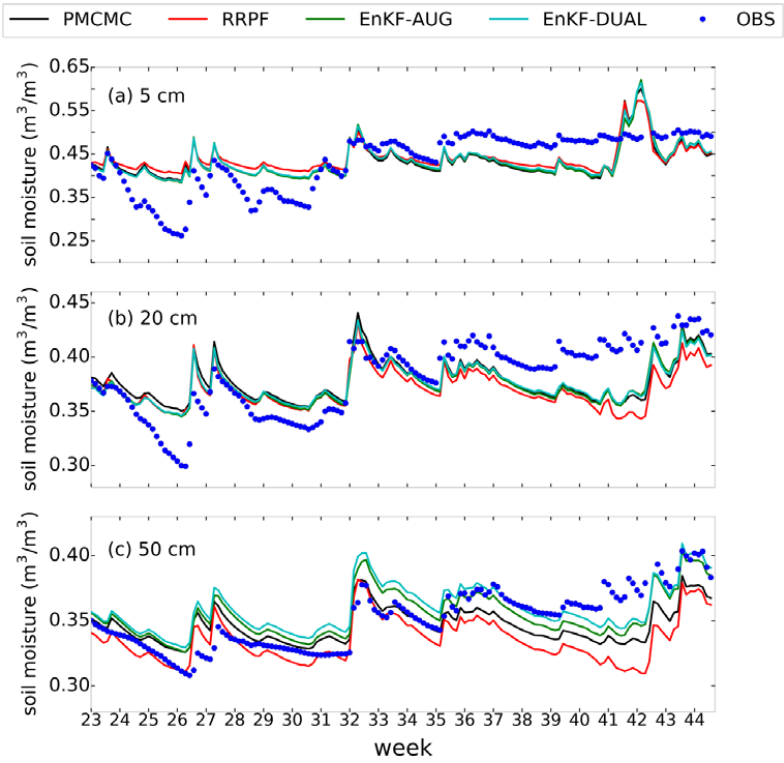

Figure 3.12 Traceplots of soil moisture contents simulated by CLM during the evaluation period at (a) 5 cm, (b) 20 cm, and (c) 50 cm depth in the Rollesbroich site using the calibrated parameter values derived from PMCMC [black], RRPF [red], EnKF-AUG [green], and EnKF-DUAL [cyan]. The measured moisture data are separately indicated in each panel with the solid blue dots. The first day of week 23 is 01-08-2012 and the last day of week 44 is 02-01-2013.

Finally, table 3.9 presents the NSE and RMSE values of PMCMC, RRPF, EnKF-AUG and EnKF-DUAL during the 5-month evaluation period. We also list the performance of VIC without data assimilation (OpenLoop) using the mean soil moisture time series derived from many different realizations of the prior parameter distribution, and display NSE and RMSE values of the EnFK using state estimation only (noParamUpdate) with CLM parameterizations drawn randomly from the prior parameter distribution. The results of this Table are in agreement with our findings for VIC. Indeed, the RMSE values of the evaluation period are much higher than their counterparts of the assimilation period. This is particularly evident for the 5 cm measurement depth where RMSE values have increased from 0.017-0.027 to 0.054-0.058. The deeper measurement depths do not appear to be as much affected, consistent with our findings from figure 3.12. The results also highlight the importance of joint CLM parameter and state estimation as state estimation alone (column noParamUpdate) results in significantly larger RMSE values during the evaluation period. This is most evident for the 50 cm measurement depth, where the RMSE value of 0.050 of noParamUpdate is much larger than its value of 0.016-0.025 derived from PMCMC, RRPF, EnKF-AUG and EnKF-DUAL. Altogether, RRPF achieves the worst performance of all four parameter-state

estimation methods during the evaluation period. PMCMC, EnKF-AUG and EnKF-DUAL provide rather similar RMSE and NSE values.

Table 3.9 Evaluation period: NSE and RMSE values for the Rollesbroich soil moisture measurements at 5, 20, and 50 cm depth using CLM. The initial states and parameter values used by the PMCMC, RRPF, EnKF-AUG and EnKF-DUAL data assimilation methods originate from the 5-month calibration data period. For completeness, we also list the performance of the EnKF using state estimation (noParamUpdate) using CLM parameter values drawn randomly from the prior parameter distribution, and the performance of an open loop run of CLM (OpenLoop) using the mean simulation of many different CLM parameterizations drawn randomly from the prior parameter distribution.

Criteria	Soil depth	PMCMC	RRPF	EnKF-AUG	EnKF-DUAL	noParamUpdate	OpenLoop
NSE (-)	5cm	0.26	0.23	0.32	0.33	-0.19	-0.14
	20cm	0.39	0.21	0.44	0.46	0.24	-0.11
	50cm	0.35	-0.23	0.51	0.42	-3.87	-4.58
RMSE (m^3/m^3)	5cm	0.057	0.058	0.055	0.054	0.072	0.071
	20cm	0.026	0.029	0.025	0.024	0.031	0.035
	50cm	0.018	0.025	0.016	0.017	0.050	0.053

3.6 Discussion

In this study, we have evaluated the usefulness and applicability of four different data assimilation methods for joint parameter and state estimation of the VIC and CLM land surface models using a 5-month calibration (assimilation) data set of distributed SPADE soil moisture measurements at 5, 20 and 50 cm depth in the Rollesbroich test site in the Eifel mountain range in western Germany. We used the EnKF with state augmentation or dual estimation, respectively, and the PF with a simple, statistically deficient, or more sophisticated, MCMC-based parameter resampling method. The "calibrated" LSM models were tested using water content data from a 5-month evaluation period. The uniqueness of the present work resides in the application of these four joint or dual parameter and state estimation methods to real-world data.

Our results demonstrated that joint inference of the VIC and CLM soil parameters improved considerably soil moisture characterization during the evaluation period compared to the mean water content predictions of an open loop run derived via averaging of simulations of many different realizations drawn randomly from the prior parameter distribution. This is particularly true for CLM, the two deeper soil layers, and the EnKF-AUG and EnKF-DUAL methods (but followed closely by PMCMC). Despite this improvement in model performance over an open-loop simulation, VIC and CLM do not adequately characterize soil moisture dynamics of the top layer (5 cm measurement depth) during the evaluation period (RMSE

values of about 0.05 cm^3/cm^3). We posit that these two models do not characterize adequately processes such as water infiltration, soil evaporation, and/or root water uptake (transpiration), which govern rapid variations in soil moisture storage in the top soil. VIC also appeared deficient at 50 cm depth during the evaluation period with RMSE values of about 0.07 cm^3/cm^3 which are much larger than their counterparts of approximately 0.02 cm^3/cm^3 derived from CLM. These results favour the use of CLM which uses a more physics-based description of soil water movement, storage, and associated hydrological fluxes at the Rollesbroich site.

The improvement in quality-of-fit of the VIC and CLM models compared to an open-loop run does not necessarily imply that the estimated parameter values of VIC and CLM characterize better the hydraulic properties and maximum baseflow velocity of the soils of the Rollesbroich experimental test site. Assimilation studies with synthetically generated data help to ascertain whether the model parameters converge properly to their "true" values, yet this is difficult to confirm with real-world measurements. State estimation will, without doubt, help reduce the impact of epistemic errors and systematic biases of LSM input and forcing data on parameter inference during the assimilation period (e.g. Vrugt et al., 2005). But the calibrated parameter values derived with state estimation do not necessarily guarantee a consistent and adequate model performance during an independent evaluation period without state estimation. Indeed, without assimilation the simulated states may diverge from their "measured" values and deteriorate model performance in an evaluation period. This begs the question which parameter values we should use to predict future system behaviour outside an assimilation period? Should we use parameter estimates derived with state estimation or should we use their values derived via batch calibration (optimization) without recursive adjustments to the state variables? This dilemma is illustrated further in Vrugt et al. (2006) by modelling of a subsurface tracer test using data from Yucca Mountain, Nevada, USA. We conclude that the enhanced performance of VIC and CLM during the evaluation period compared to our open-loop simulation is due to improved estimates of the initial states and the soil parameters.

In our implementation of the EnKF and PF, the VIC and CLM parameters were assumed to be time-variant and their values updated jointly with the model states at each assimilation time step. The 5-month calibration period we used herein involves several large precipitation events, and as a consequence, the soil profile is rather wet. The resulting parameter estimates might therefore not be representative for dry periods with much lower moisture values of the soil profile. What is more, the assumption of spatial homogeneity might not characterize adequately the distributed soil properties of the Rollesbroich site and induce temporal variability in the VIC and CLM parameters. Bias in model input and measurement errors of the forcing data also contribute to the temporal fluctuations of the estimated parameter values. These temporal parameter variations are meaningful in some cases as they can help diagnose structural model inadequacies and/or biases in model input and forcing data. Kurtz et al. (2012) successfully estimated a temporally-variant parameter with the EnKF, but these authors concluded that the algorithm needs a considerable spin-up period to "warm-up" to new parameter values. Vrugt et al. (2013) found considerable temporal non-stationarity in the

parameters estimated by PMCMC as a result of the small time period used to calculate the acceptance probability of candidate particles. This finding is in agreement with the results of PMCMC in our study. Of course, we could have assumed time-invariant parameters via a method such as SODA, yet this would have enhanced significantly computational requirements. Fortunately, parameters estimated via our implementation of the EnKF exhibit asymptotic properties during the assimilation period (e.g. see Shi et al. (2015)). This is particularly true for highly sensitive parameters. An example of this was parameter D_m of VIC which quickly converged to values of around 1 – 2 mm after assimilating just a handful of soil moisture observations.

It is difficult to assess whether the inferred VIC and CLM parameter values will do a good job at predicting soil moisture dynamics at the different measurement depths during a much longer evaluation period with wet and dry conditions. As the estimated parameters represent apparent properties of the Rollesbroich site, one may expect their calibrated values not to change too much over time. We would need additional soil moisture data and/or other type of measurements to corroborate this. Nevertheless, the apparent parameter values derived herein improve characterization of soil moisture dynamics at the Rollesbroich site compared to a separate state estimation run with VIC and CLM using parameters drawn randomly from the prior distribution, or open loop simulation using the ensemble mean model output of a large cohort of parameter vectors drawn randomly from the prior parameter distribution (initial parameter ensemble).

The different data assimilation methods (EnKF-AUG, EnKF-DUAL, RRPF and PMCMC) led to a rather similar performance of VIC during the calibration and evaluation period. The only exception to this was the anomalous RMSE value of RRPF at the 50 cm measurement depth during the calibration period. This was explained by the slow convergence of the maximum baseflow velocity in RRPF. Our results for VIC further demonstrated that the results of EnKF-AUG and EnKF-DUAL were equivalent for a 10% and 20% rainfall error. Moreover, the use of a larger value of the scaling s in RRPF reduced considerably the RMSE values of VIC in the calibration data period, particularly at the 50 cm measurement depth, whereas model performance was hardly improved during the evaluation period.

For CLM, larger differences were observed in the performance of the different data assimilation methods. This larger disparity among the methods is explained by the considerably larger number of soil layers (ten) used by CLM. This increased significantly the dimensionality of the parameter estimation problem. The overall best results at the 5, 20 and 50 cm measurement depths were observed for EnKF-AUG and EnKF-DUAL with RMSE values that were somewhat smaller than their counterparts derived from PMCMC. This was true for both the calibration and evaluation periods. The RRPF exhibited the worst performance, in part determined by the use of a relatively small ensemble of $N = 100$ particles. The superiority of the EnKF-AUG and EnKF-DUAL methods for CLM is consistent with our expectations articulated previously in section 3.1. The analysis step of the EnKF makes it much easier for EnKF-AUG and EnKF-DUAL to track the measured soil moisture dynamics, thereby promoting convergence in high-dimensional state-parameter spaces. PF-based methods, on the contrary, deteriorate in robustness and efficiency with

larger dimensionality of the state-parameter space as they lack a state analysis step and approximate the transient state-parameter PDF via the particles' likelihoods. This likelihood is only a low-dimensional summary statistic of the distance between the forecasted and measured values of the states. Resampling with MCMC via the likelihood thus becomes increasingly more difficult in high-dimensional state-parameter spaces. For CLM, the PMCMC method still achieves comparable results to EnKF-AUG and EnKF-DUAL as the dimensionality of the state-parameter PDF of this model is only somewhat larger than its counterpart of VIC. Of course, the use of a larger ensemble size makes it easier to characterize the transient state-parameter PDF, but at the expense of a significantly increased CPU-cost. For PMCMC, multiple different MCMC resampling steps can also enhance significantly the particle ensemble by allowing each particle trajectory to improve its likelihood. Yet, this deteriorates significantly the efficiency of implementation as each candidate particle requires a separate model evaluation of VIC or CLM to determine its likelihood. Thus, for LSMs with relatively few state variables and model parameters, we expect the EnKF and PF methods to achieve a comparable performance. For larger dimensional state-parameter spaces we would recommend EnKF-AUG and EnKF-DUAL, unless one can afford a very large number of particles.

Finally, our results demonstrated that the differences between the soil moisture simulations of VIC and CLM are much larger than the discrepancies among the four data assimilation methods. Overall, CLM performed better than VIC, especially at 50 cm measurement depth. Of course, we cannot generalize this finding to other sites, but VIC's rather poor characterization of soil moisture dynamics at 50 cm depth (systematic underestimation during first 2-3 months) warrants investigation into the use of a variable water table depth in this model to account for interactions between the variably-saturated soil domain and the groundwater reservoir of the Rollesbroich site. CLM simulates such interactions and the resulting variations in the water table depth affect soil water movement in the unsaturated zone.

3.7 Conclusions

In this study, we have evaluated the usefulness and applicability of four different data assimilation methods for joint parameter and state estimation of the Variable Infiltration Capacity Model (VIC) and the Community Land Model (CLM) using a 5-month calibration (assimilation) period (March – July, 2012) of areal-averaged SPADE soil moisture measurements at 5, 20 and 50 cm depth in the Rollesbroich experimental test site in the Eifel mountain range in western Germany. This watershed is part of TERENO observatories and extensively monitored since 2011 to catalogue long-term ecological, social and economic impact of global change at regional level. We used the EnKF with state augmentation or dual estimation, respectively, and the PF with a simple, statistically deficient, or more sophisticated, MCMC-based parameter resampling method. The "calibrated" LSM models were tested using SPADE water content measurements from a 5-month evaluation period (August – December, 2012). The performance of the four different state and parameter estimation methods appeared rather similar during the evaluation period with a slightly better

performance of the augmentation and dual estimation methods, but followed closely by PMCMC and then RRPF. The differences between the soil moisture simulations of VIC and CLM are much larger than the discrepancies among the four data assimilation methods. Overall, the best performance was observed for CLM. The large systematic underestimation of water storage at 50 cm depth by VIC during the first few months of the evaluation period questions, in part, the validity of its fixed lower boundary condition at the bottom of the modelled soil domain. This approach ignores the movement of water into and out of the groundwater reservoir of the Rollesbroich site. CLM simulates interactions of the modelled soil domain with the Rollesbroich aquifer via the use of a variable water depth at the lower boundary.

Appendix 3.A Parametrization of the VIC model

The integrated water balance in the VIC can be written as follows:

$$\partial S/\partial t = P - T - E - Q_{\mathrm{d}} - Q_{\mathrm{b}}, \tag{3.A1}$$

where S [L] is storage, t [T] denotes time, $\partial S/\partial t$ [$\mathrm{LT^{-1}}$] signifies the change in water storage, and P, T, E, Q_{d}, and Q_{b}[$\mathrm{LT^{-1}}$] represent fluxes of precipitation, canopy transpiration, soil evaporation, direct runoff, and baseflow, respectively. Bare soil evaporation, E, is calculated using the equation of Francini and Pacciani (1991). The canopy transpiration flux, T, is equivalent to the total uptake of water by plant roots in our soil profile and is estimated following Blondin (1991) and Ducoudre et al. (1993) using the bulk equation of Monteith (1963). In this "single-leaf" approach, the canopy resistance is assumed to be a function of the minimum canopy resistance and environmental variables (factors) such as photosynthetically active radiation, ambient temperature, vapour pressure deficit, and soil moisture content. We refer to Wigmosta et al. (1994) for a detailed discussion of these four limiting variables, including their mathematical description and parameterization used herein. When it rains the leaves become covered with a thin film of water and the transpiration flux is suppressed temporarily until the intercepted water has evaporated at the potential rate derived from the Penman-Monteith equation (Shuttleworth, 2007). To calculate foliage storage the maximum canopy water storage is set to a multiple of 0.2 of the leaf area index (Dickinson, 1984). Direct runoff, Q_{d}, reduces the amount of rainfall that can infiltrate in the top soil during wet conditions, and is calculated using (Liang et al., 1996):

$$Q_{\mathrm{d}} = \frac{1}{\Delta t}\begin{cases} P\Delta t - \left(z_1(\phi_1-\theta_1) + z_2(\phi_2-\theta_2) - (z_1\phi_1 + z_2\phi_2)\left(1 - \frac{P\Delta t + I_0}{I_{\max}}\right)^{(1+b)}\right) & \text{if } P\Delta t \le (I_{\max} - I_0) \\ P\Delta t - \left(z_1(\phi_1-\theta_1) + z_2(\phi_2-\theta_2)\right) & \text{otherwise,} \end{cases} \tag{3.A2}$$

where the triples $\{\theta_1, \phi_1, z_1\}$ and $\{\theta_2, \phi_2, z_2\}$ signify the volumetric moisture content [$\mathrm{L^3L^{-3}}$], porosity [-], and depth [L] of the top layer of the soil and the next or second layer immediately below it, respectively, I_0 [L] and $I_{\max}$ [L] denote the actual and maximum moisture capacity of the soil, respectively, Δt [L] signifies the integration time step that is

used to solve numerically equation (3.A1), and b [-] is an unknown shape parameter that measures the spatial variability of the soil moisture capacity. Note that the integration time step, Δt, is often missing from equation (3.A2) in VIC-manuals or literature publications. This is consistent if rainfall, P, is expressed in units of depth, say mm, but invalid in conjunction with equation (3.A1) which requires as input precipitation rates. If the integration time step is set equivalent to the time unit of the measured precipitation rates then $\Delta t = 1$. This approach, however can introduce large numerical errors, particularly if the soil is close to saturation. The dimensionless parameter b is usually determined via calibration by fitting VIC against a historical record of soil moisture observations and/or flux data.

The direct runoff in equation (3.A2) is not only a function of the water saturation of the first layer, but also depends on the moisture content of the second underlying soil layer. To be able to track adequately the large storage variations of the top soil observed in experimental data, the first layer of VIC must be taken rather small. Consequently, this top layer will saturate quickly in response to rainfall as it exhibits a rather negligible water holding capacity. Hence, VIC uses the available storage of the first and second layer to determine the excess precipitation, which is set equivalent to Q_{d}. If the rainfall depth exceeds the available moisture capacity of the soil, $(I_{\max} - I_0)$, then the excess precipitation is removed via surface runoff. Otherwise, if $P\Delta t \leq (I_{\max} - I_0)$, then a large fraction of the rainfall will infiltrate depending on the soil's available storage and the spatial variability of the moisture capacity within the grid cell. The values of I_0 and $I_{\max}$ are estimated from (Zhao, 1992):

$$I_0 = I_{\max}\left(1 - (1 - A_{\mathrm{s}})^{(1/b)}\right) \tag{3.A3}$$

$$I_{\max} = (1 + b)(z_1\phi_1 + z_2\phi_2) \quad , \tag{3.A4}$$

where A_{s} [-] is the areal fraction of the grid cell that is saturated (infiltration capacity equal to $\mathrm{I}_{\max}$):

$$A_{\mathrm{s}} = 1 - \left(1 - \frac{z_1\theta_1 + z_2\theta_2}{\phi_1 + \phi_2}\right)^{(b/(1+b))} \tag{3.A5}$$

The baseflow, Q_{b}, originates from the bottom (third) soil layer and is calculated using the formulation of the Arno model (Franchini and Pacciani, 1991):

$$Q_{\mathrm{b}} = \begin{cases} \frac{D_{\mathrm{S}}D_{\mathrm{m}}}{W_{\mathrm{S}}\phi_3}\theta_3 & \text{if } 0 \leq \theta_3 \leq W_{\mathrm{s}}\phi_3 \\ \frac{D_{\mathrm{S}}D_{\mathrm{m}}}{W_{\mathrm{S}}\phi_3}\theta_3 + \left(D_{\mathrm{m}} - \frac{D_{\mathrm{S}}D_{\mathrm{m}}}{W_{\mathrm{S}}}\right)\left(\frac{\theta_3 - W_{\mathrm{S}}\phi_3}{\phi_3 - W_{\mathrm{S}}\phi_3}\right)^2 & \text{otherwise} \end{cases} , \tag{3.A6}$$

where D_{m} [LT^{-1}] is the maximum baseflow velocity, and D_{S} and W_{S} are dimensionless fractions of D_{m} and the porosity of the third layer, ϕ_3, respectively. The baseflow flux is linearly dependent on the water content of the third layer if $\theta_3 \leq W_{\mathrm{s}}\phi_3$, and increases nonlinearly with water storage of the third layer if $\theta_3 \geq W_{\mathrm{s}}\phi_3$.

Now we have discussed the different fluxes from the soil domain simulated by VIC we can now write differential equations of the moisture dynamics in the individual soil layers (see also Liang et al., 1996).

$$\begin{aligned}\frac{\partial\theta_1}{\partial t}z_1 &= P + Q_{1,2} - Q_{\mathrm{d}} - R_1 - E\\ \frac{\partial\theta_2}{\partial t}z_2 &= Q_{2,3} - Q_{1,2} - R_2\\ \frac{\partial\theta_3}{\partial t}z_3 &= -Q_{2,3} - R_3 - Q_{\mathrm{b}}\end{aligned} \quad , \tag{3.A7}$$

where $Q_{i,i+1}$ [LT^{-1}] is the vertical flux of water between two adjacent soil layers i and $i+1$, R_i [LT^{-1}] signifies the root water uptake of the ith layer, and $i = \{1,2,3\}$. Downward fluxes are negative to be consistent with convention used in soil hydrology. The canopy transpiration flux is equal to the total water uptake by the plant roots, thus $T = R_1 + R_2 + R_3$. All three soil layers contain roots and thus contribute to transpiration in our application of VIC to the Rollesbroich site. The vertical flux of water between two adjacent soil layers is assumed to be equivalent to the hydraulic conductivity of the upper layer. VIC computes the hydraulic conductivity of each soil layer using the formulation of Brooks and Corey (1988):

$$Q_{i,i+1} = -k_{s,i}\left(\frac{\theta_i - \theta_{r,i}}{\phi_i - \theta_{r,i}}\right)^{\beta_i} \quad (i = 1,2), \tag{3.A8}$$

where $k_{s,i}$ [LT^{-1}] and $\theta_{r,i}$ [L^{3}L^{-3}] signify the saturated hydraulic conductivity and the residual volumetric moisture content of the ith soil layer, respectively. The minus sign at the right-hand-side of equation (3.A8) matches the direction of the flux. The dimensionless exponent β_i should be larger than 3.0.

The use of three soil layers by VIC makes it difficult to describe accurately the vertical moisture distribution in the vadose zone. Indeed, VIC cannot distinguish between saturated and partially-saturated areas in a given soil layer. As a consequence, the baseflow flux, Q_{b}, is made up of water from the unsaturated zone and the groundwater (Liang et al., 1996; Liang et al., 2003). Liang et al. (2003) developed a new parameterization, which considers explicitly effects of surface and groundwater interactions on soil moisture, transpiration, soil evaporation, runoff and recharge. This parameterization, coined VIC-ground, enhanced considerably water storage in the lower soil layer compared to VIC.

Appendix 3.B Parametrization of the CLM model

This Appendix summarizes the main equations of CLM which are used to describe variably-saturated water flow in the soil domain of our experimental catchment. The model uses a water balance formulation similar to equation (3.A1) of Appendix 3.A to simulate moisture storage and movement in the soil of each grid-cell of the application domain of interest. Yet, CLM includes a more exhaustive description of all the different processes that determine the water storage of the land surface. This includes canopy water, surface water, snow water, soil

water, soil ice and water stored in the unconfined aquifer. In addition to surface and subsurface runoff, CLM also considers runoff from glaciers, wetlands and lakes.

Fluxes, F [$ML^{-2}T^{-1}$], of ground evaporation, interception evaporation, and vegetation transpiration are calculated by CLM using the following general expression (Schwinger et al., 2010; Oleson et al., 2013):

$$F = \frac{\rho_a}{r_a}(q - q_a), \tag{3.B1}$$

where ρ_a [ML^{-3}] is the density of air, r_a [TL^{-1}] signifies the aerodynamic resistance, q [MM^{-1}] is the specific humidity of the soil pores (for soil evaporation) or canopy (for vegetation transpiration and interception evaporation) or the saturated specific humidity of snow or surface water, and q_a [MM^{-1}] denotes the specific humidity at atmospheric level if ground evaporation is calculated, or the saturated specific humidity within the canopy if canopy evapotranspiration is calculated. The values of r_a, q and q_a are based on Monin-Obukhov similarity theory (Schwinger et al., 2010; Oleson et al., 2013).

We use 10 soil layers (see table 3.2) in CLM to solve for the vertical storage and movement of water. Whenever the index i is used we mean 'for all $i \in \{1, \dots, 10\}$'. The saturated hydraulic conductivity, $k_{s,i}$ [LT^{-1}], saturated volumetric moisture content, $\theta_{s,i}$ [L^3L^{-3}], thermal conductivity, λ_i [$WL^{-1}K^{-1}$], soil matric head at saturation, $\psi_{s,i}$ [L], and Clapp-Hornberger exponent, B_i [-], of each soil layer are derived from built-in pedotransfer functions. These functions use as inputs textural data (Clapp and Hornberger, 1978; Cosby et al., 1984) and/or the organic matter fraction (Lawrence and Slater, 2008) of each soil layer as follows:

$$\psi_{s,i} = -10(1 - f_{\mathrm{om},i})10^{(1.88-0.0131 f_{\mathrm{sd},i})} - 10.3 f_{\mathrm{om},i} \quad \text{[mm]} \tag{3.B2}$$

$$B_i = (1 - f_{\mathrm{om},i})(2.91 + 0.159 f_{\mathrm{cl},i}) + 2.7 f_{\mathrm{om},i} \quad \text{[-]} \tag{3.B3}$$

$$\theta_{s,i} = (1 - f_{\mathrm{om},i})(0.489 - 0.00126 f_{\mathrm{sd},i}) + 0.9 f_{\mathrm{om},i} \quad , \quad \text{[-]} \tag{3.B4}$$

$$k_{s,i} = \left(1 - f_{\mathrm{p},i}\right)\left[\frac{1 - f_{\mathrm{om},i}}{0.0070556 \cdot 10^{(-0.884+1.53 f_{\mathrm{sd},i})}} + \frac{f_{\mathrm{om},i} - f_{\mathrm{p},i}}{k_{\mathrm{s,om}}}\right]^{-1} + f_{\mathrm{p},i} k_{\mathrm{s,om}} \quad \text{[mm/s]} \tag{3.B5}$$

where $f_{\mathrm{sd},i}$ and $f_{\mathrm{cl},i}$, and $f_{\mathrm{om},i}$ signify the fractions of sand, clay and organic matter, respectively, $f_{\mathrm{p},i}$ [-], denotes the fraction of connected organic matter, $k_{s,\mathrm{om}}$ [mm/s], is the saturated hydraulic conductivity of organic soils. If the organic matter fraction, $f_{\mathrm{om},i}$, is smaller than 0.5, then $f_{\mathrm{p},i} = 0$, otherwise $f_{\mathrm{p},i} = 0.5 f_{\mathrm{om},i}(f_{\mathrm{om},i} - 0.5)^{-0.139}$.

Vertical flow in the unsaturated zone is governed by rainfall infiltration, surface and subsurface runoff, root water uptake (canopy transpiration), and groundwater interactions. A modified Richards' equation is used to predict water storage and movement in the variably-saturated soils of the Rollesbroich site:

$$\frac{\partial \theta_i}{\partial t} = \frac{\partial}{\partial z}\left[k_i\left(\frac{\partial(\psi_i + z_i - C_i)}{\partial z}\right)\right] - R_i = \frac{\partial}{\partial z}\left[k_i\left(\frac{\partial(\psi_i - \psi_{\mathrm{e},i})}{\partial z}\right)\right] - R_i, \tag{3.B6}$$

where θ_i [L^3L^{-3}], ψ_i [L], k_i [LT^{-1}], z_i [L], and $\psi_{e,i}$ [L] denote the volumetric water content, matric head, hydraulic conductivity, depth, and equilibrium matric head of the ith soil layer, $C_i = \psi_{e,i} + z_i$, and R_i [T^{-1}] is the loss of water via root water uptake (canopy transpiration). Note that equation (3.B6) omits conveniently the evaporation flux from the first (top) layer. The hydraulic conductivity, k_i, of each layer depends on its moisture content, saturated hydraulic conductivity, and exponent B, and these values of the adjacent soil layer immediately below, with the exception of the bottom layer (Oleson et al., 2013; Han et al., 2014a). The use of the constant C_i in equation (3.B6) allows CLM to simulate matric head variations below the water table. This modification maintains a hydrostatic equilibrium soil moisture distribution, and fixes a critical deficiency of the θ-based formulation of Richards' equation (Zeng and Decker, 2009; Oleson et al., 2013).

The matrix head, ψ_i, and equilibrium matric head, $\psi_{e,i}$, of each soil layer are computed as follows:

$$\psi_i = \psi_{s,i}\left(\frac{\theta_i}{\theta_{s,i}}\right)^{-B_i} \quad \text{and} \quad \psi_{e,i} = \psi_{s,i}\left(\frac{\theta_{e,i}}{\theta_{s,i}}\right)^{-B_i}, \tag{3.B7}$$

with

$$\theta_{e,i} = \theta_{s,i}\left(\frac{\psi_{s,i} + z_\nabla - z_i}{\psi_{s,i}}\right)^{(-1/B_i)}, \tag{3.B8}$$

where z_∇ [L] is the depth of the water table.

The bottom boundary condition of equation (3.B6) depends on the depth of the water table. This depth, z_∇, is calculated following Niu et al. (2007) and assumes the presence of an unconfined aquifer below the soil column. If the water table is within the modelled soil column (top 10 layers), then a constant water storage is assumed in the unconfined aquifer (soil column is saturated with water below water table) and a zero-flux bottom boundary condition is used. Recharge, q_{rec} [LT^{-1}], to the unconfined aquifer is calculated as follows:

$$q_{rec} = -k_{wt}\left(\frac{-\psi_{wt}}{z_\nabla - z_{wt}}\right), \tag{3.B9}$$

where k_{wt} [LT^{-1}], ψ_{wt} [L], and z_{wt} [L] signify the hydraulic conductivity, matric head, and depth of the layer that contains the groundwater table. Drainage, q_{drain} [$ML^{-2}T^{-1}$], from the aquifer is calculated via a simple TOPMODEL-based (SIMTOP) scheme (Niu et al., 2005) using:

$$q_{drain} = 10\sin(\varepsilon)\exp(-2.5z_\nabla), \tag{3.B10}$$

where ε [Rad] signifies the mean topographic slope of the respective grid cell. The change in the water table depth is then given by:

$$\Delta z_\nabla = \frac{(q_{rec} - q_{drain})\Delta t}{S_y}, \tag{3.B11}$$

where S_y [-] denotes the specific yield which depends on the properties of the soil.

Chapter 4 : Comparison of different assimilation methodologies of groundwater levels to improve predictions of root zone soil moisture with an integrated terrestrial system model

*adapted from: Zhang, H., Kurtz, W., Kollet, S., Vereecken, H., and Hendricks Franssen, H.-J.: Comparison of different assimilation methodologies of groundwater levels to improve predictions of root zone soil moisture with an integrated terrestrial system model, Advances in Water Resources, 111, 224-238, https://doi.org/10.1016/j.advwatres.2017.11.003, 2018.

4.1 Introduction

Precise knowledge of spatial and temporal variations in root zone soil moisture content is important for agriculture, weather prediction and drought monitoring (Lue et al., 2011). However, information about root zone soil moisture is usually limited due to the small volume support of point scale measurements (Grayson and Western, 1998) and the high level of uncertainty associated with (land surface) model predictions, which is caused by uncertain input parameters and atmospheric forcings (Houser et al., 2001). Remote sensing techniques allow monitoring of surface soil moisture content over large areas, but these measurements are limited to the top few centimeters of the soil and are not reliable for dense vegetation (Du et al., 2000). In recent years, some work has been carried out to improve the prediction of root zone soil moisture content. Using data assimilation techniques, ground-based surface soil moisture measurements or remotely-sensed surface soil moisture data have been combined with land surface models, which simulate surface and root-zone soil moisture content, to update soil moisture estimates for all soil layers (Walker et al., 2002; Walker et al., 2003b; Sabater et al., 2007; Crow et al., 2008; Das et al., 2008; Kumar et al., 2009; Pipunic et al., 2011; Ford et al., 2014; Han et al., 2014a; De Lannoy and Reichle, 2016). Kumar et al. (2009) concluded that the potential of surface soil moisture assimilation to improve root-zone soil moisture characterization was higher when the surface–root zone coupling was stronger. Walker et al. (2002) showed that the soil moisture profile cannot be retrieved from near-surface soil moisture measurements when the near-surface and deep soil layers become decoupled, such as during extreme drying events. Das et al. (2008) found that the assimilation of remotely sensed surface soil moisture content improved soil moisture content estimation for shallow soil (0-0.50m) but hardly for the deeper soil layers (0.50m-3.86m). Frod et al. (2014) demonstrated that the relationship between near-surface (5-10cm) and root zone (25-60cm) soil moisture was generally strong. Pipunic et al. (2011) stated that there was no clear evidence of an ability to strongly improve soil moisture content prediction for deeper layers using only surface information. In summary, the updating of root zone soil moisture by combining surface soil moisture from satellite and land surface model predictions via data assimilation is a way forward, but often improvement is only limited.

Groundwater effects on root zone soil moisture are either neglected or not explicitly treated in most land surface models (Chen and Hu, 2004; Kollet and Maxwell, 2008). A shallow groundwater table is more likely to lead to surface runoff because of saturation excess, and to

supply water to the atmosphere at the rate demanded by the atmosphere. On the other hand, deeper groundwater tables generally indicate drier areas. In this situation, surface runoff is likely to be generated by the infiltration excess runoff mechanism, the groundwater is recharged when the infiltration is enhanced, and evaporation is more often limited by the available soil moisture. Under both conditions, soil moisture content is changed through its interaction with the groundwater (Liang and Guo, 2003; Miguez-Macho et al., 2008; Miguez-Macho and Fan, 2012; Zhu et al., 2013).

Recently, a number of modeling platforms with varying complexity which couple groundwater, land surface, and atmospheric models have emerged aiming to improve the estimation of water flow in the unsaturated zone (Kollet and Maxwell, 2008; Maxwell, 2009; Davin et al., 2011; Tian et al., 2012; Maxwell et al., 2015). For example, the HIRHAM regional climate model is coupled with the MIKE-SHE hydrological model (Larsen et al., 2014), the Common Land Model is integrated into ParFlow (ParFlow-CLM) (Maxwell and Miller, 2005; Kollet and Maxwell, 2008). Another example is the atmosphere-surface-subsurface Terrestrial System Modeling Platform (TerrSysMP) (Shrestha et al., 2014). TerrSysMP and ParFlow-CLM have been used in a number of simulation studies like the investigation of the role of topography and subsurface heterogeneity on the interactions between land surface energy fluxes and groundwater dynamics (Rihani et al., 2010), the role of topography and subsurface heterogeneity on spatial soil moisture variability and discharge (Gebler et al., 2017), the impact of subsurface hydrodynamics on the lower atmosphere (Shrestha et al., 2014), the influence of crop-specific physiological properties on the partitioning of land surface energy fluxes and the resulting modifications in the heat and moisture budgets of the atmospheric boundary layer (Sulis et al., 2015), and the influence of groundwater dynamics on land surface processes (net radiation, latent heat flux, sensible heat flux and ground heat flux) (Kollet and Maxwell, 2008).

Information of groundwater level is available in many places and at regional and national scales as it can be continuously measured by automatic sensing devices at low cost and high accuracy, like the Collaborative National Groundwater Monitoring Network Program for the United States (Subcommittee on Ground Water, 2011). As mentioned above, near surface soil moisture content hardly provides information about root zone soil moisture content and groundwater levels may contain valuable information about the unsaturated zone. Integrated models like TerrSysMP are expected to be suited to explore in an optimal way the information provided by groundwater levels as well as near surface soil moisture content data, using sequential data assimilation techniques like ensemble Kalman Filter (EnKF) (Evensen, 1994; Burgers et al., 1998).

EnKF has been applied successfully in unsaturated flow and groundwater flow problems. The contributions relevant in the context of this study are the assimilation of water table depth or piezometric head (Chen and Zhang, 2006; Franssen and Kinzelbach, 2008; Li et al., 2012; Kurtz et al., 2014; Shi et al., 2014), soil moisture content (Margulis et al., 2002; Reichle et al., 2002; Montzka et al., 2013; Erdal et al., 2014; Shi et al., 2014; Pasetto et al., 2015), brightness temperature (Margulis et al., 2002; Crow and Wood, 2003; Sabater et al., 2007; Das et al., 2008; Han et al., 2014a), and surface radiometric temperature (Crow et al., 2008).

However there are few studies focusing on the assimilation of groundwater levels to improve the characterization of the unsaturated zone. Zhang et al. (2016) assimilated both groundwater head and soil moisture content with ensemble transform Kalman filter (ETKF) in the MIKE SHE hydrological model and emphasized the necessity of using localization when assimilating both groundwater head and soil moisture. Rasmussen et al. (2015) also used ETKF to assimilate groundwater head and stream discharge to study the relationship between the filter performance and the ensemble size. Shi et al. (2014, 2015b) and Shi et al. (2015a) employed EnKF to investigate the impacts of multivariate hydrological data assimilation including groundwater levels on estimating unsaturated flow parameters with synthetic experiments and real-world experiments. In our study we focus on the comparison of different methodologies for the assimilation of groundwater levels in integrated hydrological models. In addition, the methodological developments made in this work aim for high-dimensional problems and spatially heterogeneous fields of hydraulic parameters. If groundwater levels are assimilated in terms of pressure head the strongly skewed and non-Gaussian pressure distributions for dry soils cause problems for sequential data assimilation algorithms as these algorithms perform optimally only for Gaussian distributions. The water retention function maps the very negative values to a very small range of water content values, and is highly nonlinear. Therefore, if EnKF is applied in a standard form, the nonlinear state propagation would cause large errors. Erdal et al. (2015) discussed the importance of state transformations in EnKF when dealing with strong nonlinearities for unsaturated flow modeling. In this work, a complication is that groundwater level data, although often showing a correlation with soil moisture content, are in general only weakly correlated with soil moisture content of the upper soil layers. This raises the question what is the sphere of influence of groundwater level data and whether the complete unsaturated zone should be updated with groundwater level data. In summary, two problems to be solved for assimilating groundwater level data in integrated hydrological models are: (1) strongly skewed pressure distributions under dry conditions; (2) detection of the sphere of influence of groundwater level data in the context of cross-compartmental data assimilation.

In order to test different methodologies for groundwater level (and surface soil moisture) assimilation in the integrated model TerrSysMP, a series of synthetic experiments was carried out in this work. The remainder of this study is organized as follows. In section 4.4.2, we briefly review the TerrSysMP model used to simulate the soil moisture and subsurface pressure distributions, as well as energy exchange fluxes between the land and the atmosphere. The land surface model CLM and subsurface model ParFlow are described separately. Assimilation methodologies with the EnKF are also explained in this section. Section 4.4.3 then introduces our experiment setup and in section 4.4.4 the main findings of our assimilation study are presented. Discussion and conclusion are presented in section 4.4.5 and section 4.4.6 respectively.

4.2 Materials and methods

In this study, we perform data assimilation experiments with a coupled subsurface-land surface model. In order to illustrate the technical setup for these experiments, section 4.2.1

summarizes the utilized models, section 4.2.2 explains the implementation of data assimilation methodologies for this study, and introduces our data assimilation platform.

4.2.1 Terrestrial System Modelling Platform (TerrSysMP)

TerrSysMP (Shrestha et al., 2014) is a modular, scale-consistent terrestrial system model composed of well-established models for the atmosphere (COSMO) (Baldauf et al., 2011), the land surface (CLM) (Oleson et al., 2008) and the subsurface (ParFlow) (Ashby and Falgout, 1996; Jones and Woodward, 2001; Kollet and Maxwell, 2008). Its modularity makes it possible to run in fully coupled way (COSMO+CLM+ParFlow), partly coupled way (CLM+ParFlow/CLM+COSMO), and uncoupled way by running each model individually (COSMO/CLM/ParFlow). In our work, the partly coupled (ParFlow+CLM) TerrSysMP configuration is used.

The land surface component of TerrSysMP, CLM, calculates the mass and energy balance at the land surface including evaporation from the ground surface, transpiration from plants, sensible and ground heat fluxes, and freeze-thaw processes (Oleson et al., 2008; Shrestha et al., 2014). 10 soil layers are internally defined with a total extend of about 3m. There is no lateral flow between grid cells because water and energy flows are calculated only in the vertical direction. CLM input includes atmospheric forcing data (i.e precipitation, wind speed, incoming shortwave and longwave radiation, air pressure, air temperature and humidity), land surface data including information on plant functional type (PFT), and adjustable parameters and physical constants. CLM uses soil properties like soil texture and bulk density in combination with model internal pedotransfer functions to derive soil hydraulic and thermal parameters like saturated hydraulic conductivity (Oleson et al., 2004; Oleson et al., 2008).

The subsurface part of TerrSysMP consists of the subsurface flow model ParFlow. In ParFlow, a 2D distributed overland flow simulator is implemented into a 3D variably saturated groundwater flow (Kollet and Maxwell, 2006). The overland flow boundary condition helps ParFlow to simulate fully-coupled surface and subsurface flow via a mixed form of the 3D Richards equation and the kinematic wave equation. ParFlow solves for water pressure at every time step and calculates the saturation field from which soil moisture and water table depth are determined by the pressure-saturation relationship, for example according the van Genuchten formulation (Van Genuchten, 1980). More details about the model equations, the discretization and the numerical implementation can be found in (Ashby and Falgout, 1996; Jones and Woodward, 2001; Kollet and Maxwell, 2006). ParFlow input includes soil hydraulic parameters like saturated hydraulic conductivity and residual soil water content, van Genuchten parameters like α and n, and soil porosity.

Data from CLM and ParFlow are exchanged via the coupling software OASIS-MCT (Valcke, 2013) which is a library providing a generic interface to exchange information between standalone executable codes in memory. Originally, CLM only takes into account 1D vertical flow in the unsaturated zone with a decoupled surface routing as the upper boundary condition and a simple parameterization of groundwater table as a lower boundary condition. ParFlow overcomes these limitations with an overland flow boundary condition and 3D

variable saturated groundwater flow. ParFlow provides CLM with its calculated subsurface pressure (ψ) and saturation (S_w) values for the 10 uppermost subsurface layers and, in return, CLM provides the upper boundary condition for ParFlow which consists of the soil infiltration values (q_{inf}) which are calculated based on the land surface fluxes of CLM (precipitation, interception, total evaporation, total transpiration). Thus, the 1D column soil moisture prediction of CLM is replaced by the 3D formulation in ParFlow. The information exchange between CLM and ParFlow is shown schematically in figure 4.1. The thicknesses of the 10 uppermost subsurface layers should be consistent with those of the 10 soil layers in CLM and also the porosities in both models need to be the same.

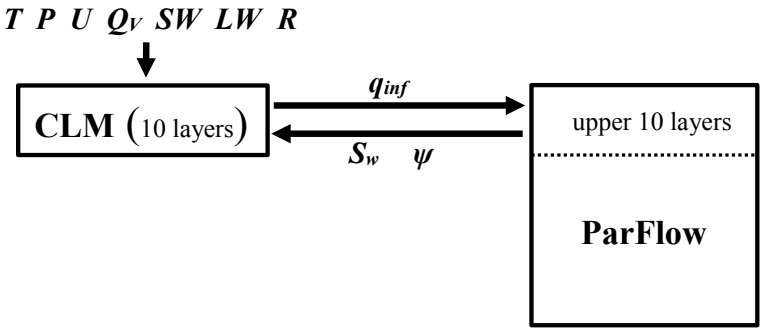

Figure 4.1 Coupling of the TerrSysMP component models ParFlow (subsurface) and CLM (land surface) by OASIS-MCT. Model forcings for the land surface component are: T (air temperature), P (air pressure), U (wind velocity), Q_v (specific humidity), SW (incoming shortwave radiation), LW (incoming longwave radiation) and R (precipitation). The exchanged fluxes and state variables are: q_{inf} (net infiltration flux), S_w (subsurface saturation), and ψ (subsurface pressure).

4.2.2 Data assimilation methodologies

4.2.2(a) Ensemble Kalman Filter, EnKF

In our study, EnKF is used in combination with the fully coupled model TerrSysMP to update soil moisture content and groundwater levels. The theory of EnKF can be referred to section 2.2.2. In our work, the observation vector **y** and the state vector **x** include pressure and/or soil moisture. As mentioned above, the correlations between pressure and soil moisture are needed to update pressure with soil moisture data. The van Genuchten model gives the relation between soil moisture and pressure:

$$\psi = -\frac{[(\frac{\theta_s-\theta_r}{\theta(\psi)-\theta_r})^{1/m}-1]^{1/n}}{\alpha} \tag{4.1}$$

where θ_s is the saturated soil moisture content which is equal to porosity (ϕ), θ_r is residual soil moisture content, α is a measure of the first moment of the pore size density function, n is an inverse measure of the second moment of the pore size density function, and m=1-1/n.

EnKF needs to be tested carefully when pressure head is the state variable. In our experiment, in the unsaturated zone, the Richard´s equation is solved for pressure head and pressure head

can vary between strongly negative values, in case of dry soil, and positive values in the aquifer, and depends on the soil hydraulic parameters and climate conditions (Fredlund, 1991). For example, when the infiltration rate exceeds the saturated hydraulic conductivity, ponding occurs and pressure head becomes positive at the top of the domain. Contrarily, during a long drying period, pressure head can become strongly negative because of evapotranspiration. In data assimilation, stochastic realizations may show a large spread of pressure head values because of varying hydraulic parameters between the realizations so that the ensemble may show a strongly skewed probability density function of pressure. This strong skewness can generate unrealistically large updates in the EnKF analysis step because the ensemble mean is largely influenced by few realizations with extreme values. In addition, EnKF performs optimally for Gaussian distributions but not for strongly skewed distributions. Erdal et al. (2014) mitigated this issue by limiting the negative pressure head to -10 m but this is not an optimal solution for arid regions. They also proposed two other methods to avoid very negative pressure heads in the unsaturated zone, that are normal score (NS) transformation and pressure head to water content (PWC) transformation with a soil water retention function (Erdal et al., 2015). Both methods improved the state distribution as well as the assimilation results. However, NS-transformation may distort the spatial corrections and in PWC-transformation all pressure heads above or below a certain limit are mapped to the same water content. We are dealing with the same issue as groundwater pressure head is assimilated to improve the pressure head distribution for the whole domain including saturated zone and unsaturated zone.

In our work, a modular high-performance data assimilation framework TerrSysMP-PDAF (Kurtz et al., 2016) which couples TerrSysMP and the pre-existing parallel data assimilation library PDAF (Parallel Data Assimilation Framework) (Nerger and Hiller, 2013) is used. Details about technical implementation, installing and running TerrSysMP–PDAF can be found in (Kurtz et al., 2016). Currently TerrSysMP-PDAF can assimilate pressure and/or soil moisture data in ParFlow with EnKF.

4.2.2(b) Assimilation Methodologies

In this work, we are concerned with groundwater level data which can be continuously measured at high accuracy and low cost with automatic sensing devices in groundwater wells. We propose two ways to introduce the groundwater level data into the model TerrSysMP. Figure 4.2 illustrates how observed groundwater level is translated into observation data. Two different variants are possible. First, at locations with groundwater level measurements, the pressure head in the saturated zone is calculated assuming hydrostatic conditions in the aquifer. Pressure head in the saturated zone is then assumed to be the observation of our assimilation system. Second, soil moisture content in the saturated zone should be equal to porosity, and then soil moisture data (porosity data) is assimilated. Based on these two observation strategies, in total five methodologies are tested and compared to assimilate groundwater level data in TerrSysMP to improve the predictions of root zone soil moisture:

(1) Assimilation of pressure (P). Here the observation is pressure head in the saturated zone at locations with groundwater level measurements. The observation error of pressure head is

assumed 0.01m. The state vector includes the pressure head for the whole domain including the saturated and unsaturated zones.

(2) Assimilation of log-transformed pressure data (P_log). To reduce problems with non-Gaussianity in method (1), pressure head is converted into log space as $\log_{10}(100 - \text{pressure})$ to improve the EnKF performance. To avoid taking log of zero or negative values, pressure head is subtracted from 100 m for both the measurement data and simulated values before calculating the Kalman gain. The observation error in log space is 4×10^{-5} log(m) which is based on the random error of 0.01 m for pressure head. We calculated the standard deviation of $\log_{10}(100 - \text{perturbed pressure})$, where perturbed pressure was generated by adding a random error of 0.01m. The state vector includes the pressure head in log space for the whole domain including the saturated and unsaturated zones. After the analysis step, the log pressure head is back-transformed.

(3) Assimilation of soil moisture (SM). Here the observation is soil moisture (porosity) in the saturated zone at locations with groundwater level measurements. The observation error is 0.02 m^3/m^3. In EnKF, the state vector includes the soil moisture for the whole domain including saturated zone and unsaturated zone. After the update with EnKF, the state vector needs to be converted to pressure head for the whole domain on the basis of the van Genuchten model as pressure head is the prognostic variable in ParFlow.

(4) Assimilation of pressure in saturated zone (P_mask). This method is similar to method (1), but for each ensemble member, grid cells in the unsaturated zone are not updated in the data assimilation procedure. Unrealistic updates for the unsaturated zone caused by extreme values in the ensemble are avoided, but the disadvantage is that the groundwater level information is not directly used to update soil moisture contents in the unsaturated zone.

(5) Assimilation of both pressure and soil moisture (Mix). In this approach, groundwater level measurements are assimilated as pressure head data with an observation error of 0.01 m. However, the state vector includes now two parts: pressure head for the saturated zone and soil moisture for the unsaturated zone. Because of different parameters, the ensemble members will show different vertical divisions between the unsaturated and saturated zone. In the data assimilation step, the definition of the state vector should be consistent for all ensemble members. This implies that a given grid cell should be updated for all ensemble members in the same way: either in terms of soil moisture or pressure head. The distinction between the saturated and unsaturated zone is firstly defined by the deepest water table depth among the ensemble members. Then, for grid columns with groundwater level measurements, we apply a correction of this depth in case the groundwater level of the observation is higher than the one of the ensemble. Grid cells above this depth are updated in terms of soil moisture and grid cells below this depth in terms of pressure head. After defining the state vector and defining which elements are updated in terms of pressure, and which elements in terms of soil moisture, the pressure head observations are assimilated via EnKF. In this mixed approach, also joint assimilation of surface soil moisture content and groundwater level was tested, where observations include both groundwater level data and surface soil moisture, with measurement errors equal to 0.01 m and 0.02 m^3/m^3, respectively.

In the methodologies SM and Mix, after data assimilation with EnKF, updated soil moisture is transformed to pressure values according the van Genuchten model (equation 4.1) because pressure head is ParFlow's prognostic variable and soil moisture (or saturation) is a derived quantity, which is not directly used as a state variable for the next time step (Kurtz et al. 2016). Before the transformation, we check if soil moisture stays within physical boundaries (between residual soil moisture content and porosity). If updated soil moisture content is less than residual soil moisture, we set updated soil moisture=residual soil moisture + 0.01*porosity, and do the transformation for this updated value. If updated soil moisture content is larger than porosity, no transformation is performed, which implies that pressure head in this grid layer is not updated and the calculated pressure value before the data assimilation step with EnKF is used. Finally, if updated soil moisture content is in the range between residual soil moisture content and porosity, transformation is done directly. The updated pressure head in the domain (either directly updated by EnKF or indirectly updated by soil moisture) is used for the next time step.

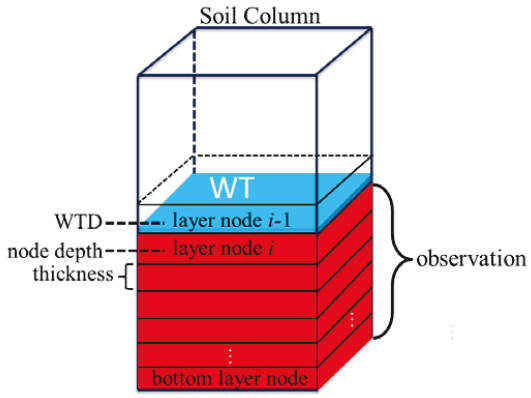

Figure 4.2 Illustration of the link between groundwater level and data to be assimilated. The blue area means groundwater level and the water table (WT) is in the layer node *i*-1. The red area (from layer node *i* to the bottom node) is saturated and can be incorporated as observations which take account of the groundwater level observation: either as pressure (hydrostatic assumption) or soil moisture content (setting soil moisture content equal to porosity).

4.3 Experiment setup

In order to test the five assimilation methodologies with TerrSysMP-PDAF, we define a synthetic experiment, which is carried out for the land surface-subsurface (CLM+ParFlow) components of TerrSysMP. A synthetic reference run provides pressure head or soil moisture observations and the ensemble needed for data assimilation experiments is generated by perturbing subsurface parameters.

4.3.1 Reference model

The synthetic domain has a horizontal extension of 2000 m × 2000 m and is discretized horizontally into 2 × 2 grid cells with a grid cell size of 1000 m × 1000 m. The domain has a vertical extension of 30 m, which is discretized into 30 soil layers with variable thickness. The uppermost 10 layers are with layer thicknesses exponentially increasing with depth. These ten layers extend in total over 3 m and in these ten layers fluxes are exchanged between CLM and ParFlow. The deeper 20 subsurface layers have a constant thickness of 1.35 m. The slope is 1% in both x and y directions for all grid cells (hillslope), thus there is topographically driven overland flow and groundwater flow in ParFlow. Soil texture, meteorological conditions and PFTs are homogeneous over the domain. The bottom boundary and boundaries on the side are impermeable. Overland flow can be generated over the upper boundary (Kollet and Maxwell, 2006) where ponded water is routed along the land surface and allowed to exit the domain at the bottom of the hill.

In order to produce different land surface fluxes and groundwater dynamics, we use two forcing datasets from a semi-arid climate and a humid climate site. Data for the semi-arid Picassent site in Spain are from a local meteorological station, and data for the humid Kennedy Space Center site within the Merritt Island in Florida, USA are from the AmeriFlux Network (Bracho et al. 2008). For each site, climate data from two years are used, one year is for model spin-up and the other year is for the model simulation and assimilation. Figure 4.3 shows the daily accumulated precipitation, average air temperature and average incoming shortwave radiation for the two climate sites.

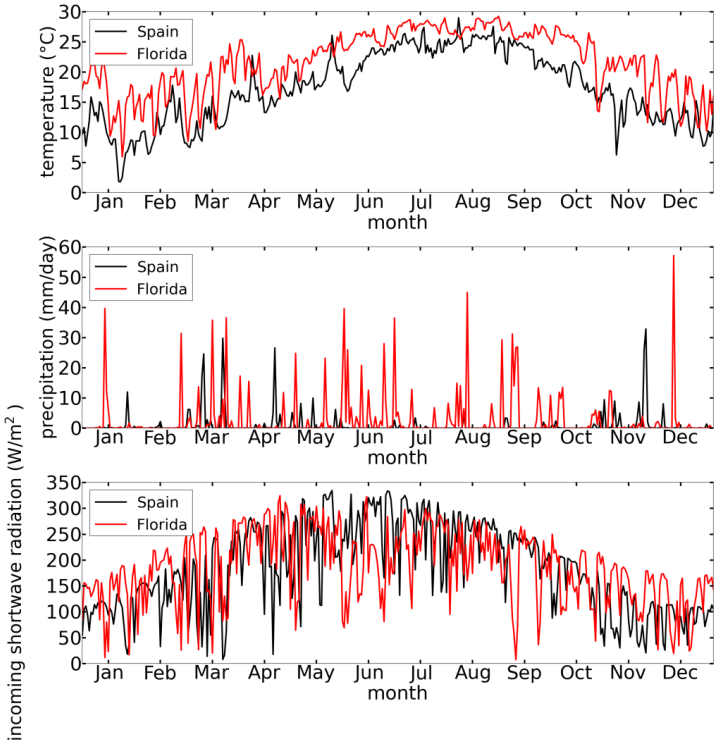

Figure 4.3 Daily accumulated precipitation, average air temperature and average incoming shortwave radiation for Picassent (Spain) and the Merritt Island (Florida, USA).

Three soil types with different soil hydraulic parameters are used. Variably-saturated flow is parameterised with the van Genuchten model. Spatially constant values of residual soil moisture content θ_r, the saturated hydraulic conductivity k_s, the van Genuchten parameters α and n are chosen from (Leij et al., 1996) (see table 4.1). To keep hydraulic consistence between CLM and ParFlow, saturated soil moisture θ_s (=porosity) for both models is calculated on the basis of the sand fraction via the following pedotransfer function in CLM:

$$\theta_s = 0.489 - 0.00126(\text{sand}\%) \quad (4.2)$$

Table 4.1 Soil properties used in simulations.

Soil texture	θ_s (m^3/m^3)	θ_r (m^3/m^3)	α (m^{-1})	n	k_s (m hr^{-1})	sand%	clay%
Loam	0.4386	0.078	3.6	1.56	0.0104	40	20
Loamy sand	0.388	0.057	12.4	2.28	0.146	80	15
Sandy loam	0.4134	0.065	7.5	1.89	0.0442	60	18

Three plant functional types (PFTs) are used in the simulations namely bare soil, shrubs/ grasland (short roots) and broadleaf tree (deeper roots). Bare soil, shrub and evergreen broadleaf tree are specified for simulations for the Picassent site, and bare soil, grassland and

evergreen broadleaf tree for the Florida site. The vegetation properties are characterized by distinct physiological, PFT-specific parameters in CLM (Oleson et al., 2004).

Each configuration of the atmospheric forcings, soil texture and vegetation type is initialized with a water table depth of 1m relative to the land surface. Then TerrSysMP is run for 100 years, forced repeatedly with one year of atmospheric data. For all the simulation scenarios in this work, 100 years of spin-up is enough to reach hydrologic and dynamic equilibrium conditions. After the model has reached equilibrium the model is forced by another year of atmospheric data for the simulation and assimilation experiments.

4.3.2 Setup of data assimilation experiments

Two climate types, three soil texture types and three PFTs were combined to generate 18 TerrSysMP configurations. These configurations generate different land surface fluxes and groundwater dynamics. For each configuration, groundwater dynamics and land surface fluxes also differ between the four hillslope grid cells. Only one grid cell is observed. The results for the highest situated grid cell and the grid cell at medium elevation are analyzed resulting in 36 (2 climate types × 3 soil types × 3 vegetation types × 2 grid cells along slope) synthetic scenarios with different groundwater levels.

For the data assimilation experiments, a synthetic reference run is created for each scenario mentioned above. The synthetic runs use the "true" hydraulic parameters shown in table 4.1 and provide virtual observation data of pressure head or soil moisture as specified in section 4.2.2(b). Although groundwater level data are assimilated, we refer to them in terms of pressure head or soil moisture data below. The synthetic reference simulations are run for 1 year with an hourly time step for both ParFlow and CLM. The synthetic reference runs also provide the true values of root zone soil moisture. The five assimilation methodologies are evaluated by comparing the assimilation results of root zone soil moisture and their corresponding "true" values.

For the assimilation experiments, an ensemble of 128 realizations of $\log_{10}(k_s)$ is created. For each scenario, individual $\log_{10}(k_s)$ realisations are generated by perturbing the reference value of $\log_{10}(k_s)$ (see table 4.1) with an additive random perturbation which is sampled from the standard normal distribution $\mathcal{N}(0,1)$. The spin-up is done for each ensemble member individually for 100 years using the different ks-values as input. The ensemble is used in addition for an open loop run and data assimilation experiments. Observation data from the reference run (groundwater level data in the form of pressure head or soil moisture) are assimilated on a daily basis for the observation grid point. The root zone soil moisture is updated directly or indirectly by assimilating observation data. The model uncertainty from the physical parametrizations in the model is ignored in this study.

4.4 Results

Groundwater level assimilation experiments for all the scenarios mentioned above are performed with the five assimilation methodologies, and joint assimilation experiments of

groundwater level and surface soil moisture with method (5) described in section 4.2.2(b). Some representative results are shown below to illustrate the possibility and potential of the assimilation strategies under different groundwater dynamics and compare the performance of the five methodologies. To evaluate the performances of the different assimilation strategies/methodologies, the Root Mean Square Error (RMSE) of soil moisture from the surface to the depth of 3m (the 10 upper soil layers, which is assumed to be the root zone) is calculated as:

$$\mathrm{RMSE}^j = \sqrt{\frac{1}{T}\sum_{t=1}^{T}(\bar{\theta}_{t,j}^{\mathrm{sim}} - \theta_{t,j}^{\mathrm{true}})^2} \tag{4.3}$$

where $\bar{\theta}_t^{\mathrm{sim}}$ is the ensemble mean soil moisture at time step t, θ_t^{true} the true soil moisture at time step t, j the jth soil layer and T is the number of time steps. The weighted average of RMSE for these 10 layers is also calculated:

$$\mathrm{RMSE} = \sum_{j=1}^{10}(\omega_j * \mathrm{RMSE}^j) \tag{4.4}$$

where ω_j is the weight for the jth soil layer, which is calculated by the depth of the jth soil layer D_j:

$$\omega_j = \frac{D_j}{\sum_{j=1}^{10} D_j} \tag{4.5}$$

The deeper layers get larger weights in correspondence to their larger vertical extend.

4.4.1 Assimilation of groundwater levels

In this section, only groundwater level (in the form of pressure head or soil moisture) is assimilated in TerrSysMP-PDAF. The scenario name is specified by the soil type, climate site, plant type and grid ("Top" means the highest grid cell and "Medium" the grid cell with medium elevation).

As in this work the soil moisture observation error is 0.02 m^3/m^3, we assume that if the RMSE value of root zone soil moisture from the open loop run is less than 0.02 m^3/m^3 the model performs well. The scatterplots in figure 4.4 illustrate that if the water table depth is very deep (< -10m) the open loop RMSE values are below 0.02 m^3/m^3. When the water table is very deep, root zone soil moisture content is low for all realizations in the open loop run so that the difference between the ensemble mean and the reference is small. On the other hand, in some scenarios when the water table is very shallow (close to surface), all realizations have very wet root zones, which also result in low RMSE values (< 0.02 m^3/m^3). Notice that in the simulation experiments the meteorological forcings and porosity were known. We analyze the results of the assimilation experiments for some scenarios with (with open loop RMSE values above 0.02 m^3/m^3 and water table depth between -5m to 0m) where data assimilation is necessary for improving the model performance.

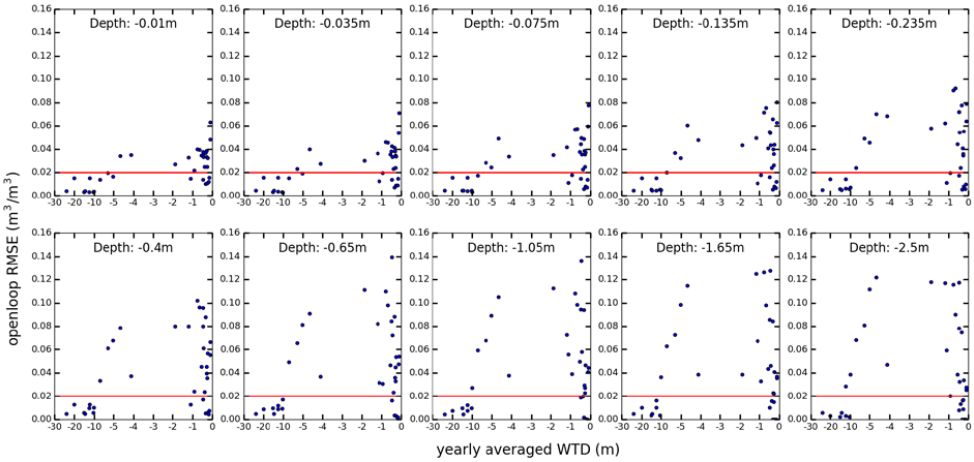

Figure 4.4 Scatterplots of RMSE values (m^3/m^3) of soil moisture at 10 different depths in the soil profile for the open loop runs as a function of yearly averaged reference water table depth (m) for the 36 synthetic scenarios. The red line indicates a RMSE value of 0.02 m^3/m^3. Please note the uneven scales on the x-axes.

4.4.1(a) Aggregated results

Figure 4.5 shows the scatter plots of weighted average of RMSE values for the open loops versus weighted average of RMSE values for the five data assimilation methodologies, for the different scenarios with open loop RMSE values above 0.02 m^3/m^3. The 1:1 line corresponds to equal weighted averages of RMSE for the open loop and data assimilation runs. Points which are situated below the 1:1 line indicate that assimilation of groundwater level improves soil moisture characterization compared to the open loop. From the figure we can see that methodologies P_mask, SM and Mix work well for most scenarios, especially the methodology Mix, which results for all the scenarios in weighted average RMSE values smaller than 0.02 m^3/m^3 after assimilation. Root zone soil moisture characterization is greatly improved compared to the open loop for this scenario. P_mask also improves the root zone soil moisture characterization for all the scenarios but the improvement is not as significant as for Mix. For a few scenarios, the methodology SM performs bad. Methodology P shows the worst performance and P_log works a little better than P. For these last two methodologies for many scenarios soil moisture characterization is worse after assimilation.

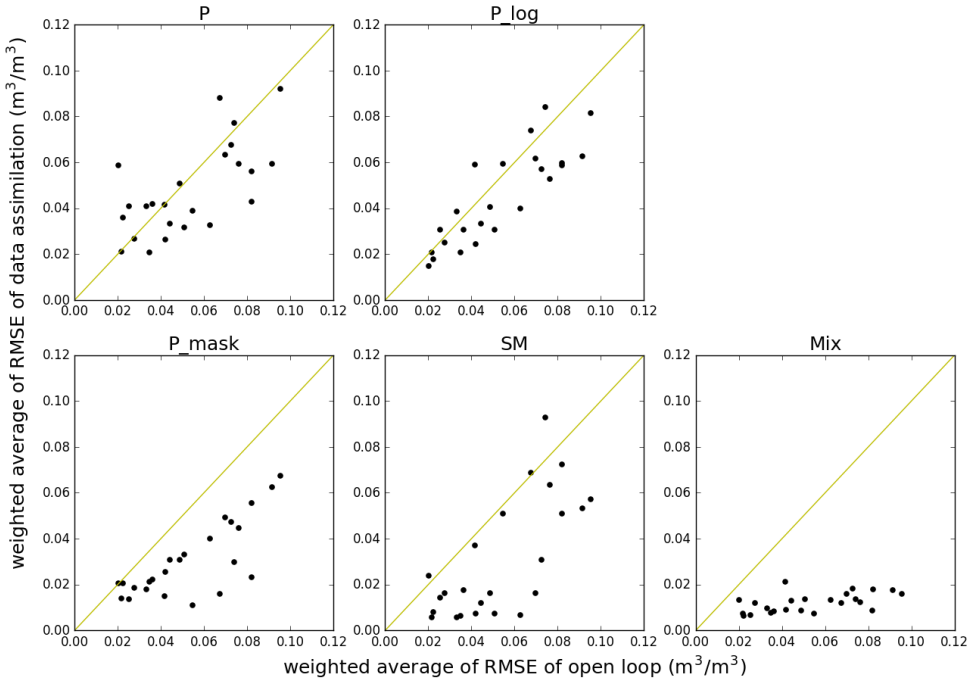

Figure 4.5 Scatter plots of weighted averages of RMSE values (m^3/m^3) for the open loop run and each of the data assimilation methods. The subfigures correspond to different assimilation methodologies. Black dots represent scores for individual data assimilation experiments. The yellow line is the 1:1 line.

More details are shown for the scenario Loam_Florida_Broadleaf_Top. Figure 4.6 shows the ensemble spread of groundwater levels as a function of time for the open loop and the five assimilation methodologies for this scenario during the assimilation. Table 4.2 shows the corresponding RMSE values of soil moisture for the upper 10 soil layers (calculated by Equation (4.3)) and weighted average of RMSE values (calculated by Equation (4.4)). In this scenario (see table 4.2), all the five methodologies improve the soil moisture profile estimation after assimilation compared with the open loop run. The improvement for the upper layers is limited for the methodologies P and P_log when compared with the other 3 methodologies, and the deeper layers are greatly improved by all the methodologies. From Figure 4.6, we can see that all methodologies improve the ensemble towards the reference groundwater level and reduce the ensemble variance. In particular, the ensemble converges quickly to the reference in the methodologies SM and Mix, which produce the best results according to table 4.2. There are small spikes in the ensemble for the methodologies P and P_log during the summer period which might affect their performances. In the below section, performances of the five assimilation methodologies are analyzed and compared with some representative scenarios.

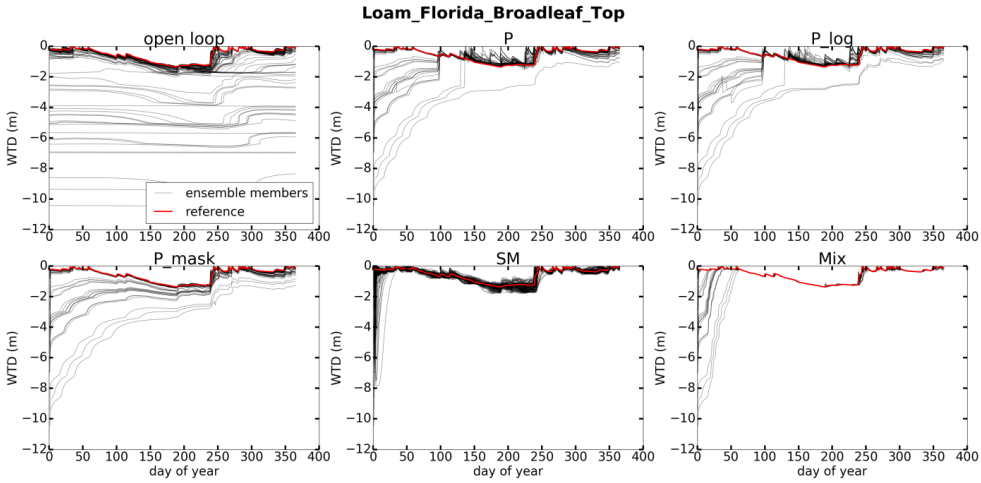

Figure 4.6 Time series of groundwater level for the open loop ensemble and the five assimilation methodologies for the scenario Loam_Florida_Broadleaf_Top. Gray is the ensemble spread and red the synthetic truth.

Table 4.2 The RMSE values (m^3/m^3) for the soil moisture characterization for the 10 upper soil layers for the open loop run and the 5 assimilation methodologies for the scenario Loam_Florida_Broadleaf_Top.

Depth	Open loop	P	P_log	P_mask	SM	Mix
-0.01m	0.035	0.028	0.026	0.023	0.007	0.011
-0.035m	0.035	0.029	0.026	0.024	0.007	0.010
-0.075m	0.037	0.029	0.026	0.025	0.007	0.010
-0.135m	0.041	0.030	0.027	0.027	0.009	0.009
-0.235m	0.044	0.030	0.028	0.029	0.010	0.008
-0.4m	0.045	0.029	0.027	0.029	0.009	0.009
-0.65m	0.047	0.029	0.027	0.029	0.007	0.010
-1.05m	0.050	0.023	0.022	0.028	0.008	0.008
-1.65m	0.043	0.017	0.017	0.021	0.002	0.008
-2.5m	0.039	0.013	0.013	0.015	0.002	0.008
Weighted average of RMSE	0.043	0.019	0.019	0.022	0.004	0.008

4.4.1(b) Comparisons of the five assimilation methodologies

The performances of the methodologies P and P_log are strongly dependent on the water content distribution in the unsaturated zone. Under some conditions, like a long dry period (Picassent site in Spain), high potential ET or erroneous hydraulic parameters k_s, the pressure head ensemble shows a strongly skewed distribution in the unsaturated zone which cannot be properly handled by EnKF. When most realizations calculate a groundwater table which is higher than the reference value, the methodology SM also has a problem as the variance

calculated at the observation point is near zero. Below some representative scenarios will be shown to discuss these issues in detail.

We analyze now the simulation results for the Spanish site which is more affected by (very) dry periods and therefore very dry topsoil conditions. We see in figure 4.7 and table 4.3 that the simulation performance is now more strongly affected by the dry conditions, which is visible in the form of high spikes in the plots for the methodologies P and P_log (scenario Sandyloam_Spain_Baresoil_Medium). From table 4.3 we can see that the methodologies P and P_log improve the soil moisture estimations below the reference water table but worsen the soil moisture estimations above the reference water table. The other three methodologies perform well above the groundwater table, especially the methodology Mix. Figure 4.7 shows that after about five months of assimilation, the reference water table is below almost all the calculated water table depths in the individual realizations for methodologies P and P_log. Related to this, these methodologies perform well in the saturated zone.

In the unsaturated zone the bad performance of methodologies P and P_log is related to the artificial large spread of the strongly skewed pressure head distribution resulting from the large updates in EnKF. In figure 4.7 there are small spikes in the ensemble for the P and P_log methods during the summer period. In the summer period soil profiles get drier, so the pressure head near the surface becomes more negative. Some ensemble members with improper ks values may generate very negative pressure heads, which result in strongly skewed, non-Gaussian local probability density functions of pressure head, as shown in figure 4.8(a) and 4.8(c), which illustrates that before the update there are a few isolated realizations with very negative pressure values while most realizations are close to the synthetic truth. The update drags the other realizations to the extreme realizations and therefore to more negative pressure values (see figure 4.8(b) and 4.8(d)). Some realizations are updated to high positive pressure heads. These positive pressure heads make no sense in the model from a physical point of view, and are the consequence of the artificial large spread of the skewed head distribution resulting from the EnKF updates. These unwanted positive pressure head updates result in the water table depth spikes in the methodologies P and P_log in figure 4.7 and bad performance for the upper layers in table 4.3. The figure also shows that the scenario P_log strongly reduces the outliers compared to the scenario P, but is not able to fully eliminate them.

In the figure 4.7 the methodology P_mask shows a much slower convergence than the other methodologies. In the P_mask methodology, only the grid cells in the saturated zone are updated in the data assimilation procedure. Unrealistic updates for the unsaturated zone caused by extreme values in the ensemble are avoided. Soil moisture contents in the unsaturated zone are indirectly updated as a result of updating groundwater levels (by data assimilation) and the action of the model equations, which leads to its slower convergence.

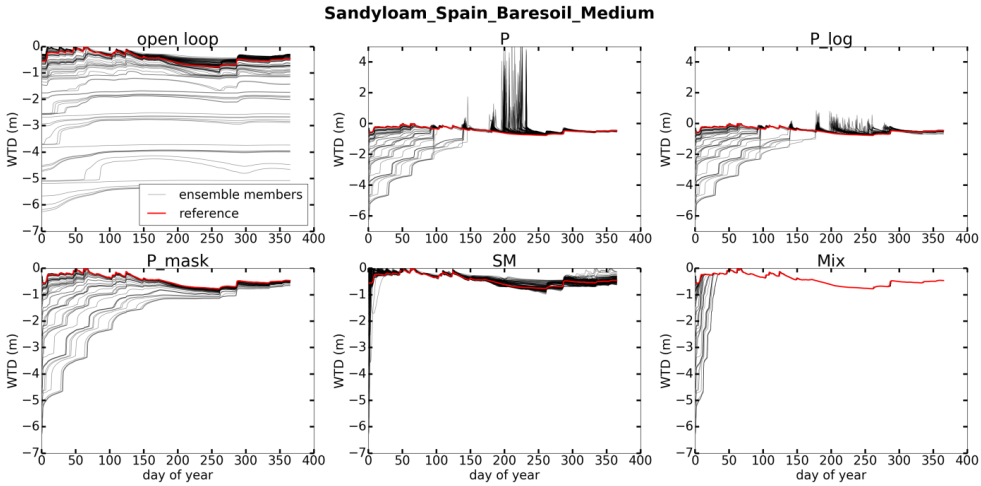

Figure 4.7 Time series of water table depth from the open loop ensemble and the 5 assimilation methodologies for the scenario Sandyloam_Spain_Baresoil_Medium. Please note the different scales on the y-axes. Gray is the ensemble spread and red the synthetic truth.

Table 4.3 The RMSE values (m^3/m^3) for the soil moisture characterization for the 10 upper soil layers for the open loop run and the 5 assimilation methodologies for the scenario Sandyloam_Spain_Baresoil_Medium. Red values highlight the RMSE values for the five assimilation methodologies which are larger than the corresponding RMSE values for the open loop.

Depth	**Open loop**	**P**	**P_log**	**P_mask**	**SM**	**Mix**
-0.01m	0.033	0.045	0.037	0.026	0.023	0.010
-0.035m	0.033	0.049	0.039	0.026	0.023	0.009
-0.075m	0.035	0.053	0.043	0.028	0.023	0.009
-0.135m	0.043	0.062	0.051	0.035	0.019	0.008
-0.235m	0.055	0.076	0.061	0.044	0.018	0.008
-0.4m	0.061	0.082	0.057	0.042	0.018	0.008
-0.65m	0.072	0.037	0.035	0.036	0.007	0.010
-1.05m	0.058	0.023	0.023	0.024	0.004	0.008
-1.65m	0.046	0.017	0.017	0.017	0.003	0.007
-2.5m	0.033	0.011	0.011	0.011	0.002	0.005
Weighted average of RMSE	0.046	0.025	0.022	0.021	0.005	0.007

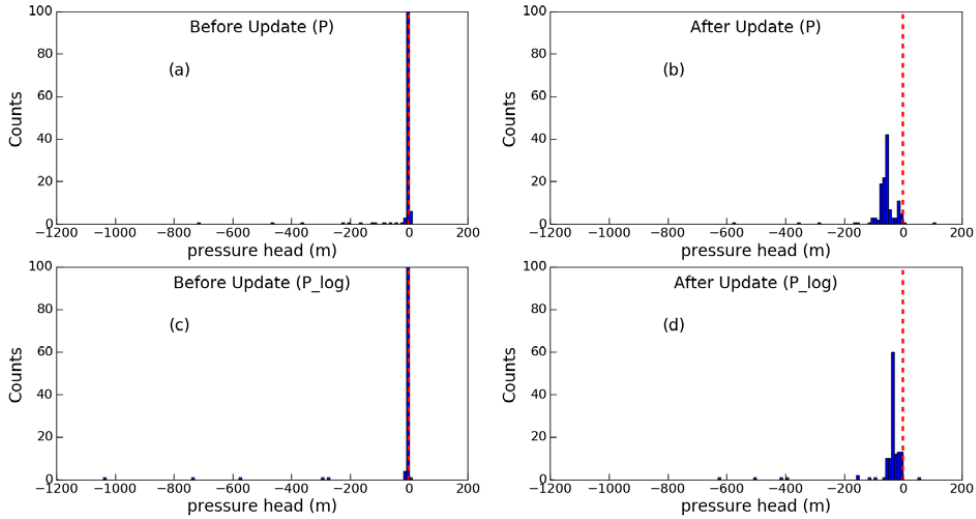

Figure 4.8 Histogram of pressure head distribution for the surface layer at 0.01m depth before and after the update at assimilation step 185 for methodologies P ((a) and (b)) and P_log ((c) and (d)) for the scenario Sandyloam_Spain_Baresoil_Medium. The dashed red line marks the synthetic truth on the x-axes at this time step.

In some scenarios, methodology SM also worsens the soil moisture estimations in the unsaturated zone while Mix still works very well (see figure 4.9 and table 4.4). For the scenario Sandyloam_Spain_Shrub_Medium, in methodology SM, after two months of assimilation, all realizations are above the reference water table (see figure 4.9(b)). As a consequence, (**y**-**Hx**) in equation (2.22) is very small for the soil moisture observations taken at the layer nodes as the ensemble spread is close to zero there (all realizations are saturated or nearly saturated), and if (**y**-**Hx**) is very small, the update in equation (2.22) is also small. Therefore, the data assimilation according to methodology SM is not able to correct the erroneous water table depth, resulting in bad performance statistics as indicated in table 4.4. For the scenario Loamysand_Spain_Baresoil_Medium, in methodology SM, even though the reference water table is covered by the ensemble spread during assimilation (see figure 4.9(e)), SM still produces bad results in the unsaturated zone (see table 4.4). In the model, the pressure head and soil moisture are defined for the centers of layers (nodes) but the groundwater table can be between those layer centers (see figure 4.2). In the methodology SM soil moisture (=porosity) for the layer nodes below the reference water table are observations (layer node *i* to the bottom layer node in figure 4.2). For this scenario, in the subfigure 4.9(e) the blue line shows the layer node depth of the uppermost saturated layer node (layer node *i* in figure 4.2) with observation, and we can see that the layer nodes which have the observation are also saturated for all realizations, which causes the same problem as the previous scenario. From figure 4.9 and table 4.4 we can see that in these two scenarios methodology Mix still performs very well with a fast convergence of the water table depth ensemble towards the true value and greatly reduced RMSE values compared to the open loop simulation.

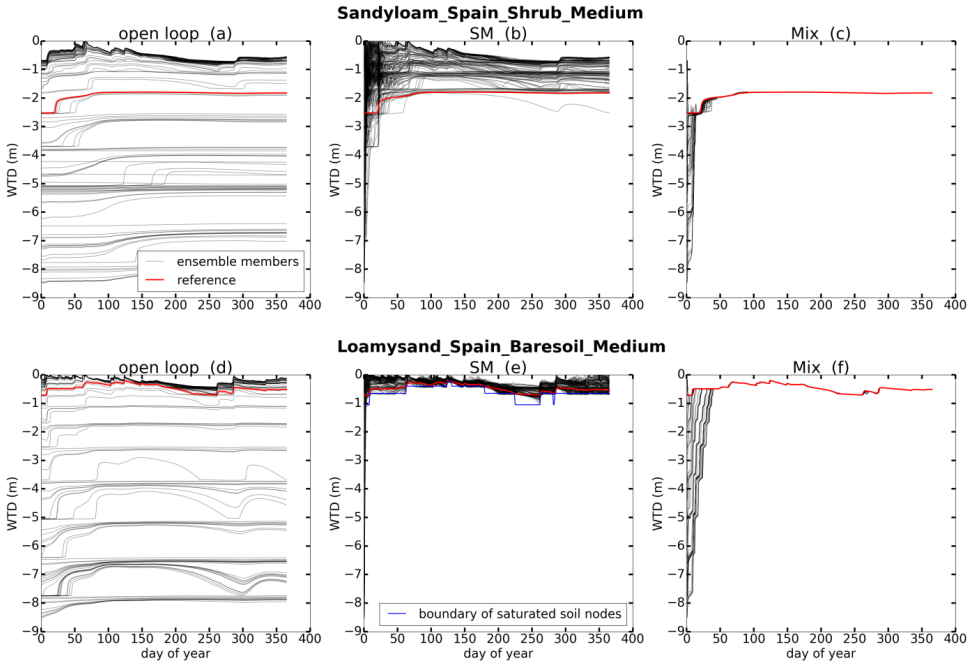

Figure 4.9 Time series of groundwater level from the open loop ensemble ((a) and (d)) and the assimilation methodologies SM ((b) and (e)) and Mix ((c) and (f)) for the scenario Loamysand_Spain_Baresoil_Medium ((a), (b) and (c)) and Sandyloam_Spain_Shrub_Medium ((d), (e) and (f)). Gray lines represent ensemble members and red the synthetic truth. The blue line in (e) marks the boundary of the saturated layer nodes. Layer nodes below the boundary are saturated which contain soil moisture observations (porosity).

Table 4.4 The RMSE values (m^3/m^3) for the soil moisture characterization for the 10 upper soil layers for the open loop run and the methodologies SM and Mix for the scenarios Loamysand_Spain_Baresoil_Medium and Sandyloam_Spain_Shrub_Medium. Red values highlight the RMSE values for the SM which are larger than the corresponding RMSE values for the open loop.

	Loamysand_Spain_Baresoil_Medium			**Sandyloam_Spain_Shrub_Medium**		
Depth	**Open loop**	**SM**	**Mix**	**Open loop**	**SM**	**Mix**
-0.01m	0.037	0.054	0.009	0.027	0.029	0.011
-0.035m	0.043	0.062	0.010	0.030	0.033	0.012
-0.075m	0.049	0.075	0.011	0.035	0.038	0.013
-0.135m	0.054	0.088	0.011	0.043	0.047	0.013
-0.235m	0.072	0.090	0.011	0.058	0.061	0.012
-0.4m	0.096	0.064	0.011	0.080	0.087	0.012
-0.65m	0.140	0.009	0.020	0.111	0.136	0.013
-1.05m	0.136	0.008	0.024	0.112	0.188	0.015
-1.65m	0.127	0.007	0.023	0.039	0.125	0.017
-2.5m	0.118	0.006	0.020	0.118	0.008	0.018
weighted average of RMSE	0.120	0.016	0.020	0.090	0.085	0.016

4.4.2 Joint assimilation of groundwater levels and surface soil moisture

In section 4.4.1 we evaluate the five assimilation methodologies for assimilating groundwater level data in the integrated subsurface- land surface model TerrSysMP. From the results above, we find that the methodology Mix works the best. Now we test this methodology to jointly assimilate groundwater levels and surface soil moisture (Joint_SSM_GWL) with more realistic experimental settings. When jointly assimilating groundwater levels and surface soil moisture, the state vector of Mix methodology still includes pressure for the saturated zone and soil moisture for the unsaturated zone. The observation vector includes also the top surface soil moisture (0.01 m below the soil surface) besides pressure head measurements in the saturated zone. The soil moisture observation is taken at 0.01 m in order to mimic remote sensing observations.

In addition, the experiments presented in this section mimic more realistic conditions. Vertically heterogeneous saturated hydraulic conductivity k_s and van Genuchten parameters (α and n) are used as input. For the data assimilation experiments, a synthetic reference run is created for each scenario. The synthetic "true" k_s value for the top surface layer is taken from Table 1. Saturated hydraulic conductivity decreases exponentially with soil depth (Niu et al., 2005):

$$\begin{cases} k_s(z_i)=k_s(z_1)*e^{-f(z_i-z_1)}, & i=1:10 \\ k_s(z_i) = k_s(z_{10}), & i=11:20 \end{cases} \quad (4.6)$$

where z_i is the soil depth of the ith layer, z_1 is the depth of the top surface layer, $k_s(z_1)$ is the saturated hydraulic conductivity of the top surface layer, and f is the decay factor, which indicates the decrease of k_s with soil depth (Beven, 1997). f is set to 2.0 m^{-1} (Niu et al., 2005). The remaining k_s values for the deeper 20 layers use the same values as the 10th layer. The "true" van Genuchten parameters (α and n) for each soil layer are generated based on the k_s values by sampling a multivariate Gaussian distribution described in Carsel and Parrish (1988) for each soil type. Carsel and Parrish (1988) used four kinds of transformation on k_s, α and n to get a multi-normal distribution among the three parameters: no transformation (NO), lognormal (LN), log ratio (SB) and hyperbolic arcsine (SU). Details about the transformation for each soil type can be found in Carsel and Parrish (1988). This procedure takes correlations among the three parameters into account. Table 4.5 shows the covariance among the three transformed parameters for loam and loamy sand. Residual soil moisture content θ_r and porosity θ_s are deterministic and spatially constant (see table 4.1). Please note that k_s, α and n are vertically heterogeneous, but with spatially homogeneous values for the different soil layers (2.5 dimensional). Other settings are similar as outlined in section 4.3.2. The synthetic "true" hydraulic parameters are used as model input to provide virtual measurement data of pressure head and soil moisture. In the experiments only loamy sand and loam are tested, in combination with the 3 PFTs and 2 climate datasets.

Table 4.5 Covariances among transformed k_s, α and n for Loam and Loamy sand. Transformations and units are shown in brackets. Transformations include no transformation (NO), log ratio (SB) and hyperbolic arcsine (SU).

	k_s (cm/hr)	α (cm^{-1})	n (-)
Loam			
k_s (SB)	1.41	0.611	0.055
α (SB)	0.982	0.093	0.026
n (SU)	0.632	0.591	0.029
Loamy sand			
k_s (SB)	1.48	0.037	0.211
α (NO)	0.986	0.014	0.019
n (SB)	0.730	0.354	0.108

For the assimilation experiments, an ensemble of 128 realizations of k_s, α and n is created as outlined above. Precipitation is also perturbed in the data assimilation experiments with multiplicative noise sampled from a uniform distribution with values between 0.5 and 1.5.

To further investigate the performance of Joint_SSM_GWL, we also assimilate surface soil moisture alone (SSM) (for all the scenarios) as is typical done in many land surface data assimilation studies, and assimilate groundwater level alone (GWL). Figure 4.10 shows the scatter plots of open loop RMSE values versus GWL, SSM and Joint_SSM_GWL RMSE values for all the scenarios. For the upper surface layers (depth: -0.01 m, -0.035 m and -0.075 m), SSM and Joint_SSM_GWL improve the soil moisture estimation compared with open loop run, because for most cases their blue and red dots are below the 1:1 line, but many green dots of GWL distribute above the 1:1 line, which indicates that GWL-assimilation does not significantly improve surface soil moisture estimation. This is reasonable because SSM and Joint_SSM_GWL include surface soil moisture observations to constrain the soil moisture content for the upper layers. For the intermediate soil layers (depth: -0.135m, -0.235m and -0.4m), Joint_SSM_GWL still works well, while the blue dots of SSM are scattered around the 1:1 line and the green dots of GWL move towards an area slightly below the 1:1 line, indicating improved performance. In other words, the performance of SSM gets worse while GWL performs better. For the deeper soil layers (depth: -0.65m, -1.05m, -1.65m and -2.5m), SSM is not able to improve soil moisture characterization compared to the open loop runs while GWL and Joint_SSM_GWL significantly improve the soil moisture characterization. Therefore, we can conclude that assimilation of surface soil moisture alone can improve the soil moisture characterization for the upper 10-20 cm, but it may even worsen the soil moisture estimation for deep layers. Similarly, assimilation of groundwater level alone can improve soil moisture characterization for layers deeper than 40cm, but may have negative effect on soil moisture characterization for surface layers. Joint assimilation of surface soil moisture and groundwater level is able to integrate the advantages of the two observation types.

The number of dots in the figure is smaller for deeper layers, because in some scenarios the water table depths are shallower than -2.5 m so that both open loop RMSE values and

assimilation RMSE values beneath the water table are very close to zero as all ensemble members reproduce saturated conditions there.

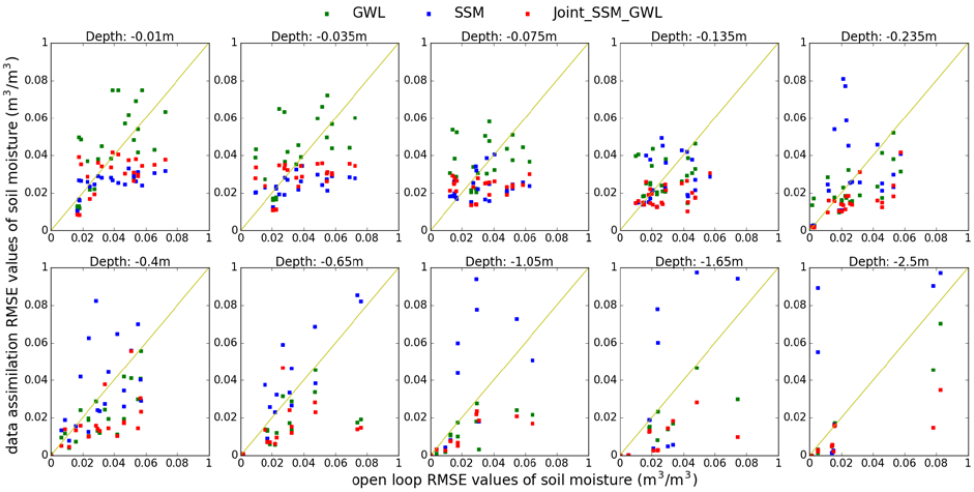

Figure 4.10 Scatter plot of RMSE values for open loop runs and the 3 assimilation strategies for all scenarios. On the x-axes the RMSE values for soil moisture characterization for the open loop run are denoted, and on the y-axes the RMSE values of GWL, SSM and Joint_SSM_GWL. Each subfigure shows a particular soil layer. Different colors donate different methods. Yellow line is 1:1 line.

Figure 4.11 compares the soil moisture results for the reference, open loop, and the data assimilation scenario Joint_SSM_GWL for Loamysand_Spain_Shrub_Medium. Data assimilation results in an ensemble closer to the reference compared with the open loop run. The ensemble does not suffer from variance underestimation. In the top four layers, soil moisture content is low with some strong fluctuations related to few precipitation events and strong potential evapotranspiration. The groundwater level data are able to correct most ensemble members for the deeper soil layers.

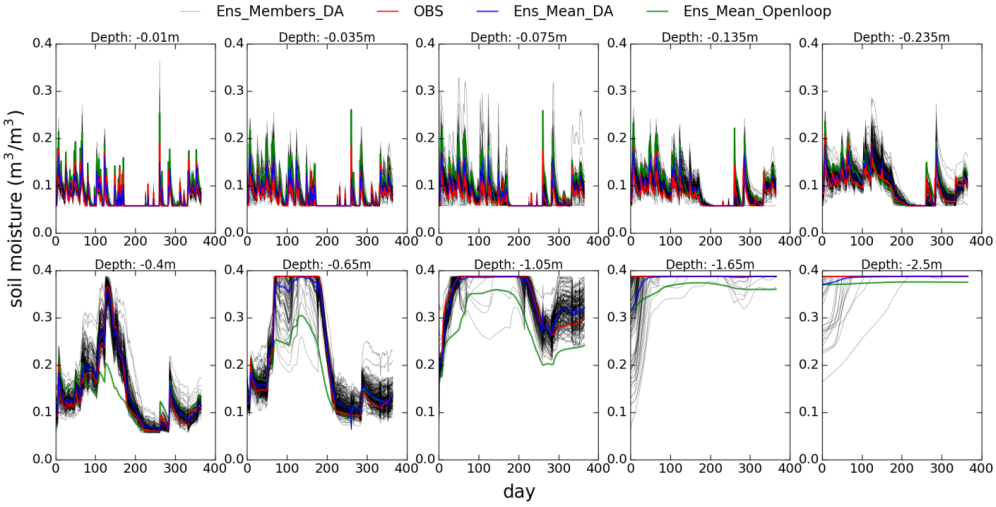

Figure 4.11 Soil moisture time series for the reference truth (OBS), the ensemble mean of open loop run (Ens_Mean_Openloop), the ensemble mean (Ens_Mean_DA) and the ensemble during assimilation (Ens_Members_DA). The scenario here is Loamysand_Spain_Shrub_Medium with Joint_SSM_GWL. Each subfigure shows a particular soil layer.

4.5 Discussion

This study compares five data assimilation methodologies for improving root zone soil moisture estimation with groundwater level data or a combination of groundwater level and surface soil moisture data. These five assimilation methodologies and assimilation of groundwater level and/or surface soil moisture data are evaluated and compared on the basis of 36 synthetic scenarios. The problem associated with the implicit Gaussian assumption in the EnKF for updating pressure heads in the unsaturated zone is illustrated.

The results of methodologies P and P_log suffer from the extreme pressure heads which drag the ensemble mean of model states far away from the “truth”. This problem happens particularly in dry periods when some realizations with extreme ks-values result in very negative pressure head values at near surface layers. One important aspect in EnKF is the ensemble size. In our study a size of 128 realizations is used which is a small size compared to groundwater data assimilation studies. However, Erdal et al. (2015) tested a very large ensemble size of 1000 members for the problem of highly skewed distributions. They pointed out that a larger ensemble size would rather increase the risk for the strong negative pressure heads since these originate from initially sampled extreme parameter values. For a large ensemble, it is more likely that a few extreme parameter values are sampled. Furthermore, the extreme state values still have a major effect on the ensemble mean even though the ensemble size is larger.

An alternative data assimilation method which could be used here is the particle filter method, which could also help to avoid extreme state values. The particle filter can deal with non-linear and non-Gaussian problems but usually requires large numbers of model evaluations to

get a reliable result. If one can afford the cost of using the particle filter method, it is obvious that the skewed pressure distribution would not pose such a problem as in the EnKF. For the small synthetic examples shown here, it would be possible to apply the particle filter. However, most real cases involve many more unknowns and a much higher dimensionality. Under those conditions, the particle filter is expected to need an extremely large ensemble size. Erdal et al. (2015) also discussed if the most common ad-hoc methods would have any positive effect on the performance with such a strongly skewed pressure distribution. They concluded that dampening the state update only has limited effect as it cannot remove the extreme realizations which still have an unwanted, but dampened, impact. They concluded that also localization would not improve the performance significantly.

Groundwater level information which is assimilated in the form of soil moisture data works well in most scenarios but there are some exceptions when the simulated water tables from all or most realizations are above the reference water table. Increasing the ensemble size could solve this specific problem, but it is unclear whether this would work in all scenarios. For example, in real-world cases with bias where the simulated water table depths are systematically closer to the surface than the observed water table depth, correction is difficult. In addition, a larger ensemble size also implies of course increased computational costs.

From section 4.4.1 we find that the methodology Mix, which updates model states in terms of pressure for the saturated zone and in terms of soil moisture for the unsaturated zone, outperforms the other methods and results in a very good root zone soil moisture characterization. This might be related to the simple setting in our experiments where only the saturated hydraulic conductivity k_s is perturbed. The van Genuchten parameters (α and n) and porosity which link the pressure head and soil moisture in the unsaturated zone are constant. While this setting is relatively simple, the focus is on developing assimilation methodologies with TerrSysMP to improve the estimation of root zone soil moisture by assimilating groundwater levels. Additional experiments (section 4.4.2) where α and n are also perturbed together with ks further verified the feasibility of the methodology Mix.

There will be additional challenges for the application of the methodology in real-world situations. The van Genuchten model is used to transform the soil moisture to pressure head in the unsaturated zone after EnKF. In real world cases, the relation between soil moisture and pressure head might even not be described correctly by the van Genuchten model. In addition, if the updated soil moisture state is $\geqslant$ porosity (from unsaturated to saturated conditions), no back transform is made. For this grid cell, the model predicted pressure head value prior to assimilation is used. In this case, strange pressure profiles might be generated as the states of the surrounding grid cells were either directly updated in terms of pressure (saturated zone) or pressure was indirectly updated via soil moisture (unsaturated zone). It is expected that in the model simulation for the next time step the pressure profile is partly smoothed again.

In our work, we test joint assimilation of groundwater levels and surface soil moisture with 2.5 dimensional synthetic experiments, which is proven to be a promising way to improve the estimation of root zone soil moisture. Surface soil moisture is easily available temporally and

spatially from satellites like SMAP and SMOS. Groundwater level measurements are also potentially numerous and measured at low cost and high accuracy, although currently large scale groundwater level data are not systematically stored in databases. Taking full advantage of these two types of data helps to better understand the soil water profile. Various studies use data assimilation techniques to combine satellite data with land surface models to update the complete soil moisture profile including the root zone. Generally, in those works, the land surface models only consider the exchange of water and energy between atmosphere, land surface and vegetation, but water and heat fluxes from the deeper subsurface are neglected. The integrated model TerrSysMP, which couples the land surface and subsurface, makes it possible to take advantage of the surface soil moisture information (from satellite) and groundwater levels (from observation networks or satellite GRACE) to improve the soil moisture estimation in the vadose zone by data assimilation.

We impose uncertainties with respect to soil hydraulic parameters (k_s, α and n) and model forcings (precipitation) in the synthetic joint assimilation study. In reality, these parameters and model forcings (especially precipitation) are always impacted by a large uncertainty, especially for large-scale applications. It is difficult to obtain information about soil hydraulic and thermal parameter values and their statistics beyond sporadic point measurements. It is important to better constrain these parameters, which is possible by sequential data assimilation using joint state-parameter estimation or inverse modelling. In future work we will test the joint estimation of states and soil hydraulic parameters by jointly assimilating surface soil moisture and groundwater level information.

As this work focused on defining the best data assimilation strategy for data assimilation problems for coupled land surface-subsurface models, model structural errors were neglected. This provides favorable conditions for our synthetic experiments. Model structural errors could be important in practice; examples are neglecting preferential flow in the unsaturated zone or the limited number of plant functional types to cover all vegetation types. It is therefore important in future work to evaluate this data assimilation methodology for real-world land surface-subsurface data assimilation problems. Nevertheless, we think that the ParFlow-CLM is less affected by model structure errors than the CLM stand-alone model, as ParFlow eliminates some of the deficiencies of CLM, for example concerning the role of groundwater.

4.6 Conclusions

In this work, we develop and compare five data assimilation methodologies to improve root zone soil moisture estimation using groundwater level or joint groundwater level and surface soil moisture data, in an integrated model TerrSysMP. The performance of the five data assimilation methodologies is evaluated for 36 synthetic scenarios under different groundwater level dynamics. Observations of groundwater levels are assimilated in the form of pressure head data or soil moisture data in TerrSysMP to update pressure heads and/or soil moisture in the whole domain. The results for assimilation of pressure or log-transformed pressure show that it can be problematic to apply EnKF, which performs optimally for

Gaussian distributions, to scenarios with strongly non-Gaussian state distributions (caused by extreme negative pressure heads in the unsaturated zone). The results from assimilation of groundwater level data in the form of soil moisture data (i.e., for the aquifer part soil moisture content is set equal to the porosity) show that this strategy often gives satisfying results, but under certain conditions (if nearly all ensemble members have a simulated groundwater depth closer to the surface than the measured groundwater level) updating of the states in the unsaturated zone does not work. The best methodology is assimilating groundwater level data to update the pressure head in the saturated zone and soil moisture content in the unsaturated zone. This method alleviates the impact of skewed pressure distributions on the EnKF analysis step. Joint assimilation of surface soil moisture and groundwater levels also shows great potential in improving the root zone soil moisture profile in synthetic scenarios with both uncertain soil hydraulic parameters and meteorological forcings. It is important to extend this work to include estimation of unknown soil and aquifer hydraulic parameters, and test in large scale real-world applications.

Chapter 5 : Under which conditions can assimilation of groundwater level data improve root zone soil moisture characterization?

*adapted from: Zhang, H., Kurtz, W., Kollet, S., Vereecken, H., and Hendricks Franssen, H.-J.: Under which conditions can assimilation of groundwater level data improve root zone soil moisture characterization? Journal of Hydrology, 2018, under review.

5.1 Introduction

Temporal and spatial variations of root zone soil moisture content are important in hydrological and climate studies, because root zone soil moisture exerts an important control on water and energy fluxes between the subsurface, land surface and the atmosphere (Chen and Hu, 2004). However, characterization of root zone soil moisture is not trivial at large spatial scales which are typically applied in land surface models, because not enough point soil moisture measurements are available. In addition, remote sensing only provides an estimate of surface soil moisture content which has limited potential to improve root zone soil moisture-characterization. It is significant to find a way to improve the root zone soil moisture estimation. Root zone soil moisture is affected by soil type, climate condition, vegetation type, topography and also groundwater level (GWL) (Liang and Guo, 2003; Chen and Hu, 2004; Fiori and Russo, 2007; Kollet and Maxwell, 2008; Miguez-Macho and Fan, 2012; Zhu et al., 2013). This paper explores especially the potential of GWL data to improve root zone soil moisture characterization.

Many GWL measurement networks exist, such as the national framework for groundwater monitoring in the United States (Subcommittee on Ground Water, 2011), and groundwater monitoring networks in Europe (Nixon et al., 1996). The assimilation of GWL data is an interesting methodology to improve large-scale root zone soil moisture characterization. A shallow GWL is more likely to generate higher root zone soil moisture, and also higher actual evapotranspiration. A deeper groundwater table has high possibility to generate lower root zone soil moisture and soil moisture at the land surface is then mostly affected by atmospheric conditions. Thus, under water-limited condition, the available soil water may limit evapotranspiration.

Coupled land surface-subsurface models (Kollet and Maxwell, 2008; Maxwell, 2009; Larsen et al., 2014; Shrestha et al., 2014; Zhang et al., 2018) allow surface-subsurface flow simulation and produce improved root zone soil moisture predictions (Maxwell et al. 2015). Some studies analyzed the interaction between the unsaturated zone and groundwater in such integrated models. Chen and Hu (2004) studied groundwater influences on soil moisture and surface evaporation in a soil hydrological model which includes groundwater effects by allowing water exchange between the unsaturated zone and groundwater. They found that spatial variations in the GWL may result in spatial variability in soil moisture content. Kollet and Maxwell (2008) used a three-dimensional variably saturated subsurface flow model (ParFlow) coupled to a land surface model (Common Land Model) to capture the influence of

groundwater dynamics on land surface processes at the catchment scale. They detected a range of critical water table depths where land surface processes show a strong sensitivity with respect to GWL. Rihani et al. (2010) used this coupled model with idealized simulations to investigate the effects of terrain, subsurface heterogeneity, climate conditions and vegetation on water table variability and to identify regions with stronger interaction between water table depth and the land surface energy balance.

Hydrological data assimilation takes advantage of hydrological measurements to improve the performance of hydrological models. Several studies previously assimilated GWL data to improve land surface fluxes using integrated hydrological models. Zhang et al. (2016) assimilated observed groundwater heads and near surface soil moisture into the MIKE SHE integrated hydrological model using the Ensemble Transform Kalman Filter (ETKF) and analyzed the impact of ensemble size and localization. In general, assimilation improved the model performance and the necessity was shown to apply localization especially when jointly assimilating groundwater head and soil moisture data. Shi et al. (2015) also assimilated GWLs and near surface soil moisture in the variably-saturated flow model HYDRUS-1D for estimating soil hydraulic parameters with the Ensemble Kalman Filter (EnKF). They found that estimates of hydraulic parameters from GWL data may suffer from strong degradation, if a large number of parameters must be identified. They also showed that a combined use of GWL data with soil moisture data is more helpful to improve the parameter estimation. Thus GWL data assimilation in integrated land surface-subsurface models is still a topic of ongoing research. Previous studies did not specifically focus on improved root zone soil moisture characterization with help of GWL assimilation. Because it can be expected that the success of GWL data assimilation for root zone soil moisture characterization depends on the correlation between GWL and root zone soil moisture, it is important to systematically characterize the impact of climate, soil, vegetation types but also GWLs, which is done in this study. The simulations are carried out with the highly modular and scale-consistent Terrestrial System Modeling Platform (TerrSysMP) (Shrestha et al., 2014). GWLs are assimilated for all combinations of selected climate conditions, PFT's and soil types to see how the different conditions affect the assimilation performance in terms of root zone soil moisture characterization.

5.2 Methodology

5.2.1 TerrSysMP

TerrSysMP is a recently developed model to simulate the coupled water and energy cycles for the atmosphere, the land surface and the subsurface. TerrSysMP couples three existing component models: the groundwater flow model ParFlow (Ashby and Falgout, 1996; Jones and Woodward, 2001), the land surface model CLM (Community Land Model, version 3.5) (Oleson et al., 2008), and the atmospheric model COSMO (Baldauf et al., 2011). For more details about the model physics see Shrestha et al. (2014). In our work, only the land surface part CLM and subsurface part ParFlow were used.

Information between CLM and ParFlow is exchanged via the library OASIS-MCT (Valcke, 2013). ParFlow provides CLM with the calculated subsurface pressure (ψ) and saturation (S_w) values for the first 10 subsurface layers and in return CLM provides the upper boundary condition for ParFlow, which consists of depth differentiated net infiltration values which are calculated based on the land surface fluxes of CLM (precipitation, interception, total evaporation, total transpiration). Thus, the 1D column soil moisture prediction of CLM is replaced by the 3D ParFlow simulations.

5.2.2 Assimilation of GWLs with EnKF

EnKF was first proposed by Evensen (1994) as a Monte Carlo variant of the classical Kalman Filter. The governing model equations are solved many times, for different input states, model forcings and/or parameters. The ensemble of model realizations (e.g., with different initial conditions, forcings and/or parameters) is propagated forward, until new measurement data $\mathbf{y}_t$ are available at time t and EnKF then performs a Bayesian update on the ensemble of state vectors $\mathbf{x}_t$. $\mathbf{y}_t$ is perturbed to generate an observation vector for the j^{th} ensemble member at time t:

$$\mathbf{y}_{j,t} = \mathbf{y}_t + \boldsymbol{\varepsilon}_{j,t} \tag{5.1}$$

where $\boldsymbol{\varepsilon}_{j,t}$ is a vector with perturbation terms drawn from a normal distribution $N(0, \sigma)$ where the standard deviation σ is equal to the expected measurement error, which is set to 0.01m for GWL measurements in this study. For each ensemble member j at time step t, the state vector $\mathbf{x}_{j,t}$ is updated according to:

$$\mathbf{x}_{j,t}^{a} = \mathbf{x}_{j,t}^{f} + \mathbf{K}_t(\mathbf{y}_{j,t} - \mathbf{H}\mathbf{x}_{j,t}^{f}) \tag{5.2}$$

where $\mathbf{x}_{j,t}^{a}$ and $\mathbf{x}_{j,t}^{f}$ are the updated state vector and the model predicted state vector respectively. $\mathbf{H}$ is the observation operator which represents the relationship between the observation vector $\mathbf{y}$ and the state vector $\mathbf{x}$. The Kalman gain $\mathbf{K}_t$ is calculated by:

$$\mathbf{K}_t = \mathbf{C}_t\mathbf{H}^{\mathrm{T}}(\mathbf{H}\mathbf{C}_t\mathbf{H}^{\mathrm{T}} + \mathbf{R})^{-1} \tag{5.3}$$

where $\mathbf{R}$ is the measurement error covariance matrix. $\mathbf{C}_t$ is the covariance matrix at time step t:

$$\mathbf{C}_t = \frac{1}{N-1}\sum_{j=1}^{N}(\mathbf{x}_{j,t}^{f} - \overline{\mathbf{x}}_t^{f})(\mathbf{x}_{j,t}^{f} - \overline{\mathbf{x}}_t^{f})^{\mathrm{T}} \tag{5.4}$$

where N is the number of ensemble members and $\overline{\mathbf{x}}_t^{f}$ is a vector containing predicted ensemble mean values.

In this work, assimilated measurement data are groundwater levels, but the prognostic variable of ParFlow is pressure. Hence, groundwater level measurements are transferred into pressure in the saturated zone, which is calculated by:

$$\psi_i = \mathrm{GWL} - D_i \tag{5.5}$$

Where i is the i^{th} saturated soil layer, ψ_i is the pressure for the i^{th} saturated layer, D_i the depth of the i^{th} saturated soil layer and GWL the water table depth. All depths are negative using the land surface as reference (0m).

The observation vector $\mathbf{y}_t$ at time step t includes pressure values for the saturated grid cells (at locations with a groundwater table observation).

Pressure heads simulated for the saturated zone and soil moisture for the unsaturated zone are stored in the state vector $\mathbf{x}$. This approach assures that the state vector only consists of positive values and avoids skewed and strongly non-Gaussian distributions of states which can worsen the performance of EnKF (Zhang et al., 2018). At each time step, after model prediction and before assimilation, we reconstruct the state vector and the division between the saturated and unsaturated zone for the domain is re-defined again and shared by all the ensemble members. The division is firstly defined by the deepest GWL among the ensemble members. Then for grid columns with observations, a correction of this depth is applied, if the GWL of the observation is higher than this depth. Grid cells above this depth are updated in terms of soil moisture and grid cells below the depth in terms of pressure head. Further details are provided in Zhang et al. (2018). The state vector at time step t is defined as:

$$\mathbf{x}_t = \begin{pmatrix} \boldsymbol{\psi}_t \\ \boldsymbol{\theta}_t \end{pmatrix} \tag{5.6}$$

where $\boldsymbol{\psi}_t$ is the pressure vector and $\boldsymbol{\Theta}_t$ the soil moisture vector at time step t. Note that the dimensions of $\boldsymbol{\psi}_t$ and $\boldsymbol{\Theta}_t$ change over time. The dimension of $\mathbf{x}_t$ is constant and equal to the total number of grid cells.

After assimilation by EnKF, $\boldsymbol{\Theta}_t$ in $\mathbf{x}_{j,t}^{a}$ in equation (5.2) is transferred to pressure by the pressure-saturation relationship as pressure is the prognostic variable in ParFlow. In this work, the van Genuchten model (van Genuchten, 1980) is used:

$$\psi = -\frac{[(\frac{\theta_S - \theta_r}{\theta(\psi) - \theta_r})^{1/m} - 1]^{1/n}}{\alpha} \tag{5.7}$$

where θ_s is the saturated soil moisture content which is equal to porosity (Ø), θ_r is residual soil moisture content, α is a measure of the first moment of the pore size density function, n is an inverse measure of the second moment of the pore size density function, and $m = 1 - 1/n$. ParFlow solves for pressure for the next time step and calculates the saturation field also by the van Genuchten model.

In our work, the modular high-performance data assimilation framework TerrSysMP-PDAF is used which couples TerrSysMP and a parallel data assimilation library PDAF (Parallel Data Assimilation Framework) (Nerger and Hiller, 2013) to do data assimilation within TerrSysMP. For more details about the framework see Kurtz et al. (2016).

5.3 Experiment Setup

Assimilation experiments were performed for simplified synthetic set-ups at small spatial scales. All the experiments include a domain of 2 by 2 grid columns (1km × 1km). Each grid column has 30 vertical cells (soil layers) of variable thicknesses for the upper 10 soil layers

and fixed depths for the lower 20 soil layers resulting in a total depth of 30m. The land surface slope is 0.01 in both x and y directions to allow for topographically driven overland flow and groundwater flow based on the terrain following grid implementation of ParFlow (Maxwel, 2013). Overland flow is the upper boundary condition and zero fluxes for the bottom boundary and lateral boundaries are imposed. The climatic forcings are homogeneous over the domain, the same holds for PFT and soil type while soil hydraulic parameters are vertically heterogeneous.

In order to study assimilation of GWLs for improving root zone soil moisture estimation under different climate conditions, PFTs and soil types, the experiments are performed for 5 PFTs, 5 climate conditions and 4 soil texture types which results in 100 (5×5×4) cases which produce different GWLs and soil moisture distributions. All simulations were performed on the supercomputer JURECA (Jülich Supercomputing Centre, 2016).

The 5 climate datasets are obtained from the CEOP (the Coordinated Energy and Water cycle Observations Project) Reference Site Data Sets and AmeriFlux Network, including humid temperate, humid tropical, arid tropical, semiarid Mediterranean and tropical monsoon climate conditions (see table. 5.1). For each site, climate data from two years are used, one year is for model spin up and the second year for model simulation/ assimilation. Note however that it was not a main aim of this research to reproduce typical groundwater levels for different climates, but to generate groundwater levels which differ between different climates. The 5 PFTs include bare soil, crop land, C3/C4 grass (arid sites have C4 grass, others have C3 grass), needle leaf tree and broadleaf tree. They have different rooting depths and their physical, phylogenetic and phenological characteristics are defined in CLM. The 4 soil texture types are clay, loam, loamy sand and silt loam. Their residual soil moisture θ_r and saturated hydraulic conductivity k_s are from Leij et al. (1996), sand fraction and clay fraction are chosen based on the soil types, and saturated soil moisture (porosity) θ_s is calculated on the basis of the sand fraction via the following pedotransfer function in CLM (version 3.5), to keep functional consistence between CLM and ParFlow:

$$\theta_s = 0.489 - 0.00126(sand\%) \tag{5.8}$$

Table 5.2 shows the values of the parameters for the 4 soil types.

Reference simulations

The synthetic reference simulations for the 100 cases are generated by imposing the climate conditions, PFTs, and the soil property values from table 5.2. The soil hydraulic parameter k_s is vertically heterogeneous. Spatial variability of k_s is created to generate a reference heterogeneous k_s. The layer specific k_s is generated by decreasing it exponentially with soil depth (Niu et al., 2005):

$$\begin{cases} k_s(z_i) = k_s(z_1) * e^{-f(z_i - z_1)}, & i = 1{:}10 \\ k_s(z_i) = k_s(z_{10}), & i = 11{:}30 \end{cases} \tag{5.9}$$

where z_i is the soil depth of the ith layer, $k_s(z_1)$ is the k_s of the top layer which is taken from table 5.2. For the upper 10 layers k_s decreases with depth and the layers 11 until 30 have the same k_s as the 10th layer. f is the decay factor taken as 2.0 m^{-1} according to Niu et al. (2005).

Van Genuchten parameters α and n are essential in describing the pressure-saturation and relative conductivity relationships to close the problem mathematically. We use the covariances among transformed k_s, α and n to get the values of α and n from the reference heterogeneous k_s, as described in Carsel and Parrish (1988). Table 5.3 shows the transformations and the covariances for each soil type. Layer specific α and n-values are generated based on the correlation between (transformed values of) k_s values and (transformed values of) α and n, given the covariances provided in table 5.3. After the multivariate sampling step, values are back transformed to k_s, α and n, which are used as reference parameters. More details can be found in Carsel and Parrish (1988).

For each case, the model spin up is performed for 100 years from an initial GWL of -1 m. Afterwards, a reference simulation is performed for 1 year to produce synthetic GWL, which are assimilated as daily values in the data assimilation experiments.

Table 5.1 Five climate types used in the data assimilation cases.

Site name	Latitude	Longitude	Average yearly temperature (°C)	Average yearly precipitation (mm)	Köppen-Geiger classification
California desert site	33.65N	-116.37E	25.3	70.2	Hot desert climates (BWh)
Picassent site in **Spain**	39.37N	-0.45E	16.7	400.5	Hot semi-arid climates (Bsh)
Northeast **Thailand** site	14.47N	102.38E	26.1	550.2	Tropical savanna climate (Aw)
Cabauw site in **Netherlands**	51.97N	4.93E	11.5	771.8	Temperate oceanic climate (Cfb)
Kennedy Space Center in **Florida**	28.61N	-80.67E	22.2	1000.5	Humid subtropical climate (Cfa)

Table 5.2 Four soil types used in the data assimilation cases. Values of θ_r and k_s (cm/hr) are from Leij et al. (1996), sand% and clay% are chosen based on the soil types, θ_s is calculated by equation (5.8).

Soil texture	θ_s	θ_r	k_s (cm/hr)	sand%	clay%
Clay	0.4575	0.068	0.02	25	50
Loam	0.4386	0.078	1.04	40	20
silt loam	0.4512	0.067	0.45	30	10
loamy sand	0.388	0.057	14.6	80	15

Ensemble generation

The parameter ensemble is generated for assimilation. Firstly $\log_{10}(k_s(z_1))$ is perturbed by an additive random perturbation which is sampled from the standard normal distribution $\mathcal{N}(0,1)$ to generate 128 ensemble members. For each ensemble member, the initial perturbation is done for the uppermost layer, equation (5.9) is then applied for the layers 2 until 30, and α and n are also sampled from the multivariate Gaussian distribution described

before. In addition, precipitation is perturbed in the data assimilation experiments by multiplicative noise sampled from a uniform distribution with values between 0.5 and 1.5. For each case, the 128 ensemble members are also spun up for 100 years from an initial GWL of -1m, and then assimilation is performed for 1 year.

Table 5.3 Covariances among transformed k_s (cm/hr), α (cm^{-1}) and n for loam, silt loam and loamy sand. Transformations include no transformation (NO), lognormal (LN), log ratio (SB) and hyperbolic arcsine (SU). Transformations and units are shown in brackets. Values are from Carsel and Parrish (1988).

clay	**SB (k_s)**	**SB (α)**	**LN (n)**
SB (k_s)	1.96	0.565	0.048
SB (α)	0.948	0.172	0.002
LN (n)	0.908	0.910	0.016
loam	**SB (k_s)**	**SB (α)**	**SU (n)**
SB (k_s)	1.41	0.611	0.055
SB (α)	0.982	0.093	0.026
SU (n)	0.632	0.591	0.029
silt loam	**LN (k_s)**	**LN (α)**	**SB (n)**
LN (k_s)	1.478	0.525	0.353
LN (α)	0.986	0.082	0.234
SB (n)	0.730	0.775	0.158
loamy sand	**SB (k_s)**	**NO (α)**	**SB (n)**
SB (k_s)	1.48	0.037	0.211
NO (α)	0.986	0.014	0.019
SB (n)	0.730	0.354	0.108

5.4 Results and Discussions

We investigate the grid columns which have the highest elevation in the domain. The results for the different cases are analyzed to study the role of the PFTs, climate conditions and soil texture on the assimilation of GWLs to improve root zone soil moisture characterization. The 10 upper soil layers are assumed to be the root zone with a depth of 3m. In order to evaluate the assimilation performance, the Root Mean Square Error (RMSE) of soil moisture for these layers is calculated as:

$$\mathrm{RMSE}^{i} = \sqrt{\frac{1}{T}\sum_{t=1}^{T}\left(\bar{\theta}_{t,\,i} - \theta_{t,\,i}^{\mathrm{ref}}\right)^{2}} \quad , i=1{:}10 \tag{5.10}$$

where T is the total number of assimilation time steps (365), $\bar{\theta}_{t,\,i}$ is the ensemble average soil moisture content of the i^{th} layer at time step t (either from open loop run or data assimilation run) and $\theta_{t,\,i}^{\mathrm{ref}}$ is the reference soil moisture content of the i^{th} layer at time step t. For each case, a vertically averaged RMSE is also calculated:

$$\mathrm{RMSE}^{\mathrm{Depth\text{-}Mean}} = \sqrt{\frac{1}{T}\,\frac{1}{N_{\mathrm{layers}}}\sum_{i=1}^{N_{\mathrm{layers}}}\sum_{t=1}^{T}\left(\bar{\theta}_{t,\,i} - \theta_{t,\,i}^{\mathrm{ref}}\right)^{2}} \quad , \; N_{\mathrm{layers}}=10 \tag{5.11}$$

where N_{layers} is the total number of root zone soil layers.

A RMSE reduction is calculated by dividing the RMSE of soil moisture from the data assimilation run $\bar{\theta}_{t,i}^{\text{ass}}$ by the RMSE of soil moisture from the open loop run $\bar{\theta}_{t,i}^{\text{ol}}$:

$$\Delta\text{RMSE}^{i} = \frac{\sqrt{\frac{1}{T}\sum_{t=1}^{T}(\bar{\theta}_{t,i}^{\text{ass}} - \theta_{t,i}^{\text{ref}})^2}}{\sqrt{\frac{1}{T}\sum_{t=1}^{T}(\bar{\theta}_{t,i}^{\text{ol}} - \theta_{t,i}^{\text{ref}})^2}},\ i=1{:}10 \tag{5.12}$$

and the Depth-Mean RMSE reduction is calculated based on equation (5.11):

$$\Delta\text{RMSE}^{\text{Depth-Mean}} = \frac{\sqrt{\frac{1}{T}\frac{1}{N_{\text{layers}}}\sum_{i=1}^{N_{\text{layers}}}\sum_{t=1}^{T}(\bar{\theta}_{t,i}^{\text{ass}} - \theta_{t,i}^{\text{ref}})^2}}{\sqrt{\frac{1}{T}\frac{1}{N_{\text{layers}}}\sum_{i=1}^{N_{\text{layers}}}\sum_{t=1}^{T}(\bar{\theta}_{t,i}^{\text{ol}} - \theta_{t,i}^{\text{ref}})^2}},\ N_{\text{layers}}=10 \tag{5.13}$$

A RMSE reduction smaller than 1.0 implies that assimilation improves soil moisture characterization.

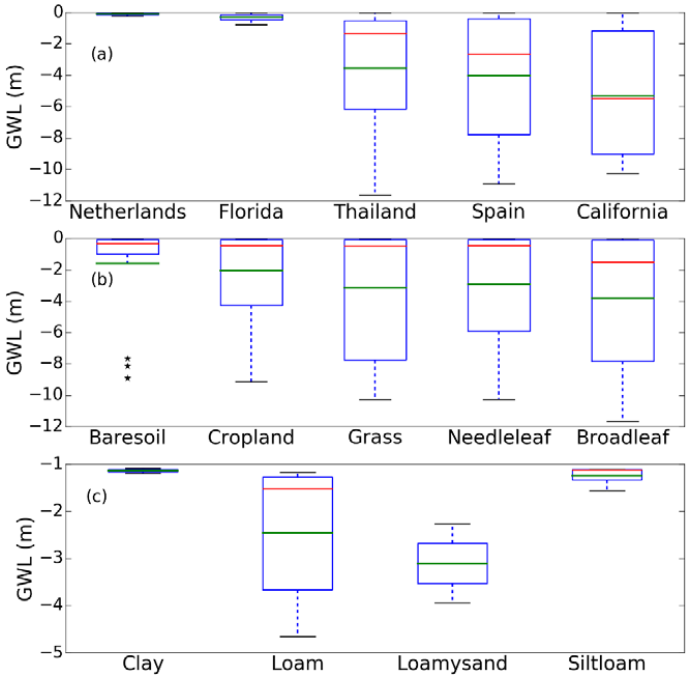

Figure 5.1 Boxplot of yearly averaged GWLs for all cases in terms of climate conditions (a), PFTs (b) and soil texture types (c) (only a subset of the simulations is used). y axis is the GWL (m). In the boxplots, the red line represents the median value and the green line mean value.

Figure 5.1 shows the boxplots of reference GWLs (yearly average for the second year) for all cases. In figure 5.1(a) each boxplot shows the effects of climate condition on GWLs (20 cases = 5 PFTs × 4 soil texture types), in figure 5.1(b) the effect of PFT (20 cases = 5 climate

conditions × 4 soil texture types), and in figure 5.1(c) the effect of soil texture (cases with GWL between -5m to -1m). In figure 5.1(c) only the GWLs between -5m to -1m are shown for soil textures in order to focus on the specific impact of soil texture on GWL-assimilation. Because of our artificial setup (like zero flux for the bottom boundary and manually generated k_s, α and n), some cases show artifacts, such as very shallow GWLs for loamy sand, while this soil type in reality is generally associated with deeper GWLs because it is more permeable and tend to have lower sorption potentials to hold water. From figure 5.1 we can see that different climate conditions, PFTs and soil textures result in different GWLs. Sites with arid/semi-arid climate or plants with deep roots like trees result in deeper groundwater tables.

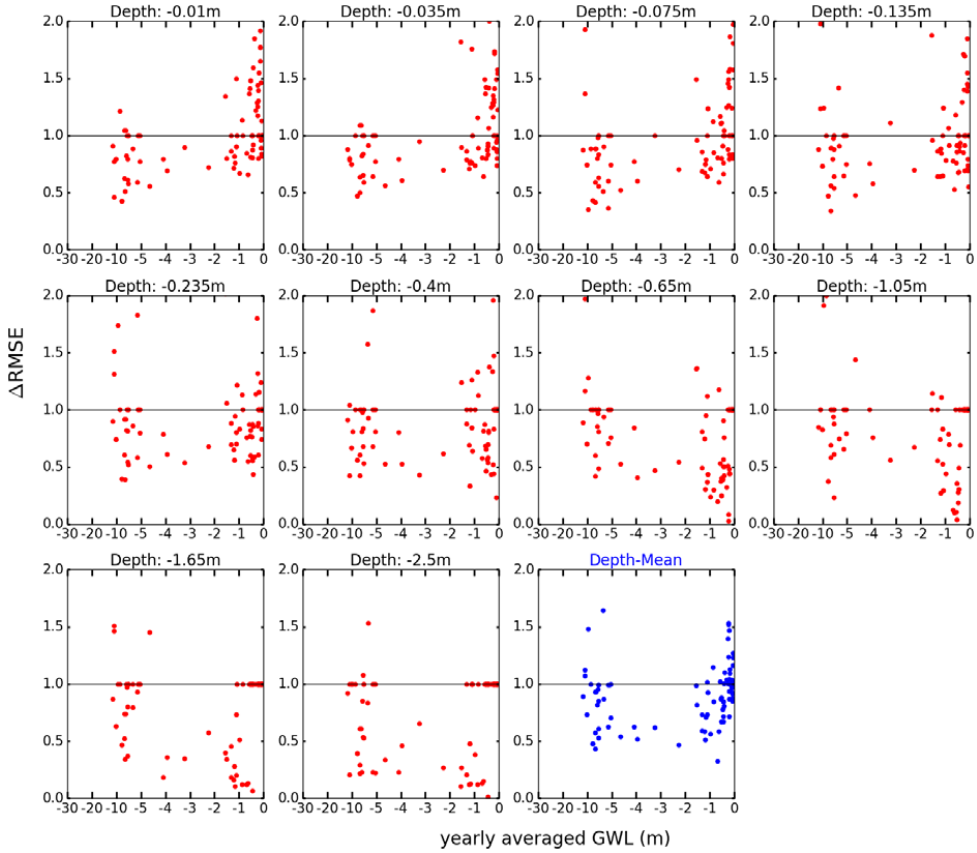

Figure 5.2 RMSE reductions of root zone soil moisture as a function of yearly averaged GWLs. Subfigures correspond to the upper 10 soil layers and the Depth-Mean, each red/blue dot represents a case, x-axis is yearly averaged GWL, y-axis is the RMSE reduction. If the RMSE reduction value is less than 1.0 (indicated by a black line), assimilation improves soil moisture estimation.

Figure 5.2 shows the RMSE reductions of soil moisture (for each soil layer and also averaged over the root zone) vs. yearly averaged reference GWL for all 100 cases (5 PFTs × 5 climate

conditions × 4 soil texture types). If GWL is too deep (<-10m) or too shallow (-1m to 0m), the assimilation does not result in an improved characterization of root zone soil moisture, depending on the combination of soil type, PFT and climate conditions. When GWL is between 1 to 10m, for almost all the cases, assimilation of GWL improves the root zone soil moisture estimation, which means that in this critical zone, soil moisture is sensitive to the water table position. This finding is consistent with the results from *Kollet and Maxwell* (2008), where the authors demonstrated that the land surface energy budget is most sensitive to the GWL when GWL is in a critical depth range.

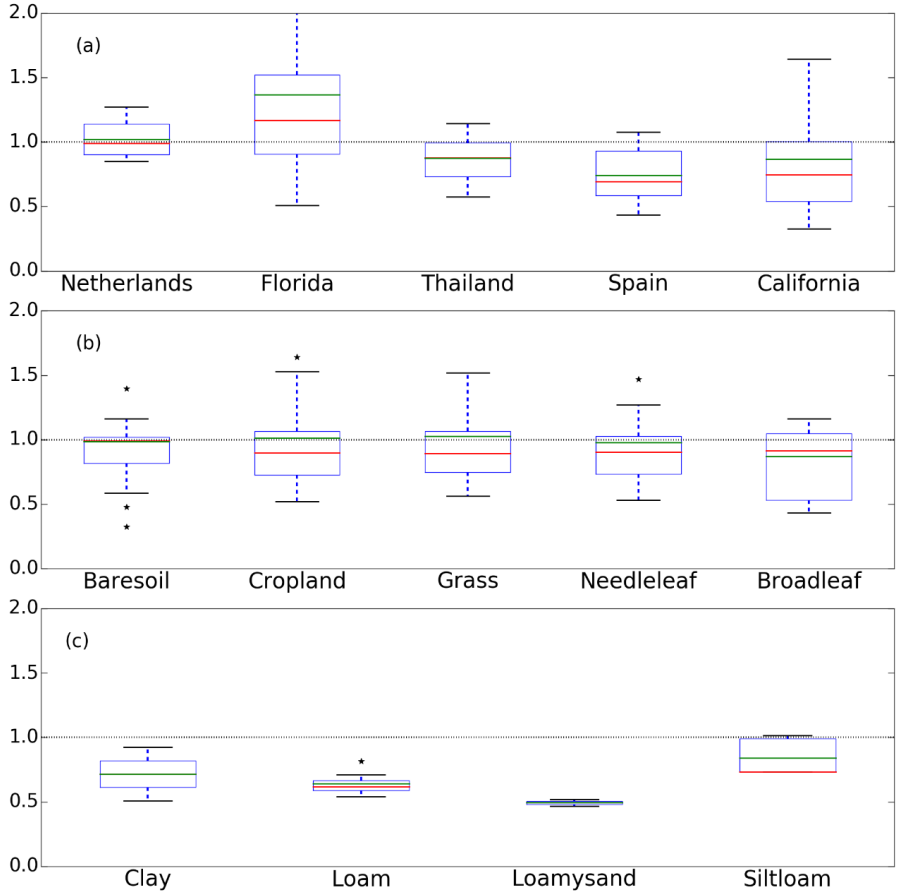

Figure 5.3 Boxplot of $\Delta RMSE^{Depth\text{-}Mean}$ for all cases in terms of climate conditions (a), PFTs (b) and soil texture types (c). In the boxplots, the red line represents median value and the green line mean value. The value 1.0 is indicated by a black dot line.

Figure 5.3 shows boxplots of the vertically averaged RMSE reduction as a function of climate, PFT and soil type. In figure 5.3(a) each boxplot shows the effect of climate condition on the assimilation of GWL (20 cases = 5 PFTs × 4 soil texture types), in figure 5.3(b) each boxplot shows the effect of PFT (20 cases = 5 climate conditions × 4 soil texture types) and

in figure 5.3(c) the effect of soil texture is shown (cases with GWL between -5m to -1m). Like figure 5.1(c) here in figure 5.3(c) effect of soil texture on the assimilation performance is studied with a subset of simulations. We assume that if the median and mean values are 1, there is no effect of the climate condition in figure 5.3(a), the PFT in figure 5.3(b) or soil type in figure 5.3(c) on the $\Delta RMSE^{Depth\text{-}Mean}$, and if the median and mean are >1, assimilation worsens root zone soil moisture characterization, and otherwise assimilation improves root zone soil moisture characterization.

The effect of climate condition on the assimilation is discussed in the following. From figure 5.3(a), we see that data assimilation does not significantly improve root zone soil moisture characterization for humid sites (Netherlands and Florida), but assimilation does improve soil moisture characterization for semi-arid and arid sites (Thailand, Spain, and California). Humid sites result in very shallow GWL and semi-arid/arid sites in deeper GWL. From figure 5.1(a), we can see that the distribution of GWL for the semi-arid/arid sites covers a broader range and includes often the aforementioned critical zone (-10m to -1m). Climate conditions affect strongly the performance of GWL assimilation as climate exerts a strong control on GWLs, which is essential in the assimilation.

The effect of PFT on the assimilation is discussed in the following. From figure 5.1(b) we can see that the 5 PFTs result in different GWL distributions because of different rooting depths (see figure 5.5). However, differences among the 5 boxplots in figure 5.3(b) for the 5 PFTs are not as large as for climate and soil texture, because their mean values, median values and box shapes are similar. Only the PFT broadleaf tree is associated with a lower mean and median values. In figure 5.1(b) even though the 5 box shapes are distinct, their mean and median values are close. All the 5 PFTs are associated with GWL values in the critical depth range, and as this critical depth is closely associated with the assimilation performance, vegetation types have a smaller impact on the assimilation performance.

The effect of soil texture on the assimilation is discussed in the following. From figure 5.3(c) we can see that even though all GWLs are in the critical range [-10m, -1m] the performances of the 4 soil textures are different. Loam soil and especially loamy sand perform better than clay and silt loam. The explanation would be that for different soil texture the correlation among soil hydraulic parameters (k_s, α and n) is different (see section 5.3 and figure 5.4), thus assimilating GWL has a differing effect on the characterization of pressure and saturation via equation (5.7). In addition, ensemble members are generated by perturbing soil hydraulic parameters which play an important role in the assimilation (e.g. ensemble spread). Therefore, soil texture also affects clearly the performance of assimilation because it affects GWL dynamics and the soil properties (e.g. k_s) affect the GWL assimilation.

In order to better illustrate the effect of climate condition, soil texture and PFT on the assimilation performance, vertically averaged RMSE reduction of root zone soil moisture as a function of yearly averaged GWLs is plotted in figure 5.6. In figure 5.6(a), 5.6(b) and 5.6 (c) different colors represent different climate conditions, PFTs and soil textures respectively. Figure 5.6(a) illustrates that the RMSE reductions for the California site are mostly lying below other climate sites, and figure 5.6(b) illustrates that the RMSE reductions for broadleaf tree are lying below others, and figure 5.6(c) shows that the RMSE reductions for loamy sand

soil are a bit below others. But there is not a very clear pattern in the figure that shows how different climate conditions, soil textures and PFTs affect the RMSE reduction. The GWL depth has the largest influence on the results and other impacts are marginal.

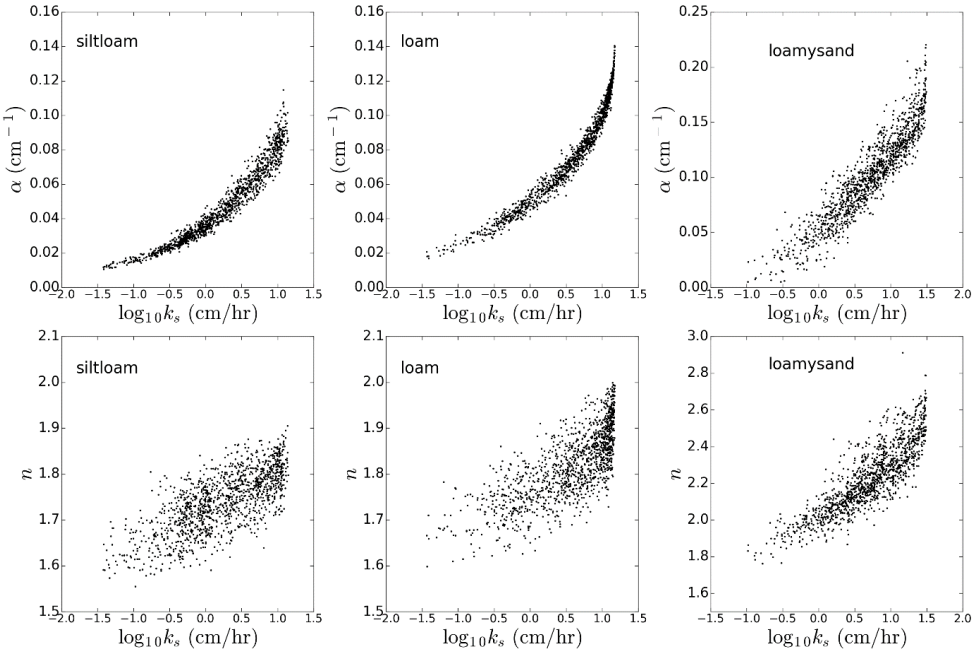

Figure 5.4 Scatter plot of α (cm^{-1}) and n as a function of $\log_{10}k_s$ (cm/hr) for the 128 ensemble members for silt loam texture (left), loam soil (middle), and loamy sand texture (right).

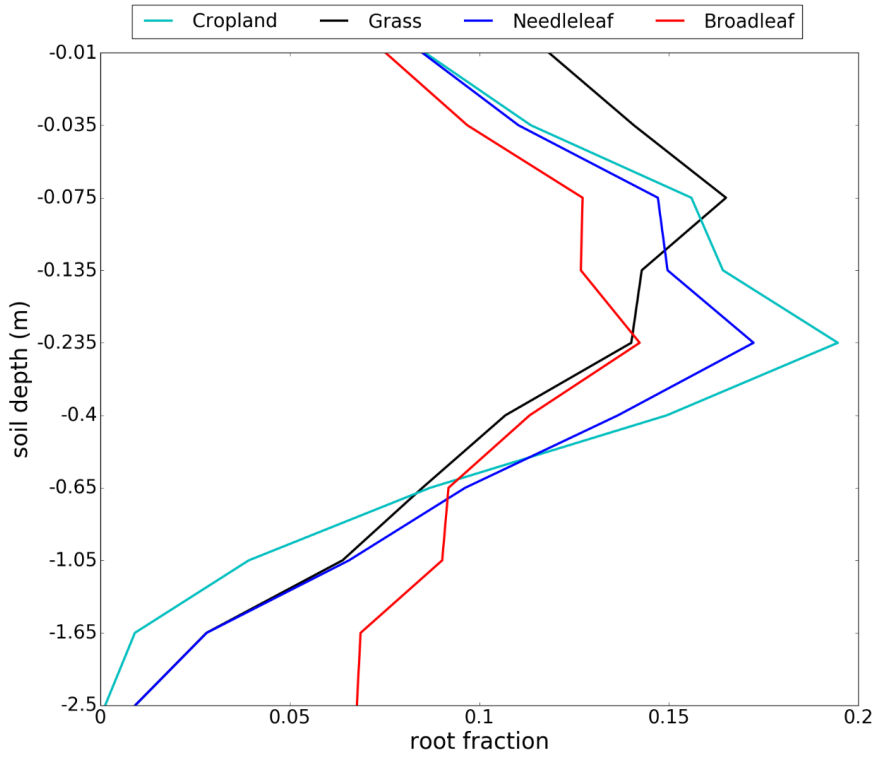

Figure 5.5 Root fraction for the upper 10 layers for the 4 PFTs: cropland, grass land, needleleaf tree and broadleaf tree. y-axis is the soil depth for the 10 layers and x-axis is the root fraction.

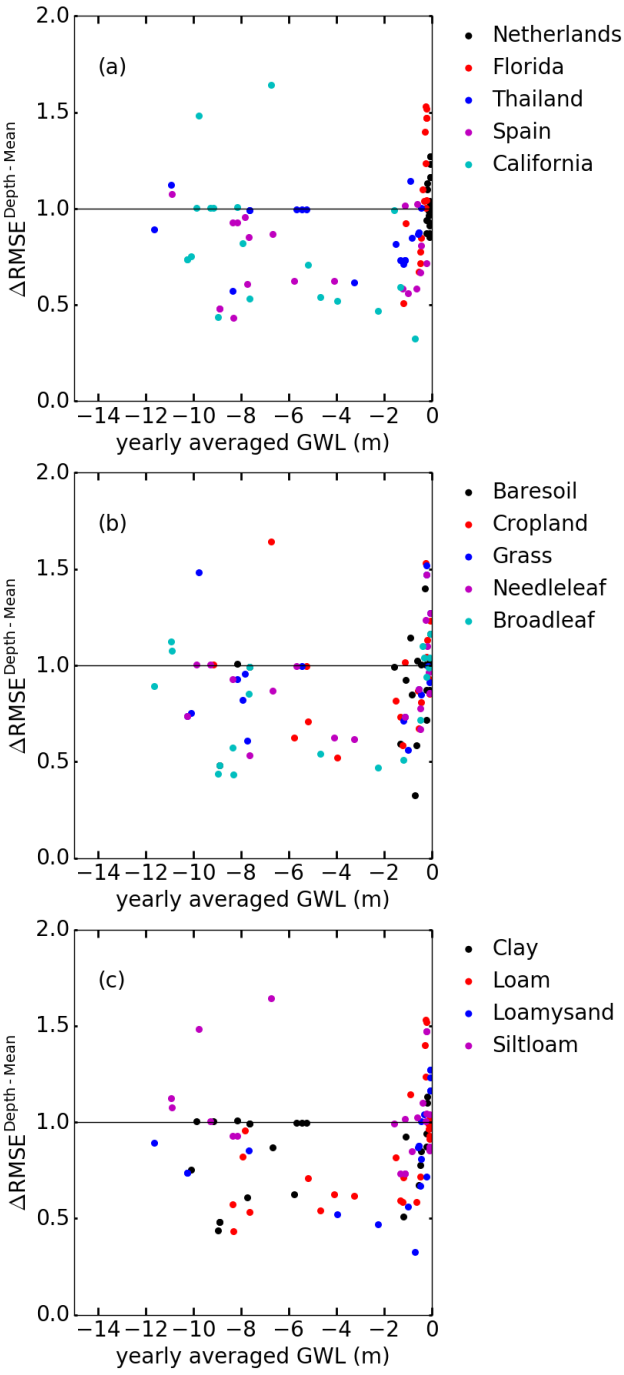

Figure 5.6 Vertically averaged RMSE reduction of root zone soil moisture as a function of yearly averaged GWLs. Each dot represents each case, and different colors show different climate conditions (a), different PFTs (b) and different soil textures (c).

5.5 Conclusions

In this study, groundwater level (GWL) data were assimilated in the integrated land surface-subsurface model TerrSysMP. Synthetic experiments were used to study under which conditions assimilation of GWLs can help to better characterize root zone soil moisture content. In particular, the influence of climate, plant functional type (PFT) and soil texture on the assimilation performance were analyzed. The 5 considered climate conditions were humid temperate, humid tropical, arid tropical, semiarid Mediterranean and tropical monsoon, the 5 plant functional types were needleleaf, broadleaf, grassland, cropland and bare soil and the 4 soil textures were clay, loam, silt loam and loamy sand. This resulted in 100 data assimilation cases in total. We find that there is a critical depth range (GWL between 1 to 10m) where assimilation leads to the largest improvements in root zone soil moisture estimation, due to pronounced sensitivity of root zone soil moisture to the GWL in this zone. The range of GWL (-10m to -1m) mainly determines the effectiveness of assimilation. In addition, GWL assimilation performance is influenced by the combination of climate condition, soil texture and PFT. Climate conditions can greatly affect the performance of assimilation as they strongly control GWL. Soil texture also affects the assimilation performance independent of its impact on GWL. Different soil textures have different soil hydraulic parameters which have different impacts on the pressure-saturation relationship and finally affect the assimilation performance. The PFT is found to have a relatively small effect on the assimilation performance. These results point to the potential of the available large scale networks of groundwater level observations for improving root zone soil moisture characterization in simulations with large scale land surface models, especially in areas with GWLs between 1m and 10m depth.

Chapter 6 : Summary and outlook

Surface and root zone soil moisture play an important role in the global and regional water and energy cycle, as they influence the partitioning of water into infiltration, runoff and evapotranspiration at the land-atmosphere interface and also the partitioning of incoming radiation into latent and sensible heat flux. Soil moisture contents can for example be estimated by field observations, remote sensing retrievals and land surface models. These methods provide soil moisture at different spatial and temporal scales but have individual shortnesses. For example, land surface models have high uncertainties which are related to simple parameterization of hydrologic processes, uncertain model input data and parameters. In this work, data assimilation was used to merge observations with land surface models (or an integrated terrestrial system model) to provide an improved dynamic representation of surface and root zone soil moisture. A central goal of the PhD work was to evaluate four different data assimilation methods in joint estimation of states and parameters and investigate the interaction between groundwater level and root zone soil moisture by assimilating groundwater level in an integrated model to update root zone soil moisture.

Therefore, first four different assimilation methods were evaluated in terms of joint estimation of states and parameters with two land surface models. Land surface models (LSMs) use a large cohort of parameters and state variables to simulate the water and energy balance at the soil-atmosphere interface. Many of these model parameters cannot be measured directly in the field, and require calibration against measured fluxes of carbon dioxide, sensible and/or latent heat, and/or observations of the thermal and/or moisture state of the soil. Data assimilation provides an approach to estimate model parameters (e.g. soil hydraulic parameters, soil thermal parameters and vegetation parameters) while considering model structural and model forcing uncertainties. There are several commonly used assimilation methods for joint state and parameter estimation. These methods not only update model states but also model parameters in the data assimilation framework. In this work we chose four important data assimilation methods for joint parameter and state estimation: the Ensemble Kalman Filter (EnKF) with state augmentation (EnKF-AUG) or dual estimation (EnKF-DUAL), respectively, and the residual resampling Particle Filter (RRPF) with a simple, statistically deficient, or more sophisticated, MCMC-based parameter resampling method (PMCMC). These four methods were implemented in two land surface models to compare and evaluate their usefulness and applicability: the Variable Infiltration Capacity Model (VIC) and the Community Land Model (CLM version 4.5). These two models had different parameterization mechanisms with different model parameters and CLM took into account groundwater while VIC didn't. The Rollesbroich experimental test site locates in the Eifel mountain range in western Germany. A soil moisture sensor network (with measurements at 5, 20 and 50 cm depth) has been installed at the Rollesbroich site. Areal-averaged soil moisture measurements at 5, 20 and 50 cm depth of the sensor network were used to do data assimilation with the four assimilation methods and the two models. The atmospheric forcing data for the models were measured at the eddy covariance tower located in the experimental site. The soil texture, bulk density and organic carbon data were determined by soil samples using laboratory experiments. Then they were averaged to obtain

mean values for the listed depths. As VIC and CLM have different representations of the physical processes of the land surface hydrology, different model parameters were chosen to be updated in the data assimilation. The assimilation period was from March to July, 2012 where soil moisture and model parameters were updated jointly via assimilation methods. The performance of the "calibrated" models was investigated using water content measurements of a 5-month evaluation period (August – December, 2012). As expected, all data assimilation methods enhanced the ability of the VIC and CLM models to describe spatiotemporal patterns of moisture storage within the vadose zone of the Rollesbroich site, particularly if the maximum baseflow velocity (VIC) or fractions of sand, clay, and organic matter of each layer (CLM) were estimated jointly with the model states of each soil layer. The differences between the soil moisture simulations of VIC and CLM were much larger than the discrepancies among the four data assimilation methods. The EnKF with state augmentation or dual estimation yielded the best performance of VIC and CLM during the calibration and evaluation period, yet results were in close agreement with the PF using MCMC resampling. Overall, CLM demonstrated the best performance for the Rollesbroich site. The large systematic underestimation of water storage at 50 cm depth by VIC during the first few months of the evaluation period questioned, in part, the validity of its fixed water table depth at the bottom of the modelled soil domain.

Based on the investigation of data assimilation methods in previous work, we used EnKF for following works. By studying the LSMs VIC and CLM (version 4.5), we found that the linkage between root zone soil moisture and groundwater was either neglected in VIC or simplified in CLM, which resulted in the large biases in the soil moisture predictions at 50cm depth. This neglect or simplification exists in most LSMs. However, the interaction between root zone soil moisture and groundwater plays an important role in subsurface hydrologic processes. Root zone soil moisture changes as a result of precipitation recharge and water exchange with both the atmosphere and groundwater. Excessive root zone soil moisture recharges groundwater by gravity drainage and groundwater can move upward to the root zone by capillary forces. The lack of understanding of the effect of groundwater on soil moisture prompted our following study.

To explicitly investigate the effects of groundwater on soil moisture we used the fully-coupled subsurface-land surface model TerrSysMP including variably saturated groundwater dynamics. TerrSysMP features three model components: an atmospheric model COSMO, a land surface model CLM (version 3.5) and a groundwater flow model ParFlow. These component models are integrated in a scale-consistent way conserving moisture and energy from the subsurface across the land surface into the atmosphere. In our work the land surface and subsurface components of TerrSysMP, CLM and ParFlow, were used. CLM calculates net infiltration for the upper ten layers of ParFlow and ParFlow in turn passes the subsurface saturation and pressure head to CLM. ParFlow is capable of simulating high-resolution groundwater flow with high-performance parallel computing.

As groundwater level can be continuously measured by automatic sensing devices at low cost and high accuracy, many groundwater monitoring networks are developed. Groundwater level measurements from these measurement networks are a valuable source of information.

We assimilated groundwater levels in TerrSysMP via the data assimilation framework TerrSysMP-PDAF to see how much root zone soil moisture prediction was improved. In order to assimilate groundwater levels in TerrSysMP via EnKF, groundwater levels were transformed to pressure head values in the saturated zone because pressure head was the prognostic variable in ParFlow. In principle, the state vector in EnKF consisted of pressure head for the whole domain including both saturated zone and unsaturated zone. EnKFperforms optimally only for Gaussian probability distributions of states and parameters. However, the pressure head in the soil profile might show very non-Gaussian pdf´s, e.g. under very dry conditions the pressure head for the upper soil layers can be very negative. The strongly non-Gaussian distriutions are related to some very negative pressure head values for some of the ensemble members. To solve this problem our second work aimed to find a proper way to assimilate the groundwater level data in TerrSysMP to improve root zone soil moisture estimation.

We tested and compared five data assimilation methodologies for assimilating groundwater level data via the EnKF to improve root zone soil moisture estimation with TerrSysMP. Groundwater level data were assimilated in the form of pressure head or soil moisture (set equal to porosity in the saturated zone) to update state vectors. In the five assimilation methodologies, the state vector contained either (i) pressure head, or (ii) log-transformed pressure head, or (iii) soil moisture, or (iv) pressure heads for the saturated zone only, or (v) a combination of pressure head for the saturated zone and soil moisture for the unsaturated zone. These methodologies were evaluated in synthetic experiments which were performed for different climate conditions, soil types and plant functional types to simulate various root zone soil moisture distributions and groundwater levels. The results demonstrated that EnKF cannot properly handle strongly skewed pressure distributions which were caused by extreme negative pressure heads in the unsaturated zone during dry periods. This problem could only be alleviated by (iii), (iv) and (v). The last approach gave the best results and avoided unphysical updates related to strongly skewed pressure heads in the unsaturated zone. If groundwater level data were assimilated by (iii), EnKF failed to update the state vector containing the soil moisture values if for (almost) all the ensemble members the observation did not bring significant new information. Synthetic experiments for the joint assimilation of groundwater levels and surface soil moisture also supported the methodology (v) and showed great potential for improving the representation of root zone soil moisture.

In the third work we applied the best assimilation methodology (v) to more synthetic experiments to investigate under which conditions assimilation of groundwater level data can improve root zone soil moisture characterization. The integrated model TerrSysMP was set up for 100 synthetic cases which covered 5 climate conditions (humid temperate/humid tropical/arid tropical/ semiarid Mediterranean/ tropical monsoon), 5 plant functional types (PFTs) (needleleaf/ broadleaf/ grassland/ cropland/ bare soil) and 4 soil textures (clay/ loam/ silt loam/ loamy sand), to generate different groundwater levels and soil moisture distributions. Data assimilation experiments were done to investigate how climate conditions, PFTs and soil textures affect the joint assimilation of surface soil moisture and groundwater levels in terms of improving root zone soil moisture characterization. Our results showed that

assimilation performance is more sensitive to climate conditions and soil texture, and less sensitive to PFTs. It was also found that assimilation generally works better if groundwater levels are between -1m and -10m below the soil surface, and if soil hydraulic parameters are well correlated with each other.

From these synthetic experiments on the use of EnKF in an integrated model it is concluded that data assimilation with EnKF is a promising tool to assimilate groundwater level data to improve root zone soil moisture. Of course some of our results were derived on the basis of idealized and simplified conditions with synthetic experiments. The spatio-temporal variations of soil properties in nature are usually more complex and lead to distinct patterns of heterogeneity in the soil profile. The relation between pressure head and soil moisture in the unsaturated zone may differ from the Mualem-van Genuchten model. For further investigations on this topic it would therefore be desirable to also apply the TerrSysMP-PDAF model and assimilation methodology to real world catchments.

We will apply groundwater level assimilation for the Rur catchment, which is part of the TERENO infrastructure. The Rur catchment (Vereecken et al., 2010; Simmer et al., 2015) is located in western Germany with a total area of 2354 km^2. It shows a strong spatial variability with respect to weather conditions, soil types and land use. The Rur catchment is highly equipped with monitoring infrastructure including soil moisture and groundwater level measurement networks, cosmic ray soil moisture stations, eddy covariance stations and river runoff stations. This abundant measurement infrastructure provides valuable information for data assimilation into terrestrial models. The possibility of assimilation of groundwater level data in TerrSysMP-PDAF with EnKF and the potential of improvement of root zone soil moisture has already been proved by our synthetic experiments, which benefits the application in the Rur catchment with real groundwater level (and soil moisture) observations.

The model TerrSysMP has already been set up successfully for the Rur catchment and in earlier work soil moisture data from cosmic ray probes were assimilated into TerrSysMP-PDAF. Based on this work, we will continue assimilating groundwater level measurements to improve root zone soil moisture characterization. It is also possible to jointly assimilate groundwater level measurements and soil moisture data from cosmic ray probes or remote sensing data. Another possibility is estimating soil hydraulic parameters, like saturated hydraulic conductivity and van Genuchten parameters, via assimilating groundwater level measurements and/or soil moisture data. It can be expected that assimilating for the real-world case is associated with many additional complications compared to the synthetic experiments. Examples are: (i) All the groundwater wells are clustered in the northern part of the catchment; (ii) TerrSysMP simulations produce shallower groundwater levels than measurements and seem to have a systematic wet bias; (iii) Model resolution (500m) is (too) coarse for the maximally 100m broad Rur river. The improvement of root zone soil moisture might therefore not be as significant as in the synthetic experiments.

Another extension of our work in the future is estimating soil hydraulic parameters, like saturated hydraulic conductivity and van Genuchten parameters, via assimilating groundwater level measurements. From our first study (in this PhD-thesis), joint estimation of soil

moisture and model parameters by EnKF is proven to be an efficient way to improve soil moisture profile prediction of LSMs. This study can be extended with TerrSysMP to not only update groundwater levels but also soil hydraulic parameters to investigate if root zone soil moisture characterization can be further improved.

The integrated model TerrSysMP also makes multivariate data assimilation possible. In our second and third studies, we jointly assimilate surface soil moisture and groundwater levels, and conclude that this approach is superior to univariate assimilation of surface soil moisture data or groundwater level data alone. In the future soil moisture from remote sensing data and cosmic ray probes should be jointly assimilated with groundwater levels. Moreover, further data types can be included in the multivariate assimilation like evapotranspiration data and discharge data.

Bibliography

Anderson, J. L. (2007), An adaptive covariance inflation error correction algorithm for ensemble filters, Tellus Series A-Dynamic Meteorology and Oceanography, 59(2), 210-224, doi:10.1111/j.1600-0870.2006.00216.x.

Andreadis, K. M., E. A. Clark, D. P. Lettenmaier and D. E. Alsdorf (2007), Prospects for river discharge and depth estimation through assimilation of swath altimetry into a raster based hydrodynamics model. Geophysical Research Letters, 34(10).

Ashby, S. F., and R. D. Falgout (1996), A parallel multigrid preconditioned conjugate gradient algorithm for groundwater flow simulations, Nuclear Science and Engineering, 124(1), 145-159.

Baatz, D., W. Kurtz, H. J. H. Franssen, H. Vereecken, and S. Kollet (2017), Catchment tomography-An approach for spatial parameter estimation, Advances in Water Resources.

Bailey, R. T. and D. Bau (2012), Estimating geostatistical parameters and spatially-variable hydraulic conductivity within a catchment system using an ensemble smoother, Hydrology and Earth System Sciences, 16, 287–304.

Baldauf, M., A. Seifert, J. Foerstner, D. Majewski, M. Raschendorfer, and T. Reinhardt (2011), Operational Convective-Scale Numerical Weather Prediction with the COSMO Model: Description and Sensitivities, Monthly Weather Review, 139(12), 3887-3905, doi:10.1175/mwr-d-10-05013.1.

Bennett, A. F. (1992), Inverse methods in physical oceanography, Cambridge university press.

Bertoldi G. (2004), The water and energy balance at basin scale: a distributed modeling approach, University of Trento, Monograph of the School of Doctoral Studies in Environmental Engineering, 202 pp., ISBN 88-8443-069-0.

Beven, K. (1997), TOPMODEL: A critique, Hydrological Processes, 11(9), 1069-1085.

Bi, H. Y., J. W. Ma, S. X. Qin, and H. J. Zhang (2014), Simultaneous estimation of soil moisture and hydraulic parameters using residual resampling particle filter, Science China-Earth Sciences, 57(4), 824-838, doi:10.1007/s11430-013-4742-y.

Birchak, J. R., C. G. Gardner, J. E. Hipp, and J. M. Victor (1974), High dielectric constant microwave probes for sensing soil moisture, Proceedings of the IEEE, 62(1), 93-98, doi:10.1109/PROC.1974.9388.

Blasone, R.-S., J. A. Vrugt, H. Madsen, D. Rosbjerg, B. A. Robinson, and G. A. Zyvoloski (2008), Generalized likelihood uncertainty estimation (GLUE) using adaptive Markov Chain Monte Carlo sampling, Advances in Water Resources, 31(4), 630-648, doi:http://dx.doi.org/10.1016/j.advwatres.2007.12.003.

Blondin, C. (1991), Parameterization of land-surface processes in numerical weather prediction, in Land Surface Evaporation: Measurements and Parameterization, Springer-Verlag, New York, 31-54.

Bogena, H. R., M. Herbst, J. A. Huisman, U. Rosenbaum, A. Weuthen, and H. Vereecken (2010), Potential of Wireless Sensor Networks for Measuring Soil Water Content Variability, Vadose Zone Journal, 9(4), 1002-1013, doi:10.2136/vzj2009.0173.

Bonan, G. B., S. Levis, L. Kergoat, and K. W. Oleson (2002), Landscapes as patches of plant functional types: An integrating concept for climate and ecosystem models, Global Biogeochemical Cycles, 16(2), doi:10.1029/2000gb001360.

Bonan G. B. (2008), Forests and Climate Change: Forcings, Feedbacks, and the Climate Benefits of Forests, Science, 320, 1444–1449, doi:10.1126/science.1155121.

Bracho, R., T. L. Powell, S. Dore, J. Li, C. R. Hinkle, and B. G. Drake (2008), Environmental and biological controls on water and energy exchange in Florida scrub oak and pine flatwoods ecosystems, Journal of Geophysical Research, 113, G02004, doi:10.1029/2007JG000469.

Brooks, R. H., and A. T. Corey (1964), Hydraulic Properties of Porous Media, Colorado State University.

Burgers, G., P. J. van Leeuwen, and G. Evensen (1998), Analysis scheme in the ensemble Kalman filter, Monthly Weather Review, 126(6), 1719-1724, doi:10.1175/1520-0493(1998)126<1719:asitek>2.0.co;2.

Camporese, M., C. Paniconi, M. Putti, and P. Salandin (2009), Ensemble Kalman filter data assimilation for a process-based catchment scale model of surface and subsurface flow, Water Resources Research, 45, W10421, doi:10.1029/2008wr007031.

Carpenter, J., P. Clifford, and P. Fearnhead (1999), Improved particle filter for nonlinear problems, Radar, Sonar and Navigation, IEE Proceedings, 146(1), 2-7, doi:10.1049/ip-rsn:19990255.

Carsel, R. F., and R. S. Parrish (1988), Developing joint probability distribution of soil water retention characteristivs, Water Resources Research, 24(5), 755-769, doi:10.1029/WR024i005p00755.

Charney, J., M. Halem, and R. Jastrow (1969), Use of incomplete historical data to infer the present state of the atmosphere, Journal of the Atmospheric Sciences, 26(5), 1160-1163.

Chen, X., and Q. Hu (2004), Groundwater influences on soil moisture and surface evaporation, Journal of Hydrology, 297(1-4), 285-300, doi:10.1016/j.jhydrol.2004.04.019.

Chen, Y., and D. X. Zhang (2006), Data assimilation for transient flow in geologic formations via ensemble Kalman filter, Advances in Water Resources, 29(8), 1107-1122.

Cherkauer, K. A., and D. P. Lettenmaier (1999), Hydrologic effects of frozen soils in the upper Mississippi River basin, Journal of Geophysical Research Atmospheres, 104(D16), 19599-19610, doi:10.1029/1999jd900337.

Clapp, R. B., and G. M. Hornberger (1978), EMPIRICAL EQUATIONS FOR SOME SOIL HYDRAULIC-PROPERTIES, Water Resources Research, 14(4), 601-604, doi:10.1029/WR014i004p00601.

Cosby, B. J., G. M. Hornberger, R. B. Clapp, and T. R. Ginn (1984), A statistical exploration of the relationships of soil moisture characteristics to the physical properties of soils, Water Resources Research, 20(6), 682-690, doi:10.1029/WR020i006p00682.

Crow, W. T., and E. F. Wood (2003), The assimilation of remotely sensed soil brightness temperature imagery into a land surface model using Ensemble Kalman filtering: a case study

based on ESTAR measurements during SGP97, Advances in Water Resources, 26(2), 137-149, doi:10.1016/s0309-1708(02)00088-x.

Crow, W. T., W. P. Kustas, and J. H. Prueger (2008), Monitoring root-zone soil moisture through the assimilation of a thermal remote sensing-based soil moisture proxy into a water balance model, Remote Sensing of Environment, 112(4), 1268-1281, doi:10.1016/j.rse.2006.11.033.

Daley, R. (1991), Atmospheric data analysis, Cambridge atmospheric and space science series, Cambridge University Press, 6966, 25.

Das, N. N., B. P. Mohanty, M. H. Cosh, and T. J. Jackson (2008), Modeling and assimilation of root zone soil moisture using remote sensing observations in Walnut Gulch Watershed during SMEX04, Remote Sensing of Environment, 112(2), 415-429, doi:10.1016/j.rse.2006.10.027.

Davin, E. L., R. Stockli, E. B. Jaeger, S. Levis, and S. I. Seneviratne (2011), COSMO-CLM2: a new version of the COSMO-CLM model coupled to the Community Land Model, Climate Dynamics, 37(9-10), 1889-1907, doi:10.1007/s00382-011-1019-z.

DeChant, C. M., and H. Moradkhani (2012), Examining the effectiveness and robustness of sequential data assimilation methods for quantification of uncertainty in hydrologic forecasting, Water Resources Research, 48, doi:10.1029/2011wr011011.

De Lannoy, G. J. M., and R. H. Reichle (2016), Assimilation of SMOS brightness temperatures or soil moisture retrievals into a land surface model, Hydrology and Earth System Sciences, 20(12), 4895-4911, doi:10.5194/hess-20-4895-2016.

Demaria, E. M., B. Nijssen, and T. Wagener (2007), Monte Carlo sensitivity analysis of land surface parameters using the Variable Infiltration Capacity model, Journal of Geophysical Research Atmospheres, 112(D11), 15, doi:10.1029/2006jd007534.

Dickinson, R. E. (1984), Modeling evapotranspiration for three-dimentional global climate models, in Climate Processes and Climate Sensitivity, Monogr. Ser., edited by J. E. Hansen and T. Takahashi, 58-72, Washington, D.C..

Dorigo, W., P. Oevelen, W. Wagner, M. Drusch, S. Mecklenburg, A. Robock, and T. Jackson (2011), A new international network for in situ soil moisture data, Eos, Transactions American Geophysical Union, 92(17), 141-142.

Douc, R., Olivier, C. and Eric M.: Comparison of resampling schemes for particle filtering, Proceedings of the 4th International Symposium on Image and Signal Processing and Analysis, 64-69, doi: 10.1109/ISPA.2005.195385, 2005.

Du, Y., F. T. Ulaby, and M. C. Dobson (2000), Sensitivity to soil moisture by active and passive microwave sensors, Ieee Transactions on Geoscience and Remote Sensing, 38(1), 105-114, doi:10.1109/36.823905.

Ducoudre, N. I., K. Laval, and A. Perrier (1993), SECHIBA, a new set of parameterizations of the hydrologic exchanges at the land-atmosphere interface within the LMD atmospheric general circulation model, Journal of Climate, 6(2), 248-273.

Dumedah, G., and P. Coulibaly (2013), Evaluating forecasting performance for data assimilation methods: The ensemble Kalman filter, the particle filter, and the evolutionary-

based assimilation, Advances in Water Resources, 60, 47-63, doi:10.1016/j.advwatres.2013.07.007.

Dunne, S., and D. Entekhabi (2005), An ensemble-based reanalysis approach to land data assimilation, Water Resources Research, 41(2), doi:10.1029/2004wr003449.

Erdal, D., I. Neuweiler, and U. Wollschläger (2014), Using a bias aware EnKF to account for unresolved structure in an unsaturated zone model, Water Resources Research, 50, 132–147, doi:10.1002/2012WR013443.

Erdal, D., M. A. Rahman, and I. Neuweiler (2015), The importance of state transformations when using the ensemble Kalman filter for unsaturated flow modeling: Dealing with strong nonlinearities, Advances in Water Resources, 86, 354-365, doi:10.1016/j.advwatres.2015.09.008.

Evensen, G. (1994), Sequential data assimilation with a nonlinear quasi-geostrophic model using Monto-Carlo methods to forecast error statistics. Journal of Geophysical Research Oceans, 99(C5), 10143-10162.

Fiori, A., and D. Russo (2007), Numerical analyses of subsurface flow in a steep hillslope under rainfall: The role of the spatial heterogeneity of the formation hydraulic properties, Water Resources Research, 43(7), doi:10.1029/2006wr005365.

Flores, A. N., D. Entekhabi and R. L. Bras (2012), Remote Sensing and Hydrology. Neale, C. M. U. and Cosh, M. H. (eds), pp. 308-311.

Ford, T. W., E. Harris, and S. M. Quiring (2014), Estimating root zone soil moisture using near-surface observations from SMOS, Hydrology and Earth System Sciences, 18(1), 139-154, doi:10.5194/hess-18-139-2014.

Franchini, M., and M. Pacciani (1991), Comparative-analysis of several conceptual rainfall runoff models, J. Hydrol., 122(1-4), 161-219, doi:10.1016/0022-1694(91)90178-k.

Franssen, H. J. H., and W. Kinzelbach (2008), Real-time groundwater flow modeling with the Ensemble Kalman Filter: Joint estimation of states and parameters and the filter inbreeding problem, Water Resour. Res., 44(9), doi:10.1029/2007wr006505.

Fredlund, D.G. (1991), How negative can pore-water pressures get? Geotechnical News, 9(3).

Gao, H., Q. Tang, X. Shi, C. Zhu, T. J. Bohn, F. Su, and E. F. Wood (2010), Water Budget Record from Variable Infiltration Capacity (VIC) Model, In Algorithm Theoretical Basis Document for Terrestrial Water Cycle Data Records, 2010.

Gasper, F., K. Goergen, P. Shrestha, M. Sulis, J. Rihani, M. Geimer and S. Kollet (2014), Implementation and scaling of the fully coupled Terrestrial Systems Modeling Platform (TerrSysMP v1.0) in a massively parallel supercomputing environment - a case study on JUQUEEN (IBM Blue Gene/Q), Geoscientific Model Development, 7(5), 2531-2543, doi:10.5194/gmd-7-2531-2014.

Gharamti, E. M., I. Hoteit, and J. Valstar (2013), Dual states estimation of a subsurface flow-transport coupled model using ensemble Kalman filtering, Advances in Water Resources, 60, 75-88, doi:10.1016/j.advwatres.2013.07.011.

Gordon, N. J., D. J. Salmond and A. F. M. Smith (1993), Novel-approach to nonlinear non-Gaussian Bayesian state estimation. IEE Proceedings-F Radar and Signal Processing 140(2), 107-113.

Graham, D. N., and M. B. Butts (2005), Flexible, integrated watershed modelling with MIKE SHE, Watershed models, 849336090, 245-272.

Grayson, R. B., and A. W. Western (1998), Towards areal estimation of soil water content from point measurements: time and space stability of mean response, Journal of Hydrology, 207(1-2), 68-82, doi:10.1016/s0022-1694(98)00096-1.

Han, E., V. Merwade and G. C. Heathman (2012), Implementation of surface soil moisture data assimilation with watershed scale distributed hydrological model. Journal of Hydrology 416, 98-117.

Han, X., H.-J. H. Franssen, X. Li, Y. Zhang, C. Montzka, and H. Vereecken (2013), Joint Assimilation of Surface Temperature and L-Band Microwave Brightness Temperature in Land Data Assimilation, Vadose Zone Journal, 12(3), doi:10.2136/vzj2012.0072.

Han, X., H. J. H. Franssen, C. Montzka, and H. Vereecken (2014a), soil moisture and soil properties estimation in the community Land Model with synthetic brightness temperature, Water Resource Research, doi:10.1002/2013WR014586.

Han, X., R. Jin, X. Li, and S. Wang (2014b), Soil moisture estimation using cosmic-ray soil moisture sensing at heterogeneous farmland, IEEE Geoscience and Remote Sensing Letters, 11(9), 1659-1663.

Havranek, W. M., and U. Benecke (1978), The influence of soil moisture on water potential, transpiration and photosynthesis of conifer seedlings, Plant and Soil, 49(1), 91-103.

Hirpa, F. A. (2013), Hydrologic data assimilation for operational streamflow Forecasting.

Hodgkinson R. A., T. J. Pepper, and D. W. Wilson (2004), Evaluation of tipping bucket rain gauge performance and data quality, Scientific Reports, W6-048/SR, Environment Agency, Bristol, UK.

Hoppe, C. M., H. Elbern, and J. Schwinger (2014), A variational data assimilation system for soil-atmosphere flux estimates for the Community Land Model (CLM3.5), Geoscientific Model Development, 7(3), 1025-1036.

Houser, P., M. F. Hutchinson, P. Viterbo, J. Hervé Douville and S. W. Running (2004), Terrestrial data assimilation, Chapter C.4 in Vegetation, Water, Humans and the Climate. Global Change - The IGB Series. Kabat, P. et al. (eds). Springer, Berlin, pp 273-287.

Houser, P. R., W. J. Shuttleworth, J. S. Famiglietti, H. V. Gupta, K. H. Syed, and D. C. Goodrich (1998), Integration of soil moisture remote sensing and hydrologic modeling using data assimilation, Water Resources Research, 34, 3405-3420, doi:10.1029/1998WR900001.

Houser, P. R., G. De Lannoy, and J. P. Walker (2012), Hydrological Data Assimilation, InTech.

Houser, P. R., Ieee, and Ieee (2001), Land data assimilation systems, 28-30 pp., Ieee, New York.

Huang, C., X. Li, L. Lu, and J. Gu (2008), Experiments of one-dimensional soil moisture assimilation system based on ensemble Kalman filter, Remote Sensing of Environment, 112(3), 888-900, doi:10.1016/j.rse.2007.06.026.

Hübner, C., R. Cardell-Oliver, R. Becker, K. Spohrer, K. Jotter, and T. Wagenknecht (2009), Wireless soil moisture sensor networks for environmental monitoring and vineyard irrigation, 8th International Conference on Electromagnetic Wave Interaction with Water and Moist Substances (ISEMA 2009), Helsinki, Finland. Vol. 408415.

Jackson, T. J. (1993), III. Measuring surface soil moisture using passive microwave remote sensing, Hydrological processes, 7(2), 139-152.

Jones, J. E., and C. S. Woodward (2001), Newton-Krylov-multigrid solvers for large-scale, highly heterogeneous, variably saturated flow problems, Advances in Water Resources, 24(7), 763-774, doi:10.1016/s0309-1708(00)00075-0.

Jülich Supercomputing Centre (2016). JURECA: General-purpose supercomputer at Jülich Supercomputing Centre. Journal of Large-scale Research Facilities, 2, A62. doi:10.17815/jlsrf-2-121.

Kalman, R. E. (1960), A New Approach to Linear Filtering and Prediction Problems Journal of Basic Engineering, 82, 35-45.

Kollet, S. J., and R. M. Maxwell (2006), Integrated surface-groundwater flow modeling: A free-surface overland flow boundary condition in a parallel groundwater flow model, Advances in Water Resources, 29(7), 945-958, doi:10.1016/j.advwatres.2005.08.006.

Kollet, S. J., and R. M. Maxwell (2008), Capturing the influence of groundwater dynamics on land surface processes using an integrated, distributed watershed model, Water Resources Research, 44(2), doi:10.1029/2007wr006004.

Koster, R. D., P. A. Dirmeyer, Z. C. Guo, G. Bonan, E. Chan, P. Cox, C. T. Gordon, S. Kanae, E. Kowalczyk, D. Lawrence, P. Liu, C. H. Lu, S. Malyshev, B. McAvaney, K. Mitchell, D. Mocko, T. Oki, K. Oleson, A. Pitman, Y. C. Sud, C. M. Taylor, D. Verseghy, R. Vasic, Y. K. Xue, T. Yamada, and G. Team (2004), Regions of strong coupling between soil moisture and precipitation, Science, 305(5687), 1138-1140.

Kumar, S. V., R. H. Reichle, R. D. Koster, W. T. Crow, and C. D. Peters-Lidard (2009), Role of Subsurface Physics in the Assimilation of surface soil moisture Observations, Journal of Hydrometeorology, 10(6), 1534-1547, doi:10.1175/2009jhm1134.1.

Kurtz, W., H. J. Hendricks Franssen, and H. Vereecken (2012), Identification of time-variant river bed properties with the ensemble Kalman filter, Water Resources Research, 48, W10534, doi:10.1029/2011WR011743.

Kurtz, W., H. J. Hendricks Franssen, H. P. Kaiser, and H. Vereecken (2014), Joint assimilation of piezometric heads and groundwater temperatures for improved modelling of river-aquifer interactions, Water Resources Research, 50(2), 1665-1688, doi:10.1002/2013wr014823.

Kurtz, W., G. He, S. J. Kollet, R. M. Maxwell, H. Vereecken, and H.-J. H. Franssen (2016), TerrSysMP-PDAF version 1.0): a modular high-performance data assimilation framework for

an integrated land surface-subsurface model, Geoscientific Model Development, 9(4), 1341-1360, doi:10.5194/gmd-9-1341-2016.

Larsen, M. A. D., J. C. Refsgaard, M. Drews, M. B. Butts, K. H. Jensen, J. H. Christensen, and O. B. Christensen (2014), Results from a full coupling of the HIRHAM regional climate model and the MIKE SHE hydrological model for a Danish catchment, Hydrology and Earth System Sciences, 18(11), 4733-4749, doi:10.5194/hess-18-4733-2014.

Lawrence, D. M., and A. G. Slater (2008), Incorporating organic soil into a global climate model, Climate Dynamics, 30(2-3), 145-160, doi:10.1007/s00382-007-0278-1.

Lee, J. H. (2014), Spatial-Scale prediction of the SVAT soil hydraulic variables characterizing stratified soils on the Tibetan Plateau from an EnKF analysis of SAR soil moisture, Vadose Zone Journal, 13(11), doi: 10.2136/vzj2014.06.0060.

Leij, F. J., W. J. Alves, and v. G. M. Th. (1996), The UNSODA unsaturated soil hydraulic database, EPA/600/R-96/095.

Li, L. P., H. Y. Zhou, J. J. Gomez-Hernandez, and H. J. H. Franssen (2012), Jointly mapping hydraulic conductivity and porosity by assimilating concentration data via ensemble Kalman filter, Journal of Hydrology, 428, 152-169, doi:10.1016/j.jhydrol.2012.01.037.

Li, Y., D. Ryu, Q. J. Wang, T. Pagano, A. Western, P. Hapuarachchi, and P. Toscas (2011), Assimilation of streamflow discharge into a continuous flood forecasting model, in Risk in Water Resources Management, edited by G. Bloschl, K. Takeuchi, S. Jain, A. Farnleitner and A. Schumann, pp. 107-113.

Liang, X., D. P. Lettenmaier, E. F. Wood, and S. J. A. Burges (1994), simple hyhrologically based model of land-surface water and energy fluxes for general-circulation models, Journal of Geophysical Research Atmospheres, 99(D7), 14415-14428, doi:10.1029/94jd00483.

Liang, X., E. F. Wood, and D. P. Lettenmaier (1996), Surface soil moisture parameterization of the VIC-2L model: Evaluation and modification, Global and Planetary Change, 13(1-4), 195-206, doi:10.1016/0921-8181(95)00046-1.

Liang, X., and J. Z. Guo (2003), Intercomparison of land-surface parameterization schemes: sensitivity of surface energy and water fluxes to model parameters, Journal of Hydrology, 279(1-4), 182-209, doi:10.1016/s0022-1694(03)00168-9.

Liang, X., Z. H. Xie and M. Y. Huang (2003), A new parameterization for surface and groundwater interactions and its impact on water budgets with the variable infiltration capacity (VIC) land surface model. Journal of Geophysical Research Atmospheres, 108(D16), 17.

Liu, J. S. and R. Chen (1998), Sequential Monte Carlo methods for dynamic systems, Journal of the American Statistical Association, 93(443), 1032-1044, doi:10.2307/2669847.

Liu, Y. W., W. Wang, and Y. M. Hu (2017), Investigating the impact of surface soil moisture assimilation on state and parameter estimation in SWAT model based on the ensemble Kalman filter in upper Huai River basin, Journal of Hydrology and Hydromechanics, 65(2), 123-133.

Liu, Y., L. S. Pereira, and R. M. Fernando (2006), Fluxes through the bottom boundary of the root zone in silty soils: Parametric approaches to estimate groundwater contribution and

percolation, Agricultural Water Management, 84(1-2), 27-40, doi:10.1016/j.agwat.2006.01.018.

Liu, Y., and H. V. Gupta (2007), Uncertainty in hydrologic modeling: Toward an integrated data assimilation framework, Water Resources Research, 43(7), doi:10.1029/2006wr005756, 2007.

Liu, G., Y. Chen, and D. Zhang (2008), Investigation of flow and transport processes at the MADE site using ensemble Kalman filter, Advances in Water Resources, 31(7), 975-986, doi:10.1016/j.advwatres.2008.03.006.

Lo, M. H., J. S. Famiglietti, P. F. Yeh, and T. H. Syed (2010), Improving parameter estimation and water table depth simulation in a land surface model using GRACE water storage and estimated base flow data, Water Resources Research, 46(5).

Lorenc, A. C. (1986), Analysis methods for numerical weather prediction, Quarterly Journal of the Royal Meteorological Society, 112(474), 1177-1194.

Lorenz, C., M. J. Tourian, B. Devaraju, N. Sneeuw and H. Kunstmann (2015), Basin scale runoff prediction: An Ensemble Kalman Filter framework based on global hydrometeorological datasets. Water Resources Research, 51(10), 8450-8475.

Lue, H., Z. Yu, Y. Zhu, S. Drake, Z. Hao, and E. A. Sudicky (2011), Dual state-parameter estimation of root zone soil moisture by optimal parameter estimation and extended Kalman filter data assimilation, Advances in Water Resources, 34(3), 395-406, doi:10.1016/j.advwatres.2010.12.005.

Margulis, S. A., D. McLaughlin, D. Entekhabi, and S. Dunne (2002), Land data assimilation and estimation of soil moisture using measurements from the Southern Great Plains 1997 Field Experiment, Water Resources Research, 38(12), doi:10.1029/2001wr001114.

Maxwell, R. M. (2013), A terrain-following grid transform and preconditioner for parallel, large-scale, integrated hydrologic modeling, Advances in Water Resources, 53, 109-117, doi:10.1016/j.advwatres.2012.10.001.

Maxwell, R. M. (2009), Coupled Surface-Subsurface Modeling across a Range of Temporal and Spatial Scales, Vadose Zone Journal, 8(4), 823-824, doi:10.2136/vzj2009.0117.

Maxwell, R. M. (2013). A terrain-following grid transform and preconditioner for parallel, large-scale, integrated hydrologic modeling. Advances in Water Resources, 53, 109-117, doi: 10.1016/j.advwatres.2012.10.001.

Maxwell, R. M., L. E. Condon, and S. J. Kollet (2015), A high-resolution simulation of groundwater and surface water over most of the continental US with the integrated hydrologic model ParFlow v3, Geoscientific Model Development, 8(3), 923-937, doi:10.5194/gmd-8-923-2015.

Maxwell, R. M., and N. L. Miller (2005), Development of a coupled land surface and groundwater model, Journal of Hydrometeorology, 6(3), 233-247, doi:10.1175/jhm422.1.

Miguez-Macho, G., and Y. Fan (2012), The role of groundwater in the Amazon water cycle: 2. Influence on seasonal soil moisture and evapotranspiration, Journal of Geophysical Research-Atmospheres, 117, doi:10.1029/2012jd017540.

Miguez-Macho, G., H. Li, and Y. Fan (2008), Simulated water table and soil moisture climatology over North America, Bulletin of the American Meteorological Society, 89(5), 663-+, doi:10.1175/bams-89-5-663.

Milly, P. C. D., and A. B. Shmakin (2002), Global modeling of land water and energy balances. Part II: Land-characteristic contributions to spatial variability, Journal of Hydrometeorology, 296–307.

Montzka, C., H. Moradkhani, L. Weihermueller, H. J. H. Franssen, M. Canty and H. Vereecken (2011), Hydraulic parameter estimation by remotely-sensed top soil moisture observations with the particle filter. Journal of Hydrology 399(3-4), 410-421.

Montzka, C., J. P. Grant, H. Moradkhani, H. J. H. Franssen, L. Weihermüller, M. Drusch and H. Vereecken (2013), Estimation of radiative transfer parameters from L-band passive microwave brightness temperatures using advanced data assimilation. Vadose Zone Journal, Special Section on Remote Sensing of Vadose Zone Hydrology, 12(3), DOI:10.2136/vzj2012.0040.

Moradkhani, S. Sorooshian, H. V. Gupta, and P. R. Houser (2005a), Dual state-parameter estimation of hydrological models using ensemble Kalman filter, Advances in Water Resources, 28(2), 135-147, doi:10.1016/j.advwatres.2004.09.002.

Moradkhani, H., C. M. DeChant, and S. Sorooshian (2012), Evolution of ensemble data assimilation for uncertainty quantification using the particle filter-Markov chain Monte Carlo method, Water Resources Research, 48, doi:10.1029/2012wr012144.

Moradkhani, H., K. L. Hsu, H. Gupta, and S. Sorooshian (2005b), Uncertainty assessment of hydrologic model states and parameters: Sequential data assimilation using the particle filter, Water Resources Research, 41(5), doi:10.1029/2004wr003604.

Neal, J., G. Schumann, P. Bates, W. Buytaert, P. Matgen and F. Pappenberger (2009), A data assimilation approach to discharge estimation from space. Hydrological Processes, 23(25), 3641-3649.

Nerger, L., and W. Hiller (2013), Software for ensemble-based data assimilation systems-Implementation strategies and scalability, Computers and Geosciences, 55, 110-118, doi:10.1016/j.cageo.2012.03.026.

Ni-Meister, W. (2008), Recent advances on soil moisture data assimilation, Physical Geography, 29(1), 19-37, doi:10.2747/0272-3646.29.1.19.

Niu, G. Y., Z. L. Yang, R. E. Dickinson, and L. E. Gulden (2005), A simple TOPMODEL-based runoff parameterization (SIMTOP) for use in global climate models, Geophysical Research Letters Atmosphere, 110, D21106, doi:10.1029/2005JD006111.

Niu, G. Y., Z. L. Yang, R. E. Dickinson, L. E. Gulden, and H. Su (2007), Development of a simple groundwater model for use in climate models and evaluation with Gravity Recovery and Climate Experiment data, Journal of Geophysical Research: Atmospheres, 112(D7), 14, doi:10.1029/2006jd007522.

Nixon, S., Y. Rees, J. Gunby, and T. Lack (1997), European freshwater monitoring network design, Office for Official Publications of the European Communities.

Oleson, K. W., and G. B. Bonan (2000), The effects of remotely sensed plant functional type and leaf area index on simulations of boreal forest surface fluxes by the NCAR land surface model, Journal of Hydrometeorology, 1(5), 431-446, doi:10.1175/1525-7541(2000)001<0431:teorsp>2.0.co;2.

Oleson, K. W., et al. (2004), Technical Description of the Community Land Model (CLM), NCAR Technical Note NCAR/TN-461+STR, 186.

Oleson, K. W., et al. (2008), Improvements to the Community Land Model and their impact on the hydrological cycle, Journal of Geophysical Research-Biogeosciences, 113(G1), doi:10.1029/2007jg000563.

Oleson, K., et al. (2013), Technical description of version 4.5 of the Community Land Model (CLM), NCAR Technical Note NCAR/TN-503+STR, 422, doi:10.5065/D6RR1W7M.

Overgaard, J., D. Rosbjerg, and M. Butts (2005), Land-surface modelling in hydrological perspective, Biogeosciences Discussions, 2(6), 1815-1848.

Panzeri, M., M. Riva, A. Guadagnini and S. P. Neuman (2014), Comparison of Ensemble Kalman Filter groundwater-data assimilation methods based on stochastic moment equations and Monte Carlo simulation. Advances in Water Resources, 66, 8-18.

Park, S. K., and L. Xu (2013), Data assimilation for atmospheric, oceanic and hydrologic applications, Springer Science and Business Media.

Pasetto, D., M. Camporese, and M. Putti (2012), Ensemble Kalman filter versus particle filter for a physically-based coupled surface-subsurface model, Advances in Water Resources, 47, 1-13, doi:10.1016/j.advwatres.2012.06.009, 2012.

Pasetto, D., G. Y. Niu, L. Pangle, C. Paniconi, M. Putti, and P. A. Troch (2015), Impact of sensor failure on the observability of flow dynamics at the Biosphere 2 LEO hillslopes, Advances in Water Resources 86, 327-339.

Pauwels, V. and De Lannoy, G. J. (2009), Ensemble‐based assimilation of discharge into rainfall‐runoff models: A comparison of approaches to mapping observational information to state space, Water Resources Research, 45(8).

Pauwels, V. R. N., A. Balenzano, G. Satalino, H. Skriver, N. E. C. Verhoest and F. Mattia (2009), Optimization of Soil Hydraulic Model Parameters Using Synthetic Aperture Radar Data: An Integrated Multidisciplinary Approach, IEEE Transactions on Geoscience and Remote Sensing, 47(2), 455-467, doi: 10.1109/TGRS.2008.2007849.

Peng B., J. C. Shi, Y. H. Lei, T. J. Zhao, D. Y. Li (2014), Dual state-parameter estimation of land surface model through assimilating microwave brightness temperature, Proceedings SPIE 9260, Land Surface Remote Sensing II, 92600X.

Plaza, D. A., R. D. Keyser, G. J. M. D. Lannoy, L. Giustarini, P. Matgen, and V. R. N. Pauwels (2012), The importance of parameter resampling for soil moisture data assimilation into hydrologic models using the particle filter, Hydrology and Earth System Sciences, 16(2), 375-390, doi:10.5194/hess-16-375-2012.

Pipunic, R. C., K. A. McColl, D. Ryu, and J. P. Walker (2011), Can assimilating remotely-sensed surface soil moisture data improve root-zone soil moisture predictions in the CABLE

land surface model?, 19th International Congress on Modelling and Simulation (Modsim2011), 1994-2001.

Post, H., J. A. Vrugt, A. Fox, H. Vereecken, and H. J. H. Franssen (2017), Estimation of Community Land Model parameters for an improved assessment of net carbon fluxes at European sites, Journal of Geophysical Research Biogeosciences, 122(3), 661-689.

Qin, J., S. Liang, K. Yang, I. Kaihotsu, R. Liu, and T. Koike (2009), Simultaneous estimation of both soil moisture and model parameters using particle filtering method through the assimilation of microwave signal, Journal of Geophysical Research Atmospheres, 114, doi:10.1029/2008jd011358.

Qu, W., H. R. Bogena, J. A. Huisman, G. Martinez, Y. A. Pachepsky, and H. Vereecken (2014), Effects of soil hydraulic properties on the spatial variability of soil water content: evidence from sensor network data and inverse modeling, Vadose Zone Journal, 13(12), doi:10.2136/vzj2014.07.0099.

Rasmussen, J., H. Madsen, K. H. Jensen, and J. C. Refsgaard (2015), Data assimilation in integrated hydrological modeling using ensemble Kalman filtering: evaluating the effect of ensemble size and localization on filter performance, Hydrology and Earth System Sciences, 19(7), 2999-3013, doi:10.5194/hess-19-2999-2015.

Reichle, R. H., M. G. Bosilovich, W. T. Crow, R. D. Koster, S. V. Kumar, S. P. Mahanama, and B. F. Zaitchik (2009), Recent advances in land data assimilation at the NASA Global Modeling and Assimilation Office, Data assimilation for atmospheric, oceanic and hydrologic applications, 407-428.

Reichle, R. H., W. T. Crow, and C. L. Keppenne (2008), An adaptive ensemble Kalman filter for soil moisture data assimilation, Water Resources Research, 44(3), doi:10.1029/2007wr006357.

Reichle, R. H., R. D. Koster, J. Dong, and A. A. Berg (2004), Global soil moisture from satellite observations, land surface models, and ground data: Implications for data assimilation, Journal of Hydrometeorology, 5(3), 430-442.

Reichle, R. H., D. B. McLaughlin, and D. Entekhabi (2002), Hydrologic data assimilation with the ensemble Kalman filter, Monthly Weather Review, 130(1), 103-114, doi:10.1175/1520-0493(2002)130<0103:hdawte>2.0.co;2.

Rihani, J. F., R. M. Maxwell, and F. K. Chow (2010), Coupling groundwater and land surface processes: Idealized simulations to identify effects of terrain and subsurface heterogeneity on land surface energy fluxes, Water Resources Research, 46, doi:10.1029/2010wr009111.

Robinson, D., C. Campbell, J. Hopmans, B. Hornbuckle, S. B. Jones, R. Knight, F. Ogden, J. Selker, and O. Wendroth (2008), Soil moisture measurement for ecological and hydrological watershed-scale observatories: A review, Vadose Zone Journal, 7(1), 358-389.

Robock, A., K. Y. Vinnikov, G. Srinivasan, J. K. Entin, S. E. Hollinger, N. A. Speranskaya, S. Liu, and A. Namkhai (2000), The global soil moisture data bank, Bulletin of the American Meteorological Society, 81(6), 1281-1299.

Romano N., M. Palladino, and G. B. Chirico (2011), Parameterization of a bucket model for soil-vegetation-atmosphere modeling under seasonal climatic regimes, Hydrology and Earth System Sciences, doi:10.5194/hess-15-3877-2011.

Rubol, S., S. Manzoni, A. Bellin, and A. Porporato (2013), Modeling soil moisture and oxygen effects on soil biogeochemical cycles including dissimilatory nitrate reduction to ammonium (DNRA), Advances in water resources, 62, 106-124.

Sabater, J. M., L. Jarlan, J.-C. Calvet, F. Bouyssel, and P. De Rosnay (2007), From near-surface to root-zone soil moisture using different assimilation techniques, Journal of Hydrometeorology, 8(2), 194-206, doi:10.1175/jhm571.1.

Schaake, J. C., V. I. Koren, Q. Y. Duan, K. Mitchell, and F. Chen (1996), Simple water balance model for estimating runoff at different spatial and temporal scales, Geophysical Research Letters, 101(D3), 7461–7475, doi:10.1029/95JD02892.

Scheerlinck, K., V. R. N. Pauwels, H. Vernieuwe, and B. De Baets (2009), Calibration of a water and energy balance model: Recursive parameter estimation versus particle swarm optimization, Water Resources Research, 45, W10422, doi:10.1029/2009WR008051.

Schoeniger, A., W. Nowak, and H. J. H. Franssen (2012), Parameter estimation by ensemble Kalman filters with transformed data: Approach and application to hydraulic tomography, Water Resources Research, 48, doi:10.1029/2011wr010462.

Schwinger, J., S. Kollet, C. Hoppe, and H. Elbern (2010), Sensitivity of latent heat fluxes to initial values and parameters of a Land-Surface Model, Vadose Zone Journal, 9(4), 984-1001.

Seneviratne, S. I., T. Corti, E. L. Davin, M. Hirschi, E. B. Jaeger, I. Lehner, B. Orlowsky, and A. J. Teuling (2010), Investigating soil moisture–climate interactions in a changing climate: A review, Earth-Science Reviews, 99(3), 125-161.

Shi, L., X. Song, J. Tong, Y. Zhu, and Q. Zhang (2015a), Impacts of different types of measurements on estimating unsaturated flow parameters, Journal of Hydrology, 524, 549-561, doi:10.1016/j.jhydrol.2015.01.078.

Shi, Y., K. J. Davis, F. Zhang, C. J. Duffy, and X. Yu (2014), Parameter estimation of a physically based land surface hydrologic model using the ensemble Kalman filter: A synthetic experiment, Water Resources Research, 50(1), 706-724, doi:10.1002/2013wr014070.

Shi, Y., K. J. Davis, F. Zhang, and C. J. Duffy, and X. Yu (2015b), Parameter estimation of a physically-based land surface hydrologic model using an ensemble Kalman filter: A multivariate real-data experiment, Advances in water resources, doi: 10.1016/j.advwatres.2015.06.009.

Shrestha, P., M. Sulis, M. Masbou, S. Kollet, and C. Simmer (2014), A Scale-Consistent Terrestrial Systems Modeling Platform Based on COSMO, CLM, and ParFlow, Monthly Weather Review, 142(9), 3466-3483, doi:10.1175/mwr-d-14-00029.1.

Shuttleworth, W. J. (2007), Putting the 'vap' into evaporation, Hydrology and Earth System Sciences, 11(1), 210-244.

Simmer, C., I. Thiele-Eich, M. Masbou, W. Amelung, H. Bogena, S. Crewell, B. Diekkrüger, F. Ewert, H.-J. Hendricks Franssen, and J. A. Huisman (2015), Monitoring and modeling the

terrestrial system from pores to catchments: the transregional collaborative research center on patterns in the soil–vegetation–atmosphere system, Bulletin of the American Meteorological Society, 96(10), 1765-1787.

Song, X., L. Shi, M. Ye, J. Yang, and N. I. Michael (2014), Numerical Comparison of Iterative Ensemble Kalman Filters for Unsaturated Flow Inverse Modeling, Vadose Zone Journal, 13(2), doi: 10.2136/vzj2013.05.0083.

Su, H., Z. L. Yang, G. Y. Niu, and C. R. Wilson (2011), Parameter estimation in ensemble based snow data assimilation: A synthetic study, Advances in water resources, 34(3), 407-416.

Subcommittee on Ground Water of the Advisory Committee on Water Information, 2011, National Ground-Water Monitoring Network—Results of pilot studies: Advisory Committee on Water Information, accessed October 23, 2013, at http://acwi.gov/sogw/pubs/tr/pilot_results/NGWMN_pilot_studies.pdf.

Sulis, M., M. Langensiepen, P. Shrestha, A. Schickling, C. Simmer, and S. J. Kollet (2015), Evaluating the Influence of Plant-Specific Physiological Parameterizations on the Partitioning of Land Surface Energy Fluxes, Journal of Hydrometeorology, 16(2), 517-533, doi:10.1175/jhm-d-14-0153.1.

Tang Q., W. Kurtz, P. Brunner, H. Vereecken, and H. J. H. Franssen: Characterisation of river–aquifer exchange fluxes: The role of spatial patterns of riverbed hydraulic conductivities, Journal of Hydrology, doi:10.1016/j.jhydrol.2015.08.019.

Thiemann, M., M. Trosset, H. Gupta, and S. Sorooshian (2001), Bayesian recursive parameter estimation for hydrologic models, Water Resources Research, 37(10), 2521–2535.

Tian, W., X. Li, G. D. Cheng, X. S. Wang, and B. X. Hu (2012), Coupling a groundwater model with a land surface model to improve water and energy cycle simulation, Hydrology and Earth System Sciences, 16(12), 4707-4723, doi:10.5194/hess-16-4707-2012.

Tian, X., Z. Xie, and A. Dai (2008), A land surface soil moisture data assimilation system based on the dual‐UKF method and the Community Land Model, Journal of Geophysical Research Atmospheres, 113(D14).

Tong, J., B. X. Hu and J. Yang (2012), Assimilating transient groundwater flow data via a localized ensemble Kalman filter to calibrate a heterogeneous conductivity field, Stochastic environmental research and risk assessment 26(3), 467-478.

Topp, G. C., J. L. Davis, and A. P. Annan (1980), Electromagnetic determination of soil water content measurements in coaxial transmission-lines, Water Resources Research, 16, 574–582, doi:10.1029/WR016i003p00574.

Troy, T. J., E. F. Wood, and J. Sheffield (2008), An efficient calibration method for continental-scale land surface modeling, Water Resources Research, 44(9), doi:10.1029/2007wr006513.

Valcke, S. (2013), The OASIS3 coupler: a European climate modelling community software, Geoscientific Model Development, 6(2), 373-388, doi:10.5194/gmd-6-373-2013.

Van Genuchten, M. T. (1980), A Closed Form Equation for Predicting the Hydraulic Conductivity of Unsaturated Soils, Soil Science Society of America Journal, 44: 892-898.

Vereecken, H., J. A. Huisman, H. Bogena, J. Vanderborght, J. A. Vrugt, and J. W. Hopmans (2008), On the value of soil moisture measurements in vadose zone hydrology: A review, Water Resources Research, 44, 21, doi:10.1029/2008wr006829.

Vereecken, H., S. Kollet, and C. Simmer (2010), Patterns in soil–vegetation–atmosphere systems: Monitoring, modeling, and data assimilation, Vadose Zone Journal, 9(4), 821-827.

Vereecken, H., et al. (2016), Modeling Soil Processes: Review, Key Challenges, and New Perspectives, Vadose Zone Journal, 15, 5, doi: 10.2136/vzj2015.09.0131.

Vertenstein, M., K. Oleson, S. Levis, and P. Thornton (2002), CLM2. 0 user's guide, National Center for Atmospheric Research, PO Box, 3000, 1-36.

Vrugt, J. A., C. G. H. Diks, H. V. Gupta, W. Bouten, and J. M. Verstraten (2005), Improved treatment of uncertainty in hydrologic modeling: Combining the strengths of global optimization and data assimilation, Water Resources Research, 41, W01017, doi:10.1029/2004WR003059.

Vrugt, J. A., and C. J. F. Ter Braak (2011), DREAM (D): An adaptive Markov Chain Monte Carlo simulation algorithm to solve discrete, noncontinuous, and combinatorial posterior parameter estimation problems, Hydrology and Earth System Sciences, 15(12), 3701–3713.

Vrugt, J. A., C. J. F. ter Braak, C. G. H. Diks, and G. Schoups (2013), Hydrologic data assimilation using particle Markov chain Monte Carlo simulation: Theory, concepts and applications, Advances in Water Resources, 51, 457-478, doi:10.1016/j.advwatres.2012.04.002.

Walker, J. P., P. R. Houser, and R. H. Reichle (2003a), New technologies require advances in hydrologic data assimilation, EOS, Transactions American Geophysical Union, 84(49), 545-551.

Walker, J. P., N. Ursino, R. B. Grayson, P. R. Houser, and Mssanzi (2003b), Australian root zone soil moisture: Assimilation of remote sensing observations, 380-385 pp.

Walker, J. P., G. R. Willgoose, and J. D. Kalma (2002), Three-dimensional soil moisture profile retrieval by assimilation of near-surface measurements: Simplified Kalman filter covariance forecasting and field application, Water Resources Research, 38(12), doi:10.1029/2002wr001545.

Weerts, A. H., and G. Y. H. El Serafy (2006), Particle filtering and ensemble Kalman filtering for state updating with hydrological conceptual rainfall-runoff models, Water Resources Research, 42(9), doi:10.1029/2005wr004093.

Whitaker, J. S., and T. M. Hamill (2012), Evaluating Methods to Account for System Errors in Ensemble Data Assimilation, Monthly Weather Review, 140(9), 3078-3089, doi:10.1175/mwr-d-11-00276.1.

Wigmosta, M. S., L. W. Vail, and D. P. Lettenmaier (1994), A distributed hydrology-vegetation model for complex terrain, Water Resources Research, 30(6), 1665-1679.

Williams M., A. D. Richardson, M. Reichstein, P. C. Stoy, P. Peylin, H. Verbeeck, N. Carvalhais, M. Jung, D. Y. Hollinger, J. Kattge, R. Leuning, Y. Luo, E. Tomelleri, C. M. Trudinger, and Y. P. Wang (2009), Improving land surface models with FLUXNET data, Biogeoscience, 6, 1341–1359.

Wu, C. C., and S. A. Margulis (2011), Feasibility of real-time soil state and flux characterization for wastewater reuse using an embedded sensor network data assimilation approach, Journal of Hydrology, 399(3-4), 313-325, doi: 10.1016/j.jhydrol.2011.01.011.

Wu, C. C., and S. A. Margulis (2013), Real-Time Soil Moisture and Salinity Profile Estimation Using Assimilation of Embedded Sensor Data streams, Vadose Zone Journal, 12(1), doi: 10.2136/vzj2011.0176.

Xie, Z., F. Yuan, Q. Duan, J. Zheng, M. Liang, and F. Chen (2007), Regional parameter estimation of the VIC land surface model: methodology and application to river basins in China, Journal of Hydrometeorology, 8(3), 447-468, doi:10.1175/jhm568.1.

Yeh, P. J. and E. A. Eltahir (2005), Representation of water table dynamics in a land surface scheme. Part I: Model development, Journal of Climate, 18(12), 1861-1880.

Yongjiu, D., and Z. Qingcun (1997), A land surface model (IAP94) for climate studies part I: Formulation and validation in off-line experiments, Advances in Atmospheric Sciences, 14(4), 433-460.

Zhang, D. H., H. Madsen, M. E. Ridler, J. Kidmose, K. H. Jensen, and J. C. Refsgaard (2016), Multivariate hydrological data assimilation of soil moisture and groundwater head, Hydrology and Earth System Sciences, 20(10), 4341-4357, doi:10.5194/hess-20-4341-2016.

Zhang, H., H. J. Hendricks Franssen, X. Han, J. A. Vrugt, and H. Vereecken (2017), State and parameter estimation of two land surface models using the ensemble Kalman filter and the particle filter, Hydrology and Earth System Sciences, 21, 4927-4958, doi: 10.5194/hess-21-4927-2017.

Zhang, H., W. Kurtz, S. Kollet, H. Vereecken, and H. J. H. Franssen (2018), Comparison of different assimilation methodologies of groundwater levels to improve predictions of root zone soil moisture with an integrated terrestrial system model, Advances in Water Resources, 111, 224-238, doi: 10.1016/j.advwatres.2017.11.003.

Zhao, R. J. (1992), The Xinanjiang model applied in China, Journal of Hydrology, 135(1-4), 371-381.

Zeng, X., and M. Decker (2009), Improving the numerical solution of soil moisture-based Richards equation for land models with a deep or shallow water table, Journal of Hydrometeorology, 10, 308-319, doi:10.1175/2008JHM1011.1.

Zhou, Y., D. McLaughlin, and D. Entekhabi (2006), Assessing the performance of the ensemble Kalman filter for land surface data assimilation, Monthly Weather Review, 134(8), 2128-2142, doi:10.1175/mwr3153.1.

Zhu, Y., L. Ren, R. Horton, H. Lu, X. Chen, Y. Jia, Z. Wang, and E. A. Sudicky (2013), Estimating the contribution of groundwater to rootzone soil moisture, Hydrology Research, 44(6), 1102-1113, doi:10.2166/nh.2013.071.

Zreda, M., W. Shuttleworth, X. Zeng, C. Zweck, D. Desilets, T. Franz, and R. Rosolem (2012), COSMOS: the cosmic-ray soil moisture observing system, Hydrology and Earth System Sciences, 16(11), 4079-4099.

Acknowledgements

First of all, I would like to thank Prof. Dr. Harrie-Jan Hendricks Franssen for his intensive supervision for my 4 years' PhD work. During my studies we had many meetings and discussions and he provided many helpful solutions, ideas and suggestions. Especially I appreciate for his encouragements when I was frustrated. Moreover I am grateful to China government scholarship which supports my work and life in Germany. I also gratefully acknowledge Prof. Xujun Han who taught me a lot about data assimilation and Dr. Wolfgang Kurtz who helped me a lot with the framework TerrSysMP-PDAF. Many thanks to Prof. Dara Entekhabi from department of civil and environmental engineering of MIT (USA) for his support during my two-month research stay in MIT (USA).

Besides, I would like to thank my other colleagues from the Institute of bio- and Geosciences at the Juelich Research Center, especially:

- Prof. Dr. Harry Vereecken, the head of our institute, for his support
- Prof. Dr. Stefan Kollet for his help with model ParFlow
- Guowei He and Mukund Pondkule for their help with my codes
- Dr. Carsten Montzka for the SMAP data
- Dr. Hanna Post and Dr. Wei Qu for providing the data for my work
- My officemates, Anne Klosterhalfen and Anne-Katrin Röseler, for their help in my life in Germany

Then I gratefully acknowledge the Transregional Collaborative Research Centre 32 (TR32) which facilitated a valuable cooperation and exchange with other groups. Many thanks to Juelich Supercomputing Center for granting the required computation time on JURECA.

Special thanks to my parents, Hongmin and Hongling. No matter what happen they always stand beside me, support me, trust me and love me.

Band / Volume 414
Entwicklung eines Werkzeugs zur Modellierung der Nettoerosion im Hauptraum der Brennkammer eines Tokamaks und Studium der Plasma-Wand-Wechselwirkung an DEMO1
M. Beckers (2018), XIX, 150 pp
ISBN: 978-3-95806-307-5

Band / Volume 415
Fehlstellendotierung von Eisenoxid- und Bismutsulfid-Nanopartikeln
J. P. Mock (2018), v, 187 pp
ISBN: 978-3-95806-309-9

Band / Volume 416
Nanocrystalline Silicon Oxide in Silicon Heterojunction Solar Cells
A. Richter (2018), 166 pp
ISBN: 978-3-95806-310-5

Band / Volume 417
Gas-to-Particle Partitioning of Major Oxidation Products from Monoterpenes and Real Plant Emissions
G. Gkatzelis (2018), xii, 128 pp
ISBN: 978-3-95806-314-3

Band / Volume 418
The Dynamics of Electrons in Linear Plasma Devices and its Impact on Plasma Surface Interaction
M. Hubeny (2018), 141 pp
ISBN: 978-3-95806-316-7

Band / Volume 419
Tomographic reconstruction of gravity wave parameters from satellite-borne airglow observations
R. Song (2018), 136 pp
ISBN: 978-3-95806-317-4

Band / Volume 420
Reduktion von Edelmetallen in der Wasserstoffelektrode bei der Polymerelektrolyt-Wasserelektrolyse
P. Paciok (2018), VII, 187 pp
ISBN: 978-3-95806-320-4

Band / Volume 421
Mechanismen des Hochtemperaturrisswachstums in einem ferritischen Stahl an Luft und in Wasserdampf
T. Fischer (2018), VIII, 216 pp
ISBN: 978-3-95806-326-6

Band / Volume 422
Selbstheilende plasmagespritzte $Mn_{1,0}Co_{1,9}Fe_{0,1}O_4$-Schutzschichten in Festoxidbrennstoffzellen
N. Grünwald (2018), viii, 137 pp
ISBN: 978-3-95806-327-3

Band / Volume 423
Sonochemical Synthesis of Silicon Hydride Polymers and Silicon Nanoparticles from Liquid Silanes
A. P. Cádiz Bedini (2018), viii, 129, XVIII pp
ISBN: 978-3-95806-329-7

Band / Volume 424
Synthesis and Stability Assessment of Uranium Microparticles: Providing Reference Materials for Nuclear Verification Purposes
R. Middendorp (2018), X, 145 pp
ISBN: 978-3-95806-330-3

Band / Volume 425
Herstellung und Charakterisierung von Lithiumlanthanzirkonat-Funktionsschichten für Lithium-Festkörperbatterien
T. Reppert (2018), vii, 187 pp
ISBN: 978-3-95806-331-0

Band / Volume 426
Proton Conduction and Gas Permeation through Polymer Electrolyte Membranes during Water Electrolysis
M. Schalenbach (2018), VI, 212 pp
ISBN: 978-3-95806-333-4

Band / Volume 427
Improved characterization of root zone soil moisture by assimilating groundwater level and surface soil moisture data in an integrated terrestrial system model
H. Zhang (2018), x, 125 pp
ISBN: 978-3-95806-335-8

Energie & Umwelt / Energy & Environment
Band / Volume 427
ISBN 978-3-95806-335-8

Mitglied der Helmholtz-Gemeinschaft

JÜLICH
Forschungszentrum